Bending Behavior of Textile Thermosetting Composite Prepregs during Forming Processes

Hassan Abdullah Alshahrani

A Thesis

In the Department

of

Mechanical, Industrial & Aerospace Engineering

Presented in Partial Fulfillment of the Requirements

for the Degree of

Doctor of Philosophy (Mechanical Engineering) at

Concordia University

Montréal, Québec, Canada

August 2017

Concordia University

School of Graduate Studies

This is to certify that the thesis prepared

By: **Mr. Hassan Abdullah Alshahrani**

Entitled: **Bending Behavior of Textile Thermosetting Composite Prepregs during Forming Processes**

and submitted in partial fulfillment of the requirements for the degree of

Doctor of Philosophy (Mechanical Engineering)

complies with the regulations of this University and meets the accepted standards with respect to originality and quality.

Signed by the Final Examining Committee:

_____ Chair
Dr. Ashutosh Bagchi

_____ External Examiner
Dr. Abbas Milani

_____ External to Program
Dr. Michelle Nokken

_____ Examiner
Dr. Van Suong Hoa

_____ Examiner
Dr. Martin Pugh

_____ Supervisor
Dr. Mehdi Hojjati

Approved by _____
Dr. Martin D. Pugh, Chair
Department of Mechanical, Industrial & Aerospace Engineering

29th June, 2017 _____
Dr. Amir Asif, Dean
Faculty of Engineering and Computer Science

Abstract

Bending Behavior of Textile Thermosetting Composite Prepregs during Forming Processes

Hassan Abdullah Alshahrani, Ph.D.

Concordia University, 2017

Composite materials are increasingly replacing metals for many modern structures used in the aerospace and automotive industry. Textile composites are favored due to their superior forming capabilities to produce complex shapes. However, the formability of a textile composite is limited by failure modes, such as wrinkling, which remain challenging issues during the forming process. The ability to accurately predict wrinkles and ultimately prevent them during the forming process is highly desirable for process optimization in an industrial environment. To predict those defects, a thorough understanding of the deformation behavior of textile-woven prepregs is required. Out-of-plane bending is one of the deformation mechanisms that govern the appearance of wrinkles during composite forming. This thesis therefore presents an experimental, theoretical, and numerical study on the out-of-plane bending behavior of woven out-of-autoclave prepregs with application in forming simulations.

Within this thesis, a new test method for characterizing the bending behavior of prepreg materials at forming conditions was developed based on a vertical cantilever test associated with a linear actuator and load cell. This test method allowed for sufficient control of the deflection shape, testing rates, and processing temperatures within the range of the thermosetting resin. Investigations for out-of-plane bending behavior and viscoelastic behavior at the forming process conditions were undertaken using the developed test method.

Through the cantilever beam theory, where the prepreg yarn is composed of two external viscoelastic polymer plies with a linear elastic ply, a theoretical model is proposed to estimate the bending stiffness over a range of processing conditions. A new approach for considering the testing rate and temperature with respect to a reference value is also established. Experimental tests were carried out to estimate the model parameters and to validate the proposed model. The predicted bending stiffness was found to be in a good agreement with experimental values at selected conditions. However, there were slight differences due to the complexity of undulation in the woven fabric structure. Then, a finite element model for the bending behavior of multilayered prepregs was developed by considering the actual bending behavior of the material. The prepreg ply was modeled by incorporating the characterized behavior of intra-ply shear and inter-ply friction. The effect of stacking sequences on out-of-plane bending deformation during the forming process was studied experimentally and numerically. Moreover, the feasibility of using a viscoelastic approach and its application in forming simulations were analyzed.

Finally, a series of real forming experiments using a double diaphragm process were carried out to investigate the formability of textile out-of-autoclave thermoset prepregs over complex geometry for aerospace applications. A one-step procedure was used for both the forming and curing processes using the same experimental setup. A finite element model was developed to simulate the double diaphragm forming process, with consideration for the diaphragm material properties at forming conditions. In addition, important considerations, such as local fiber compressive stresses, shear angle distributions, and stacking lay-up sequences, were analyzed to identify the potential causes of wrinkles in the formed parts. The resulting knowledge from the modeling methodology allowed the designers to reliably choose the appropriate stacking sequences and suitable process parameters for complex structures prior to conducting expensive trial and error tests.

Dedication

To my dear mother, Zahrah

for her everlasting support, patience, and love

To my beloved late father, Abdullah

who passed away during this journey ..... I miss you dad

To my brothers and sisters

for their unconditional support and encouragement

"especially"

my dear brother, Khalid

Acknowledgments

First and foremost, praises and thanks to Allah for the strengths and His blessing in completing this thesis.

I would like to express my deep gratitude to my supervisor, Dr. Mehdi Hojjati, for his guidance and support throughout my PhD program at Concordia University. This work would not have been possible without his help. Also, I would like to thank my research colleagues, Rahul, Harinderpal, Muhsen and Sam for all their help and collaborations.

My gratitude goes to the Government of Saudi Arabia and Najran University for providing me with all the financial needs that enabled me to achieve the goal. Also, the support and cooperation from the Natural Sciences and Engineering Research Council of Canada (NSERC) and Bombardier Aerospace are highly appreciated.

Many thanks to my friends; Dr. Abu Ahmed, Dr. Abdullahi Gujba, Dr. Othman Hassan, Abdullah Saeed, Gassim, Gamal, Mohamad Hamdoun, Omar Yagubi, Bader Alharbi, Sultan Alqahtani, Saeed Alzahrani, Khalid Aljabri, Abdulmajeed Aloraini, Majed Almuslmani, and other friends for their continuous support during my studies.

Sincere thanks to my mother (Zahrah), my late father (Abdullah), my brothers (Nasser, Safar, and Khalid), and my sisters (Fatima, Azizah, Haila, Mastorah, Norah, and Sahar) for their moral support and their encouragement during my study. Finally, many warm thanks for him and just for him, my brother (Khalid), for his support and standing by my side during all the difficulties that I faced during this journey.

Contents

List of Figures

List of Tables

Chapter 1

Introduction

Composites are a material commonly composed of fiber reinforcements bonded together with a matrix material. Composite materials are increasingly replacing metals for many modern structures used in the aerospace and automotive industry. A variety of composites in recent decades have been developed that offer good mechanical and chemical properties, including high specific stiffness and a high strength-to-weight ratio combined with good corrosion and chemical resistance. Currently, the use of composite materials based on carbon fiber-reinforced polymers has dramatically increased in commercial aircraft. Figure 1.1 shows the materials used by weight in a Boeing 787 [1]. The composite materials used in a Boeing 787 have increased by 38% compared to a Boeing 777.

The fibers in most applications need to be arranged into some form of a sheet, known as a fabric. These fabrics can be made through different textile techniques, such as weaving, braiding and knitting [2]. Hence the fabric types are specified based on the textile method used and the orientation of fibers. Woven fabric textile composites are produced by the interlacing of warp fiber tows and weft fiber tows in a regular pattern or weave style. The weave pattern determines the fabric's drapability, which is the ability to conform to a complex shape. Figure 1.2 shows the most popular weave styles that described how the warp and weft tows are interwoven. The selected weave type in this study is a Harness-Satin (in particular 5-HS), which has advantages over plain and twill weaves in terms of drapability and conformity over complex shapes.

Fabric reinforcement that has been pre–impregnated with a resin system is called prepreg. Such materials can provide several advantages, such as a precise control of the fiber/resin ratio, reduced production costs, and direct application into manufacturing processes. The resin system used in prepreg materials is typically an epoxy. This thesis focuses on woven textile out-of-autoclave (OOA) prepreg composites. The use of out-of-autoclave (OOA) composite provides a large cost-saving opportunity because the lower curing temperatures required by OOA materials allow for lower tooling costs. Therefore, the forming and curing processes can be done as one step.

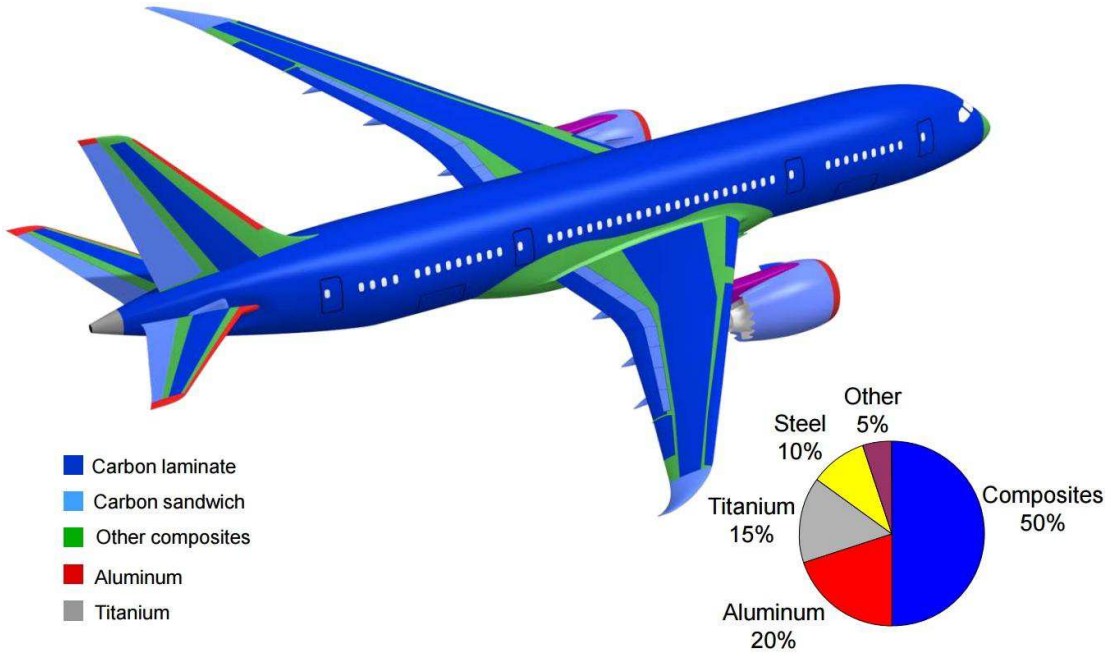

Figure 1.1: Materials used in a Boeing 787 [1].

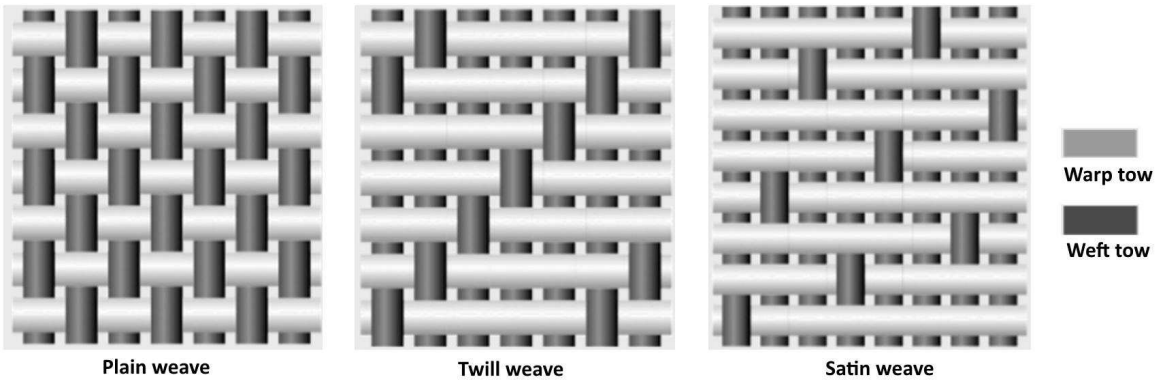

Figure 1.2: Typical woven fabrics.

1.1 Double–diaphragm forming

The most important sheet-forming processes for composite materials are the diaphragm and stamp forming methods [3, 4]. Both processes exhibit high efficiency and high productivity during formation. However, the stamp forming process is very expensive due to the need for two close-tolerance dies for each shape. Diaphragm forming is initially applied to thermoplastic matrix composites and classified into single and double diaphragm forming processes.

A typical double-diaphragm forming process can be described by three steps [5]. A prepreg stack must first be placed between two deformable sheets known as diaphragms, which are themselves clamped over a forming box as shown in Figure 1.3 (a). The space between the diaphragms is subjected to a full vacuum seal. Next, the prepreg stack between the diaphragms is heated up to processing temperature (see Figure 1.3 (b)). Finally, the forming step takes place by applying controlled vacuum pressure to the forming-box cavity below the lower diaphragm as illustrated in Figure 1.3 (c). In the diaphragm forming of thermosetting prepregs, the matrix is only heated enough to decrease its viscosity to the point where the prepreg can be formed readily.

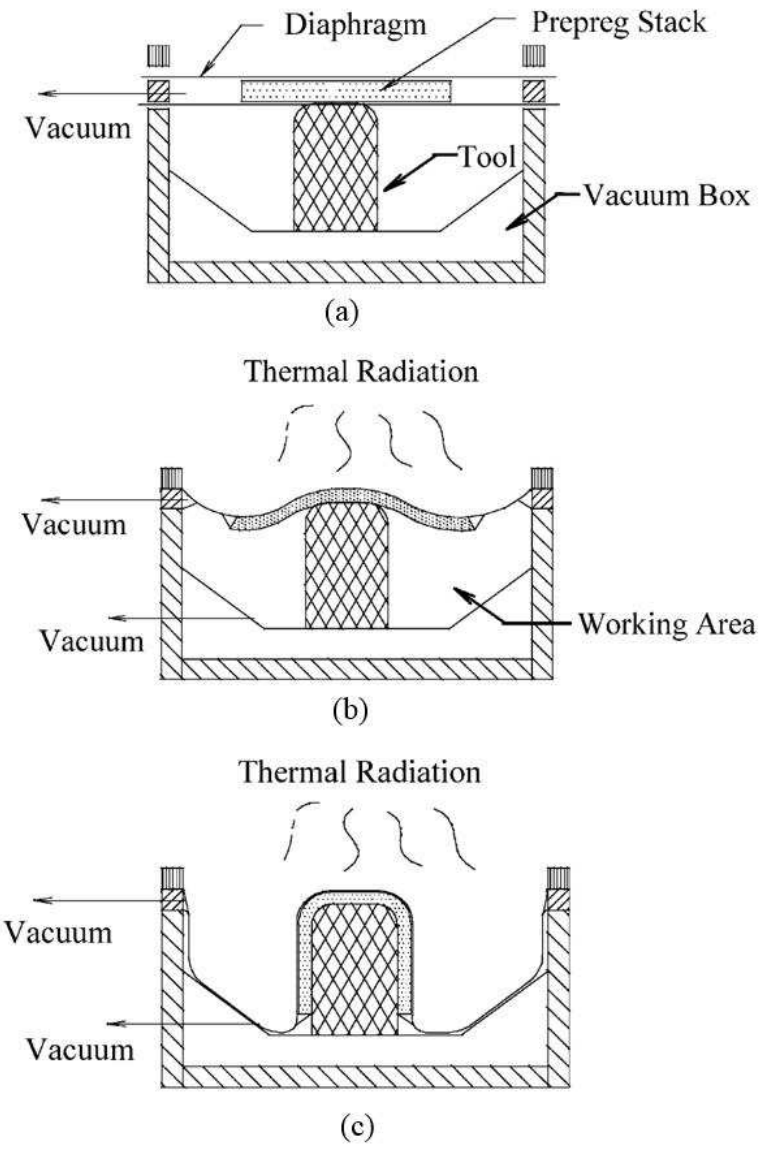

Figure 1.3: Schematic of double–diaphragm forming [5].

1.2 Forming deformation mechanisms

During the complex shapes forming process of the continuous fiber-reinforced composites, various deformation mechanisms take place to accommodate the desired geometry. Forming woven fabric to the desired shape is associated with several deformation mechanisms, of which the most common are intra-ply shearing, inter-ply sliding, and out-of-plane bending as depicted in Figure 1.4, respectively [2, 6]. Haanappel et al. [7] showed that the

formability of a composite laminate is determined by a delicate balance between these basic deformation mechanisms. To ensure successful composite forming, it is therefore necessary to thoroughly understand the mechanisms that cause defects [8]. Among numerous possible negative outcomes during forming, wrinkling is the most prevalent defect [6]. Some studies attributed the occurrence of wrinkles to the material's locking angle [9, 10]. This implies that there are wrinkles in a zone where the shear angle is larger than the locking angle. However, Boisse et al. [11] showed that the appearance of out-of-plane wrinkles is a global phenomenon that depends primarily on boundary conditions, as well as material strains and stiffness. The effect of different mechanisms also varies according to circumstances and forming processes.

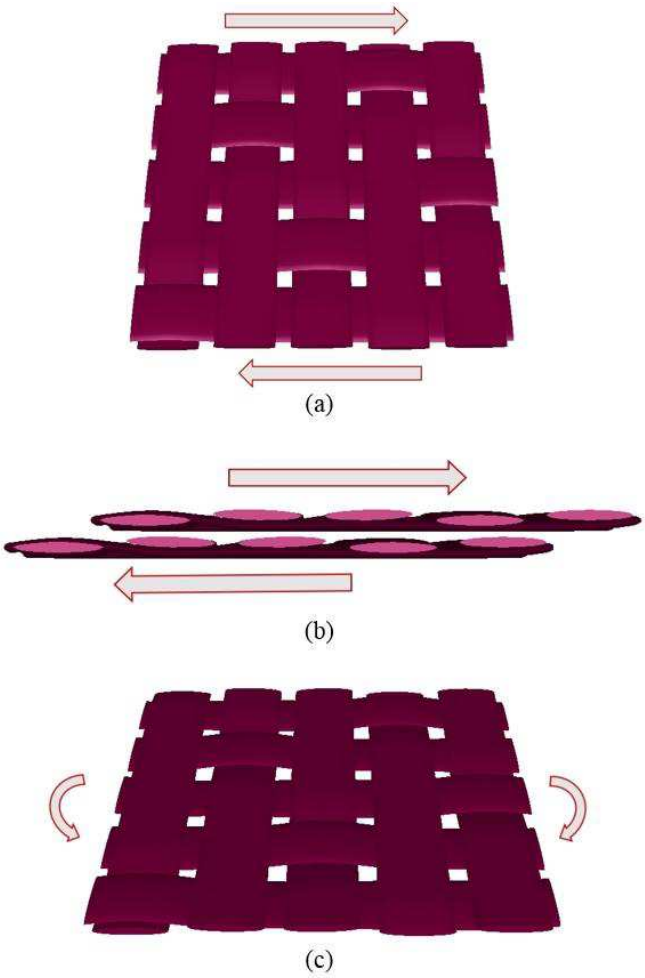

Figure 1.4: Deformation mechanisms for textile reinforcements: (a) intra-ply shear, (b) inter-ply slip, and (c) out-of-plane bending (adapted from [2, 6]).

Intra-ply shear is considered to be the primary deformation mechanism during forming and it needed to allow a material to conform to a compound curvature. This deformation mechanism is characterized by rotation of the yarns at their crossovers, which causes a change in fiber orientation. This rotation around weave crossover is mainly limited by the ability of fiber yarns to become in contact with each other. Degree of in-plane shear of woven is indicated by the shear angle between the weft and warp yarns. Both the bias extension test and the picture frame test are frequently employed to investigate the in-plane shear behavior of woven composites [12–16].

When multilayered materials are considered, adjacent plies of a laminate need to slip across one another when formed into a single or doubly curved part. Inter-ply slip is also referred to as ply–ply friction and it plays an important role for releasing the compressive stresses that may cause out of plane buckling [17, 18]. In the forming process, contact between composite laminate and the tool can also affect the final product significantly. Many researchers [19–23] investigated how processing parameters influenced frictional behavior of prepreg systems. Their results indicate that lay-up configuration, pressure, slip velocity, and temperature are greatly influence the slipping behavior. A more extensive overview of inter-ply and tool-ply slip can be found in [17, 18].

The present research focuses on out-of-plane bending mechanism both experimentally and analytically, with a goal of predicting defects during forming processes. However, in the forming simulations, the intra-ply shearing and inter-ply sliding are considered to obtain accurate results.

1.3 Out-of-plane bending of prepregs

The bending properties of ply prepreg materials are significantly lower than what would be derived from the in-plane material properties using beam or plate theory [11]. This presents a significant difficulty during forming simulations, since finite element implementations assume that bending stiffness is derived from in-plane material response using a conventional shell element. Furthermore, Liang et al [24] showed that, in forming simulations,

the bending stiffness of the prepreg at the processing temperature is an important predictor of the size and quantity of wrinkles. Wrinkling is caused by out-of-plane deformation due to compressive loading in the plane of the material during the forming process. This implies that for the forces associated with out-of-plane bending to be scaled correctly, it is necessary to first arrive at a good understanding of the relative magnitude of the bending stiffness [6]. Thus, these properties, along with their temperature and other dependencies, must be thoroughly characterized and properly represented in finite element forming simulation.

A review of current test methods, presented in Chapter 2, for characterization the bending behavior of prepreg composites showed the need for a new approach that has good control of the testing parameters and the applied load. In forming simulations, some models are presented in the literature, where bending behavior is de–coupled from in-plane by using specialized shell element in finite element forming simulation based on elastic [7,25–27], elastic with temperature-dependent [13,28], or viscoelastic approaches [29]. The latter research [29] showed that modeling rate-dependent bending behavior using a viscoelastic approach is crucial to predict wrinkling in FE forming simulation of thermoplastic pre–impregnated tapes. In their study, the bending characterization was based on isothermal investigations using the rheometer bending setup presented by Sachs [30]. Some commercial software tools, such as PAM-FORM [31] and AniForm [32], offer the possibility of modeling a number of features of composite forming. However, no details or application of out-of-plane bending behavior of prepreg composites based on viscoelastic material models are available in the literature using these commercial software tools.

1.4 Motivation

The manufacture of composite structures is often performed using conventional techniques such as hand lay-ups and vacuum bagging. However, increased demand for composite parts, together with an increase in their size and complexity, puts a strain on traditional processing methods and drives the need for fast, and cost-effective manufacturing alternatives. The low manufacturing times and costs associated with automated manufacturing

processes such as Automated Tape Laying (ATL) and Automated Fiber Placement (AFP) offer great promise to meet the growing need for composite materials in the aerospace and automotive industries [33]. The limiting factor for the viability of these automated processes is their capacity to produce complex geometries (such as highly-curved components with small radii). To improve productivity while maintaining the geometrical complexity of components, a three-step process is undertaken: first, flat laminates are laid down by automated machines; next, these laminates are subjected to a forming process; finally, the formed parts are cured. A semi–continuous forming method associated with automated machines for OOA prepreg materials, shown in Figure 1.5, is a promising direction, which offers an extreme reduction in overall manufacturing cost and time.

Textile composites are favored due to their superior forming capabilities for producing complex shapes. However, formability of textile composite is limited by failure modes such as wrinkling, which remains as a challenging issue during forming processes. The bending stiffness of prepreg ply plays an important role in determining wrinkle formation. Accurate prediction of wrinkle formation is highly desirable as a first step to prevent this defect for process optimization in an industrial environment. Minimizing failure rates of complex composite parts is of great interest to the aerospace and automobile industries. Once potential material defects during forming can be accurately predicted, designers will be able to reliably choose appropriate material types and processing parameters without the requirement for expensive trial and error tests. However, a considerable amount of knowledge of the mechanical behavior of prepreg materials and forming process conditions is still required to produce defect-free complex-shaped composite parts.

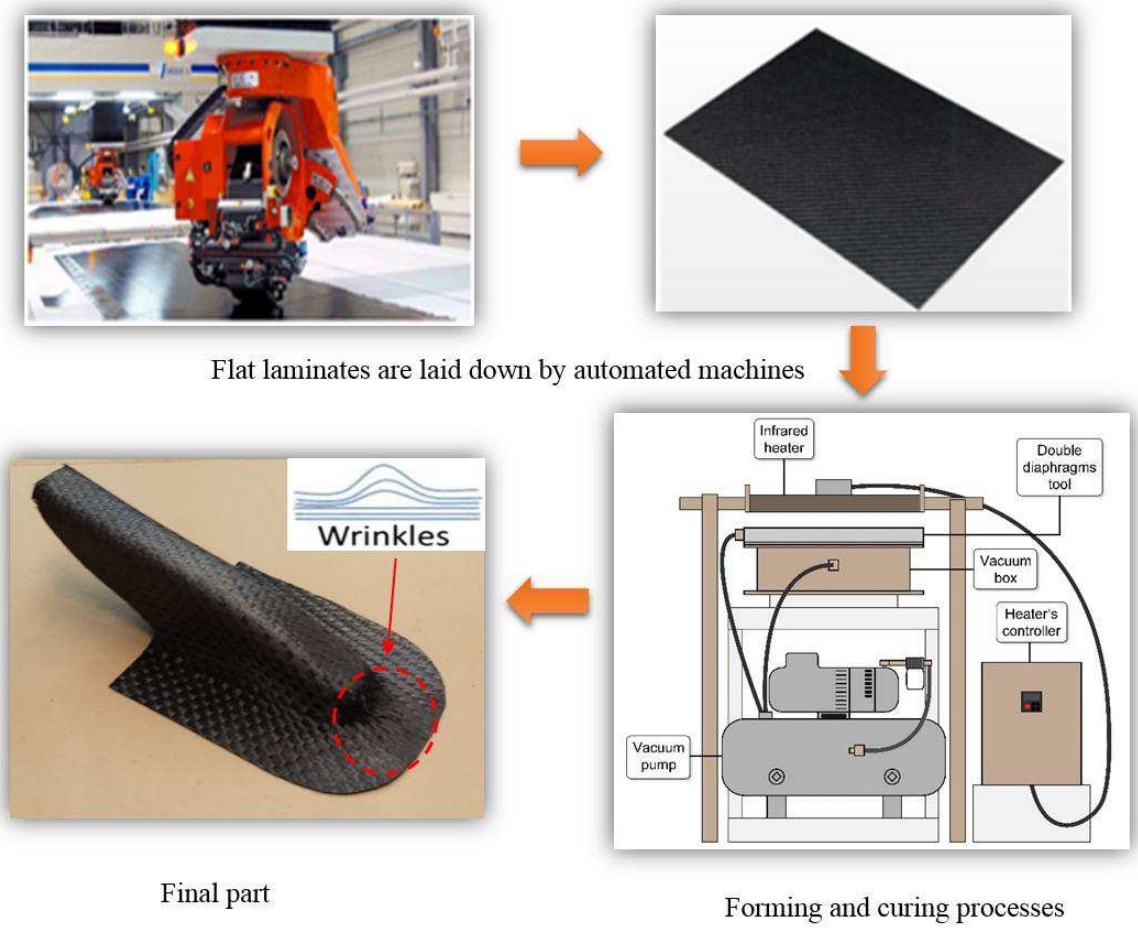

Figure 1.5: A semi-continuous production method for OOA prepreg materials.

1.5 Objectives

Currently, the test methods used to characterize the out-of-plane bending behavior of prepreg composites showed the need for a new approach that has good control of the testing parameters and the applied load. Furthermore, there are at present no accurate theoretical models available to predict bending stiffness of prepregs at processing parameters. Accordingly, the main goal of this thesis is to gain a fundamental understanding of out-of-plane bending behavior of textile woven out-of-autoclave thermoset prepregs as measured using both experimental characterization and theoretical modeling and to implement the findings into forming simulation. The specific objectives of the present research are as follows:

(1) Design a simple experimental set-up to accurately characterize the bending properties of thermosetting prepregs at processing conditions, including forming temperatures and rates.

(2) Develop a theoretical model for estimating the bending stiffness of textile prepregs to minimize the effort required for experimental investigations.

(3) Develop a finite element (FE) model for the bending behavior of multilayered textile prepregs using an independent bending stiffness.

(4) Investigate experimentally and numerically the formability of OOA thermoset textile prepregs over a complex geometry for aerospace applications using a double diaphragm forming (DDF) process.

1.6 Thesis outline

The entire thesis is divided into six chapters and formatted in accordance to the rules for a manuscript-based thesis. This thesis consists of four journal articles (Chapters 2 to 5); each chapter includes a review of the relevant studies and addresses one objective of this research. These chapters are completely self-contained and can be read independently. This implies that some introductory and parts are duplicated. A brief outline of each chapter is given below.

Chapter 1 outlines a general introduction about textile composites and the addressed problem, which is of high practical relevance in the manufacture of composite components. In particular, the prediction of material wrinkling or other defect formation mechanisms is extremely important for process optimization in an industrial environment. Motivation and objectives of the present work are presented.

Chapter 2 presents a new test method for characterization of the bending behavior of textile prepregs under conditions relevant to the forming process. This is based on a comprehensive review of existing devices and their drawbacks and limitations. The proposed setup allows for investigation into temperature, rate and viscoelastic effects. A number of

experimental considerations with different sample configurations are also evaluated.

Chapter 3 proposes a theoretical model that can be applied to a wide range of processing conditions to predict the bending stiffness of thermosetting composite perpreg during forming process. A new approach for considering the testing rate and temperature with respect to a reference value is also established. Experimental tests are carried out for estimation of the model parameters and validation of the proposed model.

Chapter 4 provides a systematic approach for a finite element (FE) prediction of bending behavior of multilayered textile prepregs based on viscoelastic material model. Experimental investigations of bending behavior of multilayered textile prepregs are conducted using the proposed test, presented in Chapter 2. The experimental results are subsequently compared against the FE model. Moreover, the feasibility of using a viscoelastic approach and its application in forming simulations are analyzed.

Chapter 5 investigates experimentally and numerically the formability of out-of-autoclave thermoset textile prepregs over a complex geometry for aerospace applications using a double diaphragm forming (DDF) process. An evaluation of the DDF process in terms of observed defects, stacking sequences, and the pre–forming state is carried out. Significant investigations are made in order to obtain the required properties for the material models in the FE simulation, including the diaphragm material properties.

At the conclusion of this thesis, **Chapter 6** summarizes the main conclusions and contributions that are drawn from this research. In addition, recommendations for future work directions are presented.

Chapter 2

A new test method for the characterization of the bending behavior of textile prepregs*

Abstract

To improve forming simulation outcomes for composite prepregs and predict wrinkle formation, the bending behavior of prepreg materials must be correctly characterized. This paper proposes a new loading-rate control bending test in which the sample deflection and applied rate are controlled by a linear actuator while the load required to achieve this deflection is recorded by a miniature-load cell. An investigation of out-of-plane bending behavior as well as viscoelastic behavior at the forming process conditions of woven fabric out-of-autoclave prepregs was undertaken using this method. The experimental results show that the proposed bending test provides sufficient control of the deflection shape, testing rates, and processing temperatures within the range of thermosetting resin. Furthermore, the bending results reveal the rate dependency and viscoelastic nature of the materials. A method is developed to derive the bending stiffness from the nonlinear relationship between bending moment and curvature.

*Reproduced from: Hassan Alshahrani, Mehdi Hojjati. A new test method for the characterization of the bending behavior of textile prepregs. Composites Part A: Applied Science and Manufacturing, 97 (2017), pp. 128–140. http://dx.doi.org/10.1016/j.compositesa.2017.02.027

2.1 Introduction

Many modern structures, including primary aerospace structures, high performance sporting goods, and marine and wind energy structures, are progressively coming to rely on advanced composite materials based on carbon fiber-reinforced thermoset polymers. Increased demand on these composite parts, together with an increase in their size and complexity, puts a strain on traditional processing methods and drives the need for fast, adaptive, cost-effective manufacturing alternatives. The low manufacturing times and costs associated with automated manufacturing processes such as Automated Tape Laying (ATL) and Automated Fiber Placement (AFP) offer great promise to meet the growing need for composite materials in the aerospace and automotive industries [33]. The limiting factor for the viability of these automated processes is their capacity to produce complex geometries (such as highly curved components with small radii). To improve productivity while maintaining the geometrical complexity of components, a three-step process is undertaken: first, flat laminates are laid down by automated machines; next, these laminates are subjected to a forming process; finally, the formed parts are cured. To ensure successful composite forming, the mechanisms that cause defects must be thoroughly understood [8]. Forming of woven fabric to the desired shape is associated with several deformation mechanisms, of which the most common are intra-ply shearing, out-of-plane bending, and inter-ply sliding [6]. The success or failure of composite forming is determined by the material properties that predominate these deformation mechanisms.

For numerical simulations to yield meaningful results, a number of different mechanical properties must considered [11, 24, 34, 35]. Thus, these properties, along with their temperature and other dependencies, must be thoroughly characterized prior forming simulation. One of the most common manufacturing-induced defect types to occur during composite forming is wrinkling. Wrinkling is caused by out-of-plane deformation due to compressive loading in the plane of the material during the forming process. Thus, for the forces associated with out-of-plane bending to be scaled correctly, it is necessary to first arrive at a good understanding of the relative magnitude of the bending stiffness [6].

Accurate prediction of wrinkle formation is highly desirable as a first step to prevent this defect. Boisse et al. [11] showed that the appearance of out-of-plane wrinkles is a global phenomenon which depends primarily on boundary conditions, as well as material strains and stiffness. Recently, Liang et al. [24] have demonstrated that the effective bending stiffness of the prepreg at the processing temperature during forming simulations is an important predictor of the size and quantity of wrinkles. Beam or plate theory models based on in-plane material properties predict significantly higher bending properties than are actually found for ply prepreg materials [11]. This presents a significant difficulty during forming simulations, because finite element implementations automatically derive bending stiffness from in-plane material response using a conventional shell element. Consequently, the bending stiffness must be represented separately in the finite element model [27].

During forming simulation, all three deformation mechanisms (out-of-plane bending, intra-ply shearing, and inter-ply sliding) must be considered to achieve an accurate prediction of wrinkling. However, more recent attention has focused on the mechanism of out-of-plane bending of prepreg composites. There exists, at present, no established method to characterize the bending behavior of prepreg materials. Thus, the present paper will propose a new test method to characterize out-of-plane bending behavior at forming-process conditions, including both rate and temperature dependencies.

2.2 Review of bending test methods

Several test methods have been developed to measure the out-of-plane bending properties of dry reinforcement and prepreg composites; the main methods are listed in Table 2.1. Most of the setups that have been proposed for characterization of bending behavior are adapted from Peirce's cantilever test [36]. In Peirces setup, a rectangular strip of fabric on a horizontal platform is slowly extended forward to project as a cantilever horizontally until the tip of the cantilever touches an inclined plane. The bending stiffness of the cantilever is then calculated at a specific inclined-angle value of 41.5° [37]. The standard cantilever

test requires the assumption that a linear elastic behavior holds between the bending moment and the strip curvature. The small deformation assumption restricts such a method to be applied to prepreg composites that require high curvature during forming process. A modification of the cantilever test, consisting of a succession of quasi-static tests with different load cases, was proposed by Bilbao et al. [38]. The test device comprises two parts: a mechanical part and an optical part. The mechanical part enables the sample to be placed in a cantilever configuration (a fixed board composed of laths) under its own weight, while the optical part takes pictures of the bent shapes using a digital camera. After the sample is placed, the drawer moves in the bending direction, causing the laths to retract and the overhang length to increase. The test is stopped for a chosen overhang length and is continued for new lengths. For each selected length, the shape of the overhang sample is extracted and image processing is undertaken. However, the obtained curves for all selected lengths were not identical; furthermore, large scatter points were observed in the zones of low curvature. Liang et al. [24] proposed a modified cantilever test setup with an environmental chamber. They followed the principles of Bilbao's method to create a moment–curvature graph for different temperatures. Their investigation showed that the bending stiffness of thermoplastic prepregs is greatly influenced by temperature. However, obtaining a uniform temperature field in the sample before starting the test is complicated due to bending under its own weight. Moreover, the influence of the deformation rate is not considered in their work.

Soteropoulos et al. [39] introduced a new test design that addresses the potential problem of twists in the samples (due to non-linear loading effects in the cantilever setup) by hanging the samples vertically. In their setup, the load was applied by attaching masses to a string tied to the tip of the sample. A digital camera was then used to capture the relative displacement of the sample under each load. Next, the digital image was graphically processed to generate data points along the sample length. Dangora et al. [40] used the vertical cantilever method with a radiant heater to characterize the bending behavior of a cross-ply thermoplastic lamina at elevated-temperature conditions.

Kawabata's Evaluation System (KES) is an alternative method of measuring the basic mechanical properties of fabrics [41,42]. In the bending test, a sample is held between a fixed clamp and a moving clamp. The moving clamp bends the sample, following a circular path, and provides full data on bending behavior, including stiffness as a function of curvature. However, it is not very well adapted for composite reinforcements or prepreg which are often thicker and stiffer than clothing textiles [38]. Additionally, the device is very expensive and its availability is limited. A three-point bending test with a V–shaped punch and thermal chamber was proposed by Martin et al. for studying the bending behavior of unidirectional thermoplastic composites [43]. It has proven difficult to prevent deformation of the sample under its own weight during this test, especially at elevated temperatures. To avoid this problem, a buckling test was suggested by Wang et al. [44]. However, the authors note that great care must still be taken during clamping of the samples to avoid any misalignment. Moreover, only small samples can be tested to obtain a symmetric bending shape.

Researchers at the University of Twente have recently developed a custom-built fixture that mounts onto a rheometer, which offers a close temperature control via an equipped thermal chamber [45,46]. The rheometer settings allow for testing at a range of rotational velocities. The main difficulty with this method is that the sample must follow a perfect circular path to ensure pure bending. Although the test has shown promising results for a selected sample size, the researchers report that further evaluations need to be performed at different sample lengths [46]. Note, however, that the choice of the sample size is limited by the size of the available rheometer.

In 2015, Margossian et al. proposed a new approach that uses a Dynamic Mechanical Analysis (DMA) system [47] to assess different test fixtures at a range of temperatures and speeds. Based on a method suggested by TA Instruments [48] , an out-of-plane bending modulus, E_B, was calculated using

$$E_B = K * GF \tag{2.1}$$

where K is the stiffness of the sample measured by the DMA system and GF (Geometry Factor) is a factor related to the geometry of the sample. For rectangular samples subjected to three-point bending tests, TA Instruments gives [48]

$$GF = \frac{L^3}{48I}\left[1 + \frac{48}{5}(1+\nu)\left(\frac{t}{L}\right)^2\right] \tag{2.2}$$

where L is the sample free span length, I the second moment of inertia, t the sample thickness and ν the Poisson's ratio. By inserting Eq. 2.2 into Eq. 2.1, the out-of-plane bending modulus E_B can be determined. However, due to a failure to record the deflections with the DMA system, the curvature was calculated using the Euler–Bernoulli theory. The authors concluded that machine acceleration makes it difficult to apply a specific test speed [47]. Newly, Ropers et al. [35] performed both Dynamic Mechanical Analysis (DMA) and rheometer-based bending experiments to assess temperature-dependent and viscoelastic behavior for thermoplastic composites.

Table 2.1: Test methods developed to determine out of plane bending properties of dry reinforcement and prepreg composites.

Ref.	**Method**	**Temperature (°C)**	**Rate control**	**Material**
Peirce [36]	Cantilever test	RT	No	Various fabrics
Bilbao et al. [38]	Modified cantilever test	RT	No	Dry reinforcement fabric
Liang et al. [24]	Cantilever test + thermal chamber	Up to 600	No	5HS thermoplastic prepreg
Soteropoulos et al. [39]	Vertical cantilever test	RT	No	Dry Non-Crimp Fabrics
Dangora et al. [40]	Vertical cantilever test with a radiant heater	Up to 120	No	Cross-ply thermoplastic
Lomov et al. [42]	Kawabata test	RT	Yes	Dry Non-Crimp Fabrics
Martin et al. [43]	V-bending test + thermal chamber	Up to 170	Yes	UD thermoplastic prepreg
Wang et al. [44]	Buckling test	Up to 150	Yes	UD thermosetting prepreg
Ten Hove [45]	Rheometer + thermal chamber	Up to 450	Yes	UD thermoplastic prepreg
Margossian et al. [47]	DMA system	Up to 260	Yes	UD thermoplastic prepreg
Ropers et al. [35]	Rheometer + thermal chamber and DMA system	Up to 260	Yes	Woven textile and UD thermoplastic prepreg

2.3 Materials

The out-of-autoclave (OOA) prepreg chosen for this study was manufactured by Cytec Engineered Materials Inc. The prepreg consists of a 5-harness (5HS) satin weave (6 K carbon fiber tows) impregnated with an epoxy resin (Cycom 5320) designed for OOA manufacturing applications. The fabric's areal weight is 380 g/m^2 and the resin content is 36% by weight. The measured thickness of an uncured single-ply is approximately 0.55 mm. A dry 5HS satin weave (6 K carbon fiber tows) was also included for comparison.

OOA prepregs differ from most autoclave prepregs in that the upper and lower fiber plies are partially impregnated with resin. This partial impregnation creates a dry porous medium between the upper and lower portions of the prepreg and permits the evacuation of any trapped air before the resin wets the dry fibers, as shown in Figure 2.1 [49]. During processing, these spaces are progressively infiltrated by resin to produce a uniform, void-free structure. OOA composite forming provides a great cost-saving opportunity for the aerospace industry, because the lower curing temperatures required by OOA materials allow for lower tooling costs.

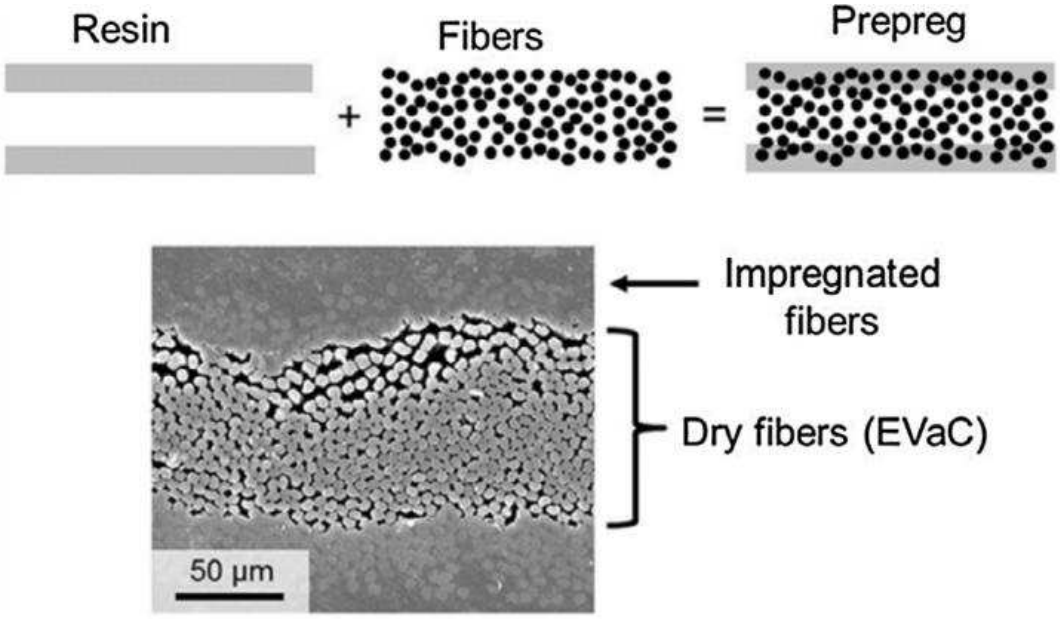

Figure 2.1: Schematic and SEM micrograph of air evacuation channels in OOA prepreg [49].

2.4 Experimental procedure

2.4.1 Test set-up

A review of current test methods for characterization the bending behavior of prepreg composites showed the need for a new approach that has good control of the testing parameters and the applied load. To meet this need, a new test method, based on the vertical cantilever test, is proposed in the present paper. The setup for the proposed test is illustrated in Figure 2.2. In this setup, metallic custom grips are used to clamp the sample vertically, while the sample deflection and applied rate are controlled by a linear actuator. A miniature-load cell is used to measure the load required to achieve this deflection. The T-NA08A50 actuator and Loadstar load cell are connected by rotating the actuator until the load cell threads into the standoff on the tip of the actuator, as shown in Figure 2.3 (a). Direct commands and change settings (such as required travel displacements, speeds, or current position) can be sent via the Zaber Console connected to the actuator, while LoadVUE software records the load during the test with high accuracy (see Figure 2.3 (b)). Note that the load cell's capacity is 9.8 N, while the maximum travel displacement of the actuator is 50 mm.

A radiant heater is employed to heat the sample to the target testing temperature. The temperature throughout the sample is monitored by an infrared camera (FLIR), as detailed in Section 2.4.2. The rate-dependent effect can be measured by adjusting the testing speed using the actuator's controller.

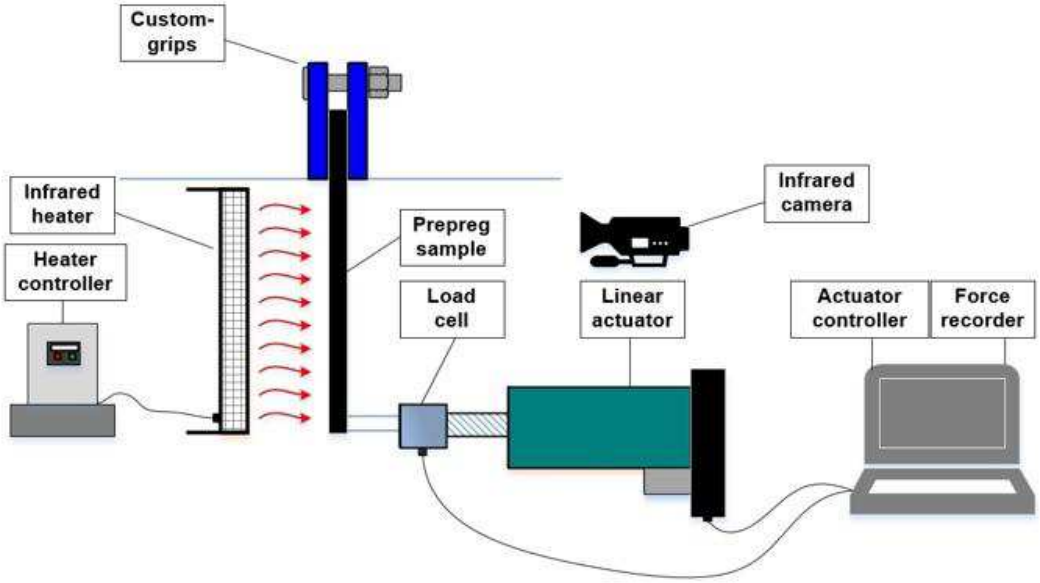

(a)

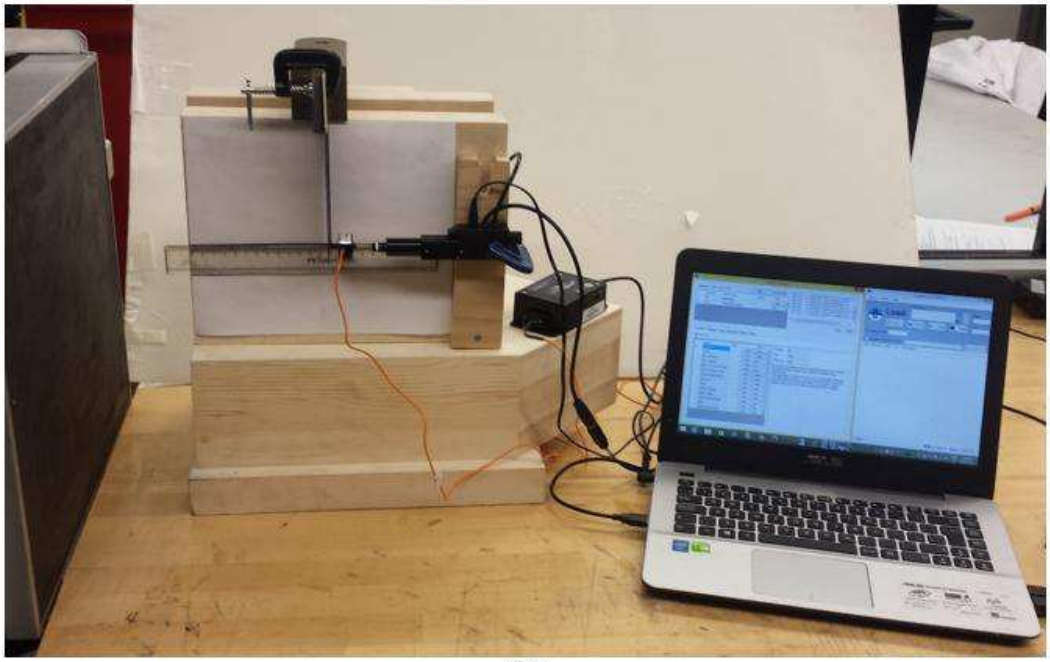

(b)

Figure 2.2: Proposed bending test setup for prepreg characterization purposes at processing conditions (a) schematic and (b) photograph.

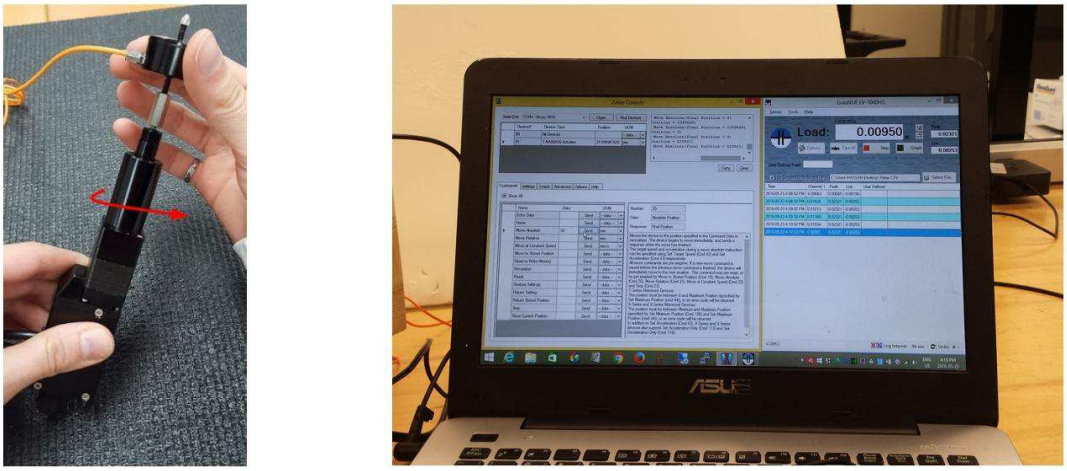

(a) (b)

Figure 2.3: (a) Method of connecting the load cell to the actuator and (b) Zaber Console and LoadVUE software.

2.4.2 Selection and analysis of temperature

To identify appropriate processing temperatures for composite forming, thermal analysis of the selected materials must be performed. Dynamic cure analysis using differential scanning calorimetry (DSC) was carried out on the Cycom-5320 OOA prepreg to determine the cure reaction onset temperature. The dynamic run of the uncured prepreg sample at 2 °C/min is plotted in Figure 2.4. The graph indicates that the cure reaction begins at approximately 110 °C. Based on this measure, the temperature range and limit for the OOA material during the forming process can be determined. Note that selection of processing temperature must take place before the aforementioned temperature is reached; otherwise, a curing reaction may commence, leading to a change in the material properties.

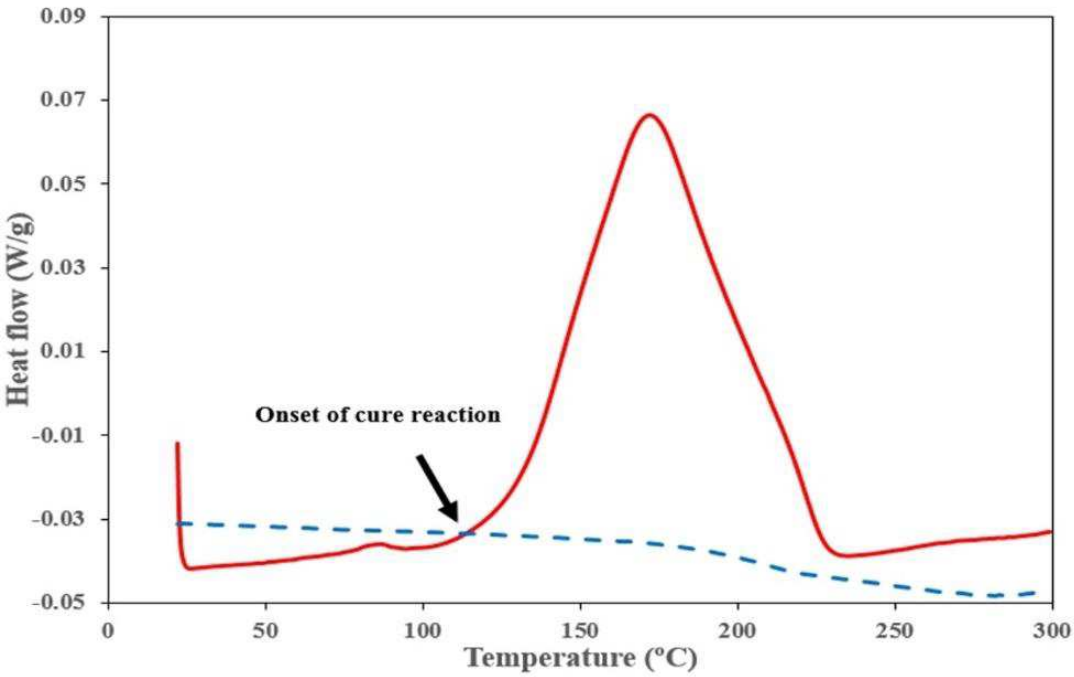

Figure 2.4: Dynamic analysis at 2 °C/min for Cycom-5320 OOA prepreg.

The temperature throughout the sample should be uniform before testing begins. To ensure uniform heating during the elevated temperature tests (using a non-contact radiant heater), the sample was held at the same temperature for 5 minutes after reaching the processing temperature. To accomplish this, the thermocouple was placed in the clamping zone. Upon reaching the required temperature, the sample's temperature field was captured by infrared camera (FLIR), as shown in Figure 2.5 (a). The pictograph (Figure 2.5 (b)) shows the surface temperature map and differences in temperature at three different points, sp1, sp2, and sp3, on the prepreg samples. A uniform temperature field is observed with a range of ±2 °C throughout the sample. Measured temperatures over a 20–90 °C range showed homogeneous temperature distributions (max. ±3 °C). Note that the lower temperatures required during the processing of thermosetting materials allow to achieve acceptable temperature fields using the non-contact radiant heater. This heating system must be contained within a closed chamber when higher temperatures (above 120 °C) are required. For thermoplastic prepregs, such a thermal closed chamber is recommended. Liang et al. [24] used a thermal chamber to study the bending properties of thermoplastic

prepreg under the horizontal bending test condition. Their results suggest that uniform temperature distributions (±5 °C) up to 600 °C can be achieved. However, Liang et al.'s temperature gradient measurements were conducted on the bent shape, due to the difficulty of controlling the sample before bending. Therefore, the vertical position of the sample may have advantages in particular in case of test at high temperature.

(a) (b)

Figure 2.5: (a) FLIR T420 IR camera and (b) Infrared images showing temperature gradient.

2.4.3 Sample preparation and test conditions

The samples selected for the bending experiments were 150-mm long by 50-mm wide, with an un-gripped length of 120 mm. Single-ply samples were used to offset any possible contribution of ply-ply friction to the bending results. Nevertheless, bending-friction coupling effects may still have some impact during the forming simulation of multi-layered composites; this possible effect will be investigated in future studies. Each sample was kept under the same conditions prior to testing (unconsolidated state). A consolidated sample under conditions relevant to double diaphragm forming was also investigated. The samples were cut so that their warp and weft directions were perpendicular to the applied load (red spot), as shown in Figure 2.6 (a) and (b), respectively. Other possible configurations can be evaluated using the same set-up.

In a 5HS woven fabric, 80% of the fibers on one face are in the strip-long direction, whereas 80% of the fibers on the other face are perpendicular to that direction. It is therefore possible that the bending behavior may be sensitive to which face is in tension and which is in compression. In Face 1 in Figure 2.6 (a), 80% of the fibers are aligned to the warp direction, implying that this face will be in tension during warp (face 1) tests. Conversely, warp (face 2) will correspond to the other face when face 1 is under compression. In the weft (face 1) sample, 80% of the fibers are perpendicular to the weft direction, as shown in Figure 2.6 (b), while the other face is indicated by weft (face 2). The bending experiments in this study were carried out on all four faces–warp (face 1 and 2) and weft (face 1 and 2)–to investigate the effect of sample configuration on the bending results. Tests were conducted on all these samples at room temperature (RT), 50 °C, 70 °C and 90 °C, i.e. below cure reaction temperature. Three test speeds were applied at room temperature: 3 mm/s, 6 mm/s, and 9 mm/s. At least three trials were conducted under each condition to ensure that the results are repeatable. The average of these three tests are plotted with error bars of the standard deviation.

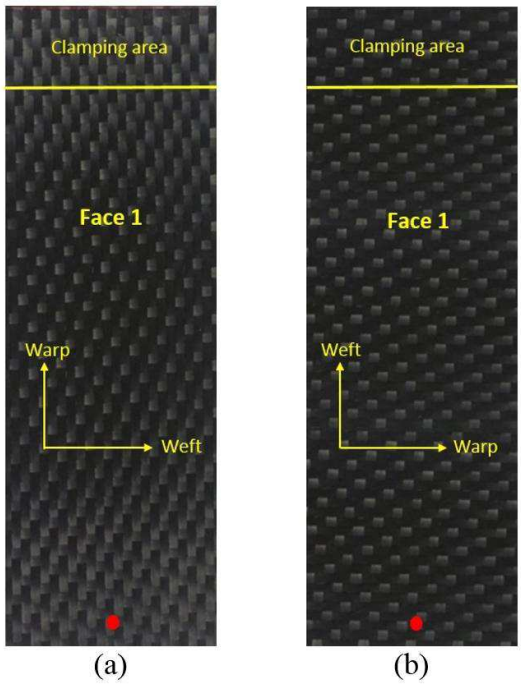

Figure 2.6: 5HS prepreg samples and tow direction to the applied load (normal to red spot) (a) warp direction and (b) weft direction.

2.4.4 Bending test procedure

The sample is clamped vertically and the actuator applies horizontal force until a certain tip displacement is achieved. The analysis of the bending behavior during composite forming process requires high curvature (higher displacement) to accurately simulate the process. Therefore, large bending deflection must be considered during the bending test to give the bending moment as a function of large curvature. Figure 2.7 (a) shows the bent shape of tested sample with large bending deflection (tip displacement of 50 mm). The force required to achieve this displacement is subsequently recorded by the load cell. Tying the tip of the load cell to the sample may create tension in the sample during bending. To avoid this, the position of applied load is lifted from the tip of the sample by approximately 3-5 mm (see red spot in Figure 2.6) to reach the required tip displacement without an attachment method. This distance is then excluded from the total length of sample during moment calculation.

Images of the bent shape are captured by a digital camera and processed in ImageJ software. The sample length is divided into several segments–10 mm per segment, in the current case–and the corresponding points of deformation are then marked, as illustrated in Figure 2.7 (a). Note that care must be taken when extracting data points during the image-processing procedure. Data points on the deflection profile are subsequently fitted using a proper polynomial function, as shown in Figure 2.7 (b). The curvature of the profile is then calculated from the obtained polynomial fit according to Euler-Bernoulli's law for large deformation produced by bending:

$$\kappa = \frac{x''}{(1 + x'^2)^{3/2}} \tag{2.3}$$

where x is the horizontal displacement at a given axial location y.

The slope of the deflection curve in the expression of the curvature cannot be neglected unless the deflections are small [50]. Thus, describing the beam's curvature using the second derivative alone (as indicated in [51]) may compromise the characterization parameters that are derived from the test data.

The value of the recorded load can now be used to calculate the moment at each selected point. According to Figure 2.8, $(M = -F(L- \Delta -y))$ is the resulting bending moment at any $0 \leq y \leq L - \Delta$, where F is the load required to achieve a certain tip displacement (d), L is the sample length, and Δ is the vertical displacement of the free end. Finally, the moments at each point can be plotted against the corresponding curvature values.

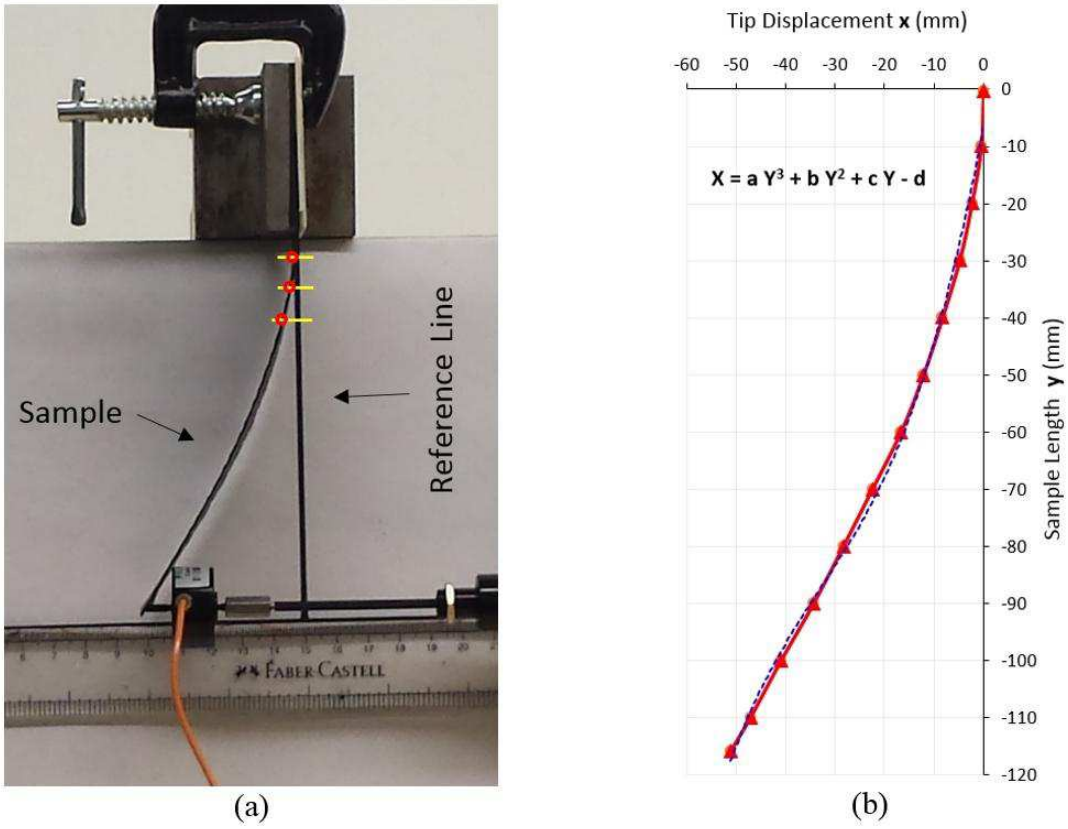

Figure 2.7: Bending profile with tip displacement of 50 mm (a) bent shape with selected segments and (b) data points along the sample length.

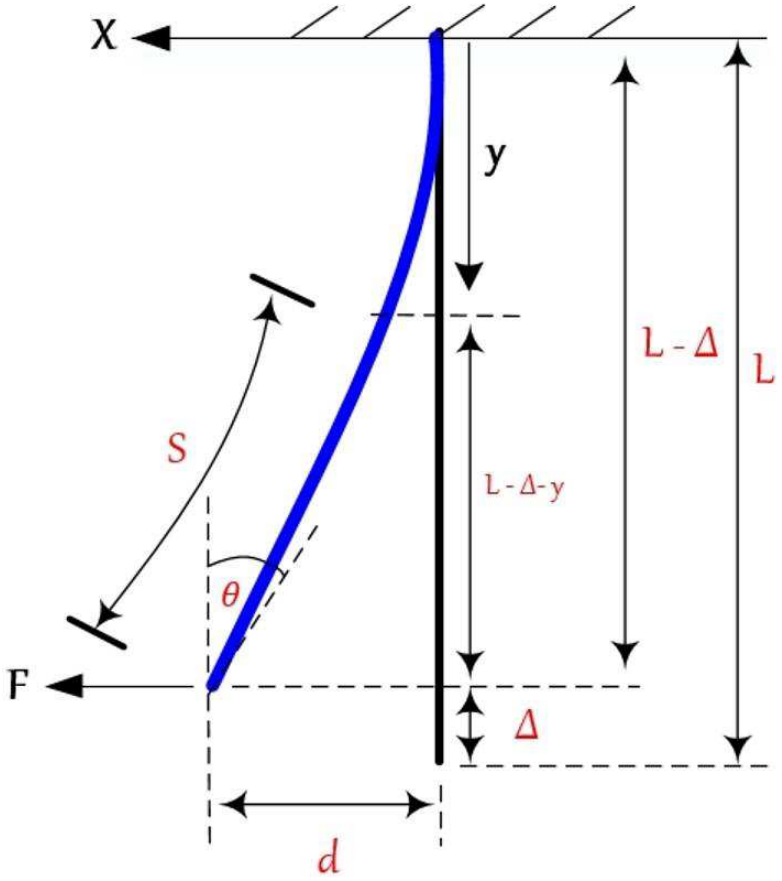

Figure 2.8: Large deformation of a cantilever beam of length L with a concentrated Load F applied at the free end.

2.5 Results and discussion

As previously mentioned, both the warp- and weft-direction samples are considered in the analysis. The bending moment and corresponding curvature values for 5HS (warp) and 5HS (weft) samples at each selected point (as described in Section 2.4.4) are plotted in Figures 2.9 and 2.10, respectively. Note that the nonlinear relationship between the bending moment and curvature is due to the utilization of Eq. 2.3, a second-order nonlinear differential equation. The data produced by this equation suggest that material deflections are not a linear function of the bending moment as long as the slope of the deflection curve is significant. The obtained polynomial fit is a third-order equation for all samples tested up to a 50-mm tip displacement. Applying Eq. 2.3 reveals a slight difference in the

curvature values along the samples. Again, the procedure for extracting the data points must be followed precisely for each sample. Figure 2.9 shows the difference between the two faces (warp direction) tested at room temperature with a speed of 3 mm/s. The maximum bending moment in the warp direction (face 1) is 4.816 N-mm, versus 4.175 N-mm in warp direction (face 2). The variation between weft (face 1) and weft (face 2) is depicted in Figure 2.10. The face 1/face 2 difference is likely to have as much impact on the outcome as the difference between warp and weft alignments. However, the results do show that the bending moment in the warp direction is approximately 20% higher than the bending moment in the weft direction. This distinction is attributed to the fact that the warp is straighter than the weft (lower number of crimps) and the number of warp threads per unit area is also higher than weft (more fabric density). Ropers et al. [35] used DMA measurements to investigate the difference between warp and weft directions in thermoplastic prepreg and conclude that this difference can be ignored. However, Liang et al. [24] showed that the difference between warp and weft for PEEK-satin prepreg is about 15%. Therefore, the bending properties of the warp and weft directions during numerical forming simulations must be considered to ensure an accurate model.

It should be noted that the difference between warp and weft directions in dry 5HS is greater than the one observed in 5HS prepreg. Results for dry 5HS in both directions are shown in Figure 2.11. The moments plotted for the warp direction differ by up to 29% from those obtained in the weft direction, whereas the equivalent warp/weft moments only differ by 18% in prepreg samples. This contrast is likely due to the prepreg manufacturing technique, which pulls the weft rovings out of alignment by slightly bending them [35]. However, it is also possible that the presence of resin in the OOA prepreg plays a role in this difference. The effect of curing degree (out-time) on the bending results was not examined in this paper; recall that all samples were kept under the same conditions before the bending experiments.

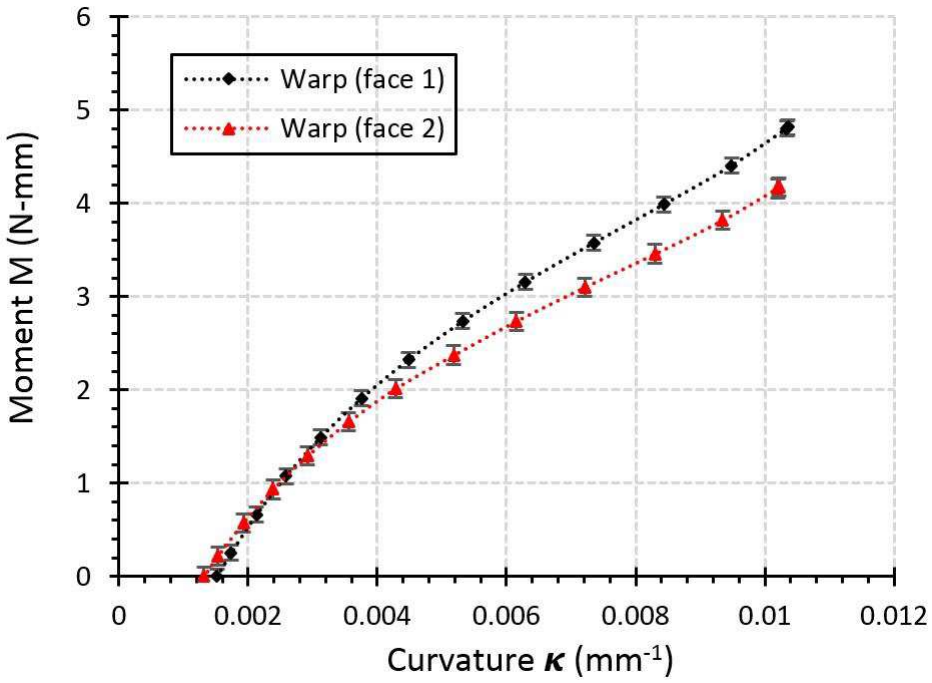

Figure 2.9: Bending moment versus curvature of 5HS prepreg sample in warp direction at room temperature.

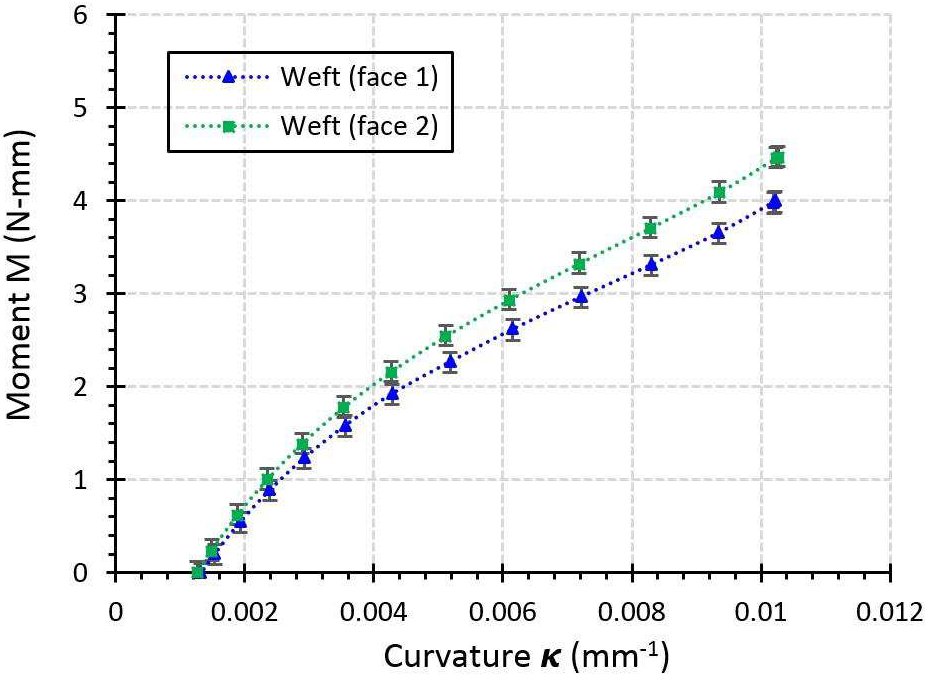

Figure 2.10: Bending moment versus curvature of 5HS prepreg sample in weft direction at room temperature.

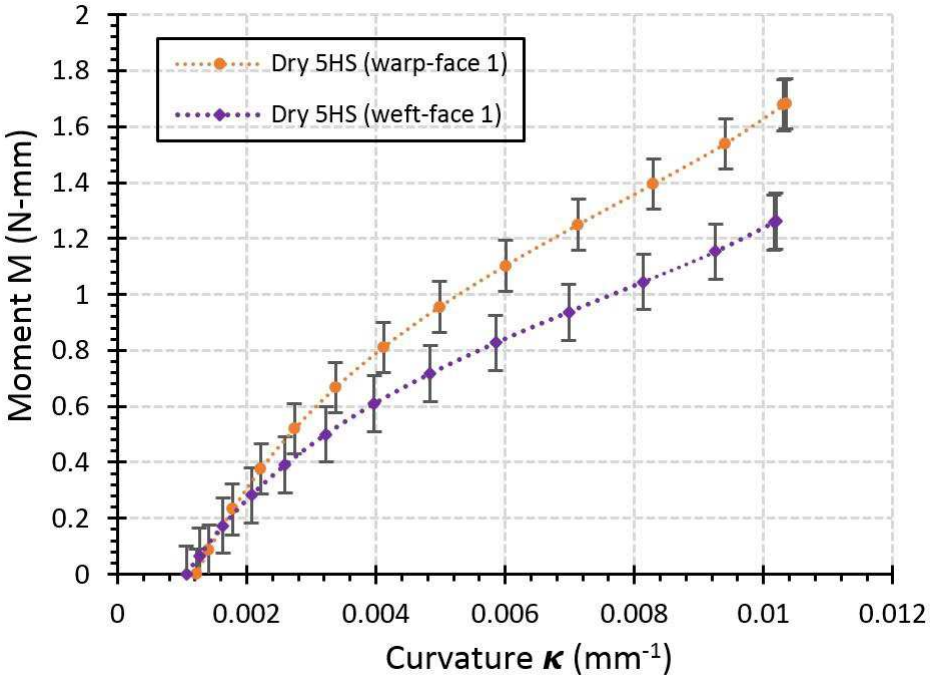

Figure 2.11: The difference between warp and weft directions in dry 5HS.

A room-temperature comparison between the prepreg sample and the dry sample can indicate the contribution of resin to the bending results. The results of this comparison, shown in Figure 2.12, reveal a significant difference between the obtained bending moments in prepreg and dry samples: the maximum bending moment in the prepreg sample was 4.816 N-mm, versus 1.681 N-mm in the dry sample. It was expected that the difference between the maximum bending moment of the prepreg sample and the dry one is related to the resin content, which is 36% of the prepreg sample's weight. However, the observed difference in maximum bending moment between the two materials is much larger than that: about a factor of 3. In a single prepreg yarn, it can be assumed that the load is mostly borne by uncured resin when the direction of the load is perpendicular to the longitudinal direction of fiber. However, it seems also that the uncured resin has a significant impact in the outcomes more than the fabric and its style. Accordingly, it is essential to assess temperature and rate dependencies as well as viscoelastic behavior during the bending experiments.

To confirm the repeatability of the results presented in this study, three tests were performed on three different prepreg samples, as illustrated in Figure 2.13. A slight difference can be seen among the three tests; the load used in the moment calculation for all tested samples was averaged across the three test trials. Note also that the applied load position must be centered to avoid twisting of the sample during the test, which can create problems for extracting the bending shape and obtaining acceptable results.

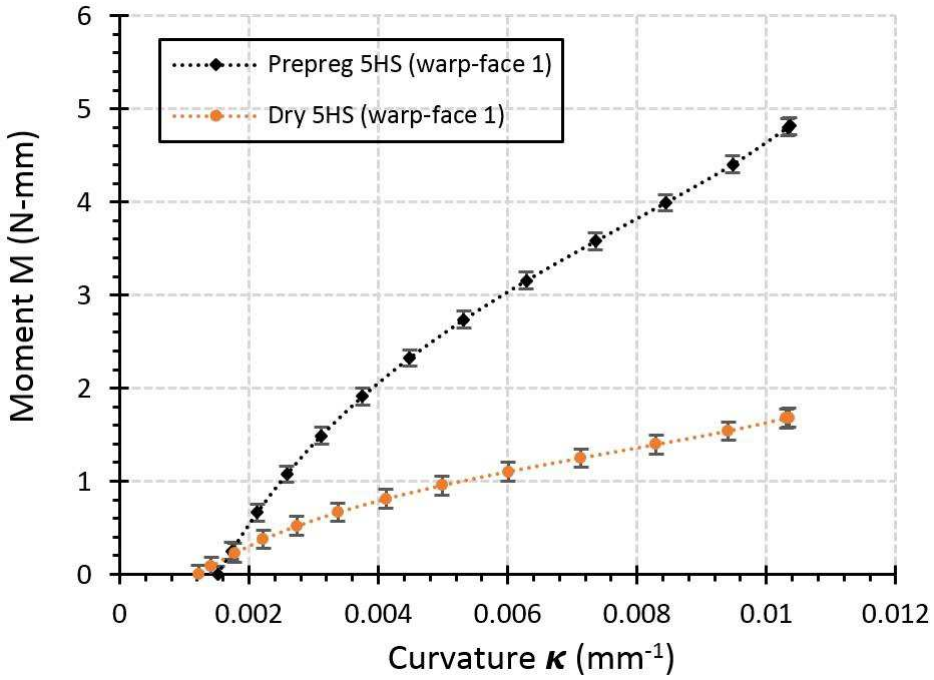

Figure 2.12: The difference between prepreg and dry samples in warp direction.

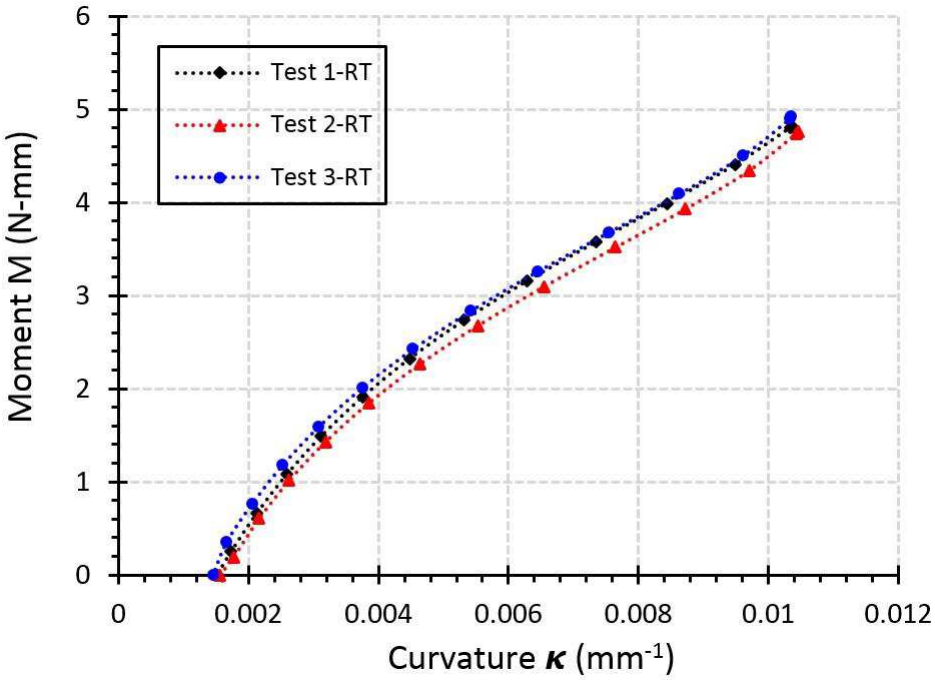

Figure 2.13: Repeatability of bending tests on 5HS prepreg sample in warp direction (face 1) at room temperature.

2.5.1 Temperature and rate dependencies

In the forming process, the sample is heated and then formed at certain rates. Because the uncured resin matrix has a significant impact on the outcomes, as previously discussed, the effect of processing temperature and rate on out-of-plane bending deformation may be an important consideration. Warp-direction and weft-direction samples revealed identical curve trends at different temperatures and rates; consequently, only warp-direction results are presented in the following sections.

To investigate the effect of temperature on bending behavior, tests were performed at a constant rate (3 mm/sec) and various temperatures: room temperature (RT), 50, 70, and 90 °C. The results, shown in Figure 2.14, reveal that bending moment decreased significantly with increasing temperature. For example, the maximum moment at room temperature was 4.816 N-mm, versus 1.298 N-mm at 90 °C, a reduction of 73%. This drop in maximum moment is strongly correlated with a reduction in resin viscosity: higher temperatures reduce the load required to achieve the same tip displacement. The variation of viscosity

with temperature was quantitatively investigated by performing rheological tests using a MCR 500 Rheometer (see Ref. [16]). Note that increased temperature may also increase the incidence of wrinkling during the forming process, because the accompanying reduction in bending stiffness decreases the resistance to compressive loading in the plane of the material.

Past simulations have found that the number of wrinkles increases with forming temperature, due to the reduction in bending stiffness [24]. Nevertheless, it remains challenging to validate these predictions via experimental forming work, where various deformation mechanisms and other processing factors also come into play. Future work can be considered through the development of a double compression test (see Ref. [51]) to measure the effect of processing temperature on out-of-plane defects (wrinkles).

It was observed that the bending profile of the material at 90 °C was relatively unsettled in all test trials: at higher temperatures, the vertical situation of the sample was already undergoing change before the load was applied. Therefore, it is recommended that the load should be applied as soon as the required temperature is reached, particularly for high–temperature (90 °C) trials. Uniform temperature distributions can still be obtainable during the test (disparity inferior to ±4 °C).

Prepreg samples tested at a constant temperature (room temperature) and various speeds (3, 6, and 9 mm/sec) are shown in Figure 2.15. Very similar behavior was observed over the range of rates. The experiments reveal that bending behavior is rate dependent and this rate dependence is likely due to the viscoelastic behavior of the prepreg. Figure 2.15 shows that a higher testing rate consequently results in the higher load required to bend the sample to the desired tip displacement (50 mm). Over a rate increase from 3 to 9 mm/sec, the maximum bending moment increased by approximately 16%. Moreover, Figure 2.16 shows the maximum bending moment for the warp-sample (face 1) at the three selected rates. The results show that the bending resistance has a relatively linear relationship with the applied testing rate. This finding is also reported by Wang et al. [44], who studied the bending behavior of unidirectional (UD) thermosetting carbon/epoxy prepreg under buckling test conditions. It is also worth noting that the rate dependence of thermoplastic prepreg may not be significant beneath melting temperature, as documented in [35].

Overall, the bending results at different temperatures and rates reported here suggest the need for a viscoelastic material model under bending for forming simulation outcomes.

Processing temperature and forming rate are known to be important parameters during the forming of prepreg materials. The effects of these parameters on in-plane shear deformation and wrinkle formation have been investigated by many researchers [15,16,52,53], and the results indicate that higher temperatures and slower rates are preferable to avoid wrinkling. At the same time, however, ply bending stiffness decreases under higher temperatures and slower rates. As discussed above, when out-of-plane deformation is the dominant deformation mechanism, both these parameters need to be optimized to increase the degree of formability of composite prepregs and thus produce a formed part without defects.

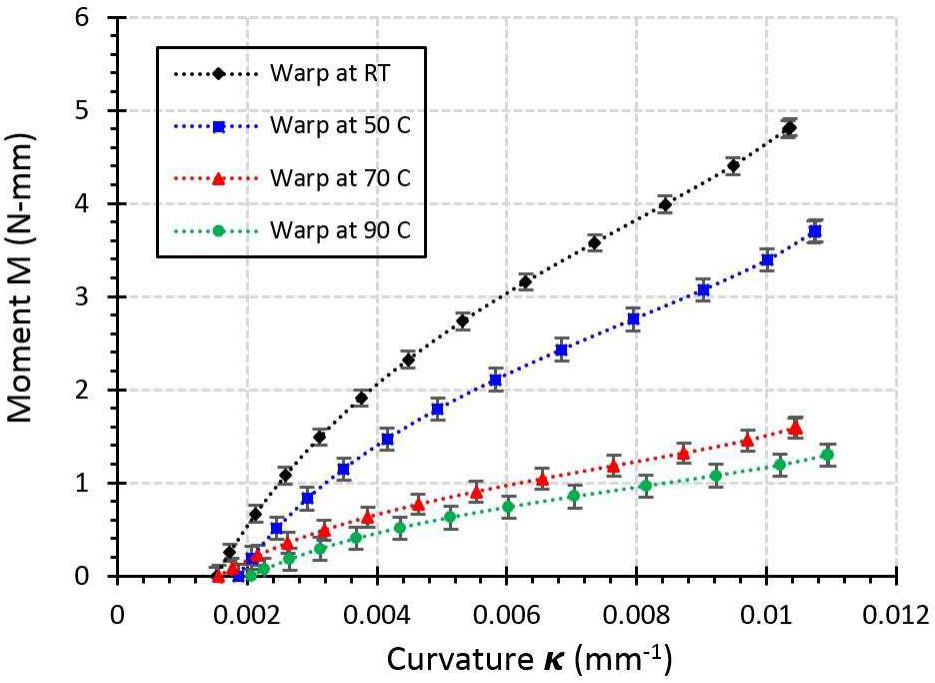

Figure 2.14: Bending moment versus curvature of 5HS prepreg sample in warp direction (face 1) at different temperatures.

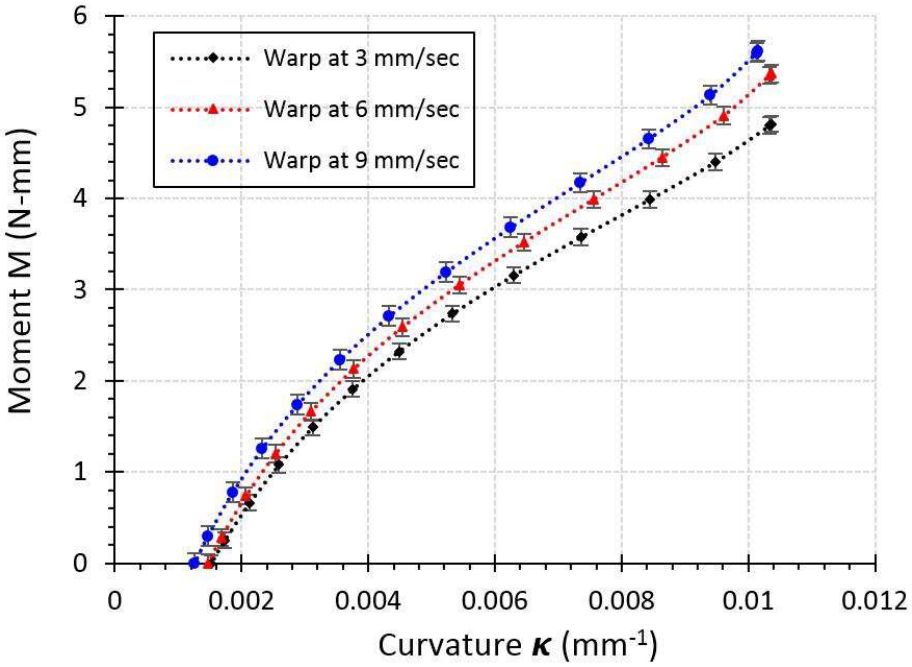

Figure 2.15: Bending moment versus curvature of 5HS prepreg sample in warp direction (face 1) at different speeds.

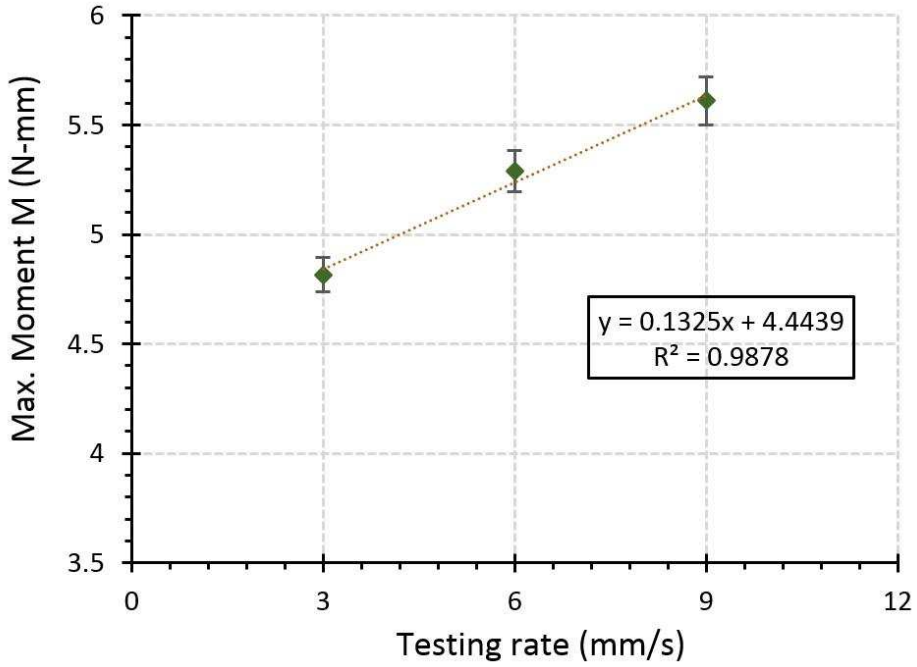

Figure 2.16: The maximum bending moment versus testing rate for warp-sample (face 1), including error bars for standard deviation of three repeats.

2.5.2 Investigation of viscoelastic behavior

The viscoelastic behavior of 5HS prepregs during bending was investigated by measuring the stress–relaxation response of the cantilever. In the proposed test, the sample can be loaded to a specific tip displacement and then held in that position, thus ensuring that the strain remains constant for the duration of the test. Load versus time curve at that displacement position can then be recorded via the load cell to capture the stress–relaxation response. Stress–relaxation tests were performed for a tip displacement of 50 mm and held in position for 5 minutes. Figure 2.17 shows the load as a function of time for three warp prepreg samples, tested at room temperature with a load rate of 3 mm/sec. The initial value of the load at time 0 sec was the load observed when the test stopped at the 50-mm tip displacement. Although the overall result was a gradual decrease (relaxation), the rate of relaxation varied across time, becoming slower over the course of the experiment: i.e., the load value decreased from 0.042 to 0.031 N in the first 50 seconds but had only decreased to 0.025 N after 200 sec. Note, furthermore, that a 0 N load was never attained; cross-linked polymers are expected to decrease to a constant value over time [54]. Although the tip displacement was held fixed across all three tests, slight differences were recorded in the maximum load to reach this displacement. Upon load removal, all samples showed a decrease in displacement, but none returned fully to their original position. Thus, stress relaxation yielded a non-reversible displacement and a slight curved shape for all samples. Investigation of this permanent displacement may help in the selection of an appropriate mathematical model to predict the behaviors of viscoelastic materials in future work. However, further investigation remains necessary to determine the significance of the influence of this displacement on the total strain. Multiple tip displacements and temperatures should also be tested to further understand the relaxation behavior of selected materials. It may well turn out that the dynamic or inertia effects induced by sudden strain can be avoided by the use of a ramped strain input and slow loading motion, which can be achieved through the proposed test.

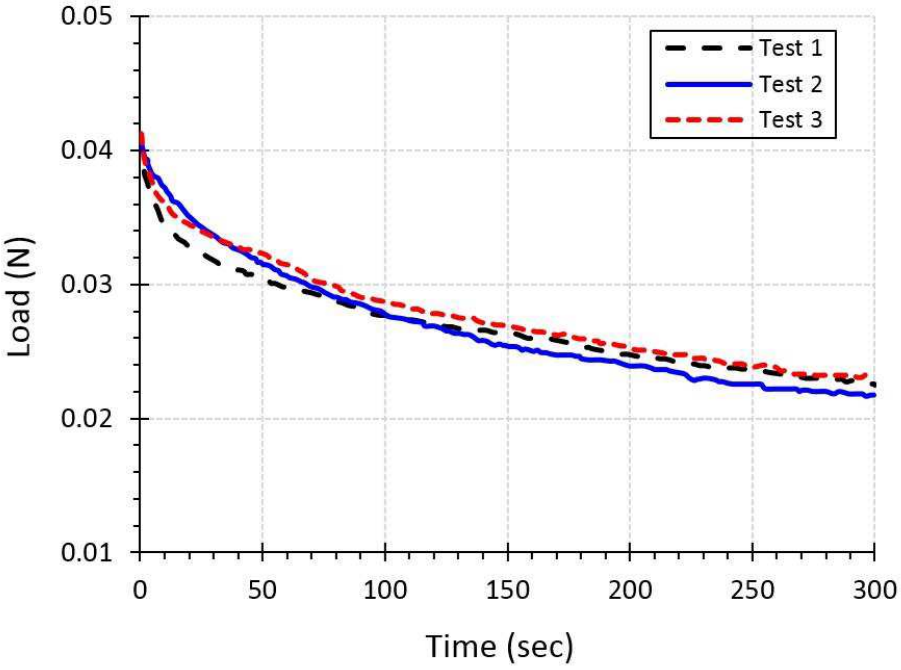

Figure 2.17: Three tests of load relaxation of 5HS prepreg sample (warp) recorded at room temperature with 50 mm tip displacement.

2.5.3 Consolidation effect

The bending properties would also be expected to depend in part on the state of consolidation of the prepreg, especially during the double-diaphragm forming; pre-heating within a vacuum necessarily causes some degree of consolidation. The experimental approach described above was carried out to measure the bending behavior of the consolidated sample under conditions relevant to double-diaphragm forming. One ply of OOA prepreg was consolidated at 70 °C with a pressure of 0.1 MPa using vacuum bagging for 30 minutes, as shown in Figure 2.18 (a). The vacuum bag-only (VBO) consolidation process of OOA prepreg includes air evacuation, fiber bed compaction, and resin flow. Once vacuum is applied, trapped air is evacuated through the dry tows, the void content decreases, and the fiber bed is compacted [49]. The dry tow areas, (see Figure 2.1), are infiltrated by the resin when the temperature is raised to produce a void-free micro-structure. The consolidated sample was then cut to the same dimensions as the unconsolidated samples with respect

to warp direction. The evacuation of entrapped air caused by the applied pressure reduced the measured average thickness of the consolidated sample to 0.49 mm.

The bending moments and the corresponding curvatures for consolidated and unconsolidated samples, tested at room temperature and 3 mm/sec, are given in Figure 2.18 (b). A notable increase in the bending stiffness of the consolidated sample was observed (almost 17%). In this context, the increase in the bending stiffness is attributed to the change in the degree of curing, as well as the increase in fiber volume fraction. Fiber volume fraction is calculated using the following equation:

$$V_f = \frac{M_f}{\rho_f \, h} \tag{2.4}$$

where M_f is the areal density of the fabric (kg/m^2), h is the ply thickness (m), and ρ_f is the density of the carbon fiber (kg/m^3). Based in our measurements, the fiber volume fraction prior to consolidation was about 43.53%, versus 48.44% in the consolidated sample. Note also that the OOA prepreg micro-structures underwent impregnation during consolidation; see Centea and Hubert [55] for further details. There is an uneven distribution of the resin through the cross-section, as shown in Figure 2.1, and the resin-rich interlayer (shear viscosity of resin inter-layers) plays an important role in terms of facilitating the through thickness shearing during bending, especially at elevated temperatures. However, the sample length-to-thickness ratio is large enough to minimize the occurrence of the through thickness shearing within the sample during the current bending experiments. Although the consolidation conditions depend on the processing parameters utilized during forming, the proposed experimental approach measures the bending stiffness as a function of the consolidation state, thus allowing the modeler to determine the correct parameter values to set during the simulation process.

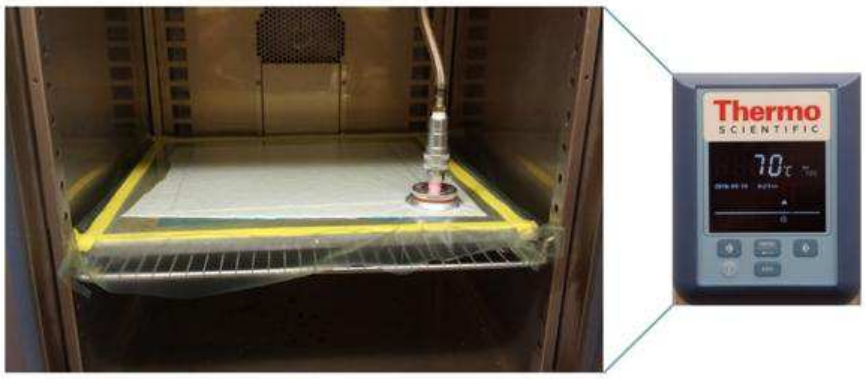

(a)

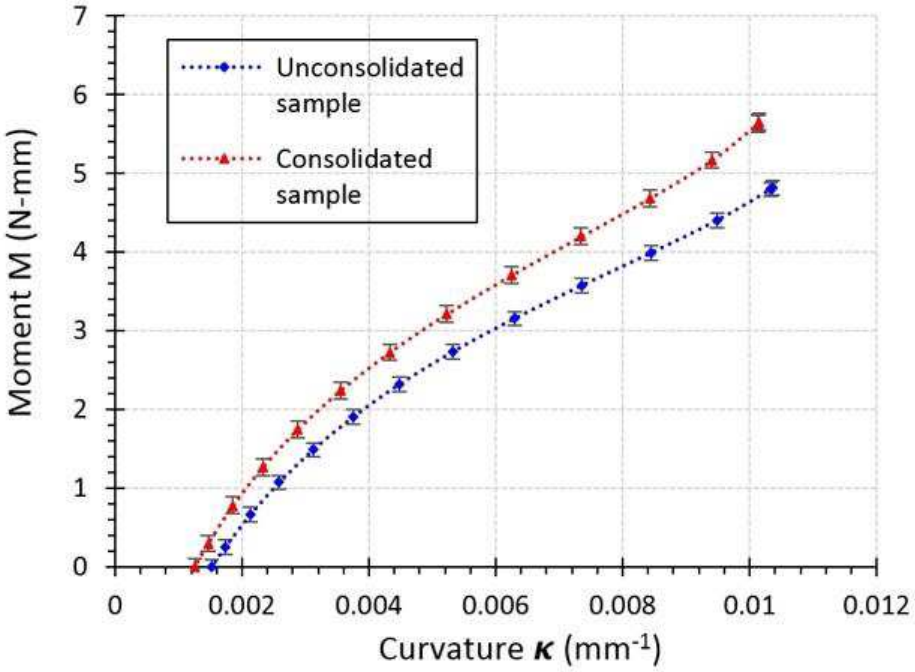

(b)

Figure 2.18: Consolidation of one-ply of OOA prepreg at 70 °C and (b) bending moment versus curvature for consolidated and unconsolidated samples (warp-face 1).

2.5.4 Bending stiffness calculation

Given the nonlinear nature of the relationship between bending moment and curvature, this paper proposed a new method for calculating the bending stiffness from the obtained load and the maximum slope (tangent of θ). Accordingly, the effort needed to extract the data points for obtaining the deflection equation and then calculate the curvature can be minimized. Observed bending stiffness (corresponding to the slope of the linear fit) can be used to validate the proposed method. The procedure for the proposed method is as follows:

From the elastica theory of a flexible uniform cantilever beam loaded with a concentrated load at the free end [50] (see Figure 2.8), a large deflection equation *x (y)* can be obtained:

$$x(y) = \int_0^y \frac{G(y)}{\left\{1 - [G(y)]^2\right\}^{1/2}} dy \tag{2.5}$$

where

$$G(y) = \frac{P}{2EI}\left[y^2 - (L - \Delta)^2\right] \tag{2.6}$$

Taking *EI* as the bending stiffness (Bs), and solving Eq. 2.5 with reference to *x'(y)* and Eq. 2.6 for (Bs) gives,

$$B_s = \frac{P\left[y^2 - (L - \Delta)^2\right]\sqrt{1 + x'(y)^2}}{2\ x'(y)} \tag{2.7}$$

where P is the load required to achieve a certain tip displacement, L is the sample length, Δ is the vertical displacement of the free end, and $x'(y)$ is the first-derivative (slope). The maximum slope can be obtained graphically as the tangent of θ (see Figure 2.8). The vertical displacement Δ can be determined graphically from the obtained image. However, the value of Δ is calibrated when the applied load position is shifted from the tip of the sample, as discussed in Section 2.4.4. In the case of a 50-mm tip displacement, the value of Δ is found to be 5-6 mm. The calculated bending stiffness at selected test conditions are listed in Table 2.2.

The bending stiffness value was confirmed by repetition of the method under various tip displacements (50 and 30 mm). Figures 2.19 (a) and (b) show the bending stiffness corresponding to the slope of the linear fit between bending moment and curvature for a 50-mm and 30-mm tip displacement, respectively. The percent error in bending stiffness values between a tip displacement of 50 mm and a tip displacement of 30 mm was found to be small– approximately 2.63%. These values can then be used to validate the bending stiffness calculated according to Eq. 2.7. A good agreement between the calculated bending stiffness and the slope of the linear fit was observed for all results, as listed in Table 2.3. However, minor errors among the values do arise due to the inaccuracy of the fit line, as shown in Figures 2.19 (a) and (b). Figure 2.19 (c) shows the curvature-moment curve and the bending stiffness value based on calculating the curvature as the second derivative. A significant difference in bending stiffness value using Eq. 2.3 (Figure 19 (a)) and the second derivative alone (Figure 2.19 (c)) was observed. Therefore, Eq. 2.3 should be used to calculate the curvature as long as the slope of the deflection curve cannot be neglected (i.e., higher displacement).

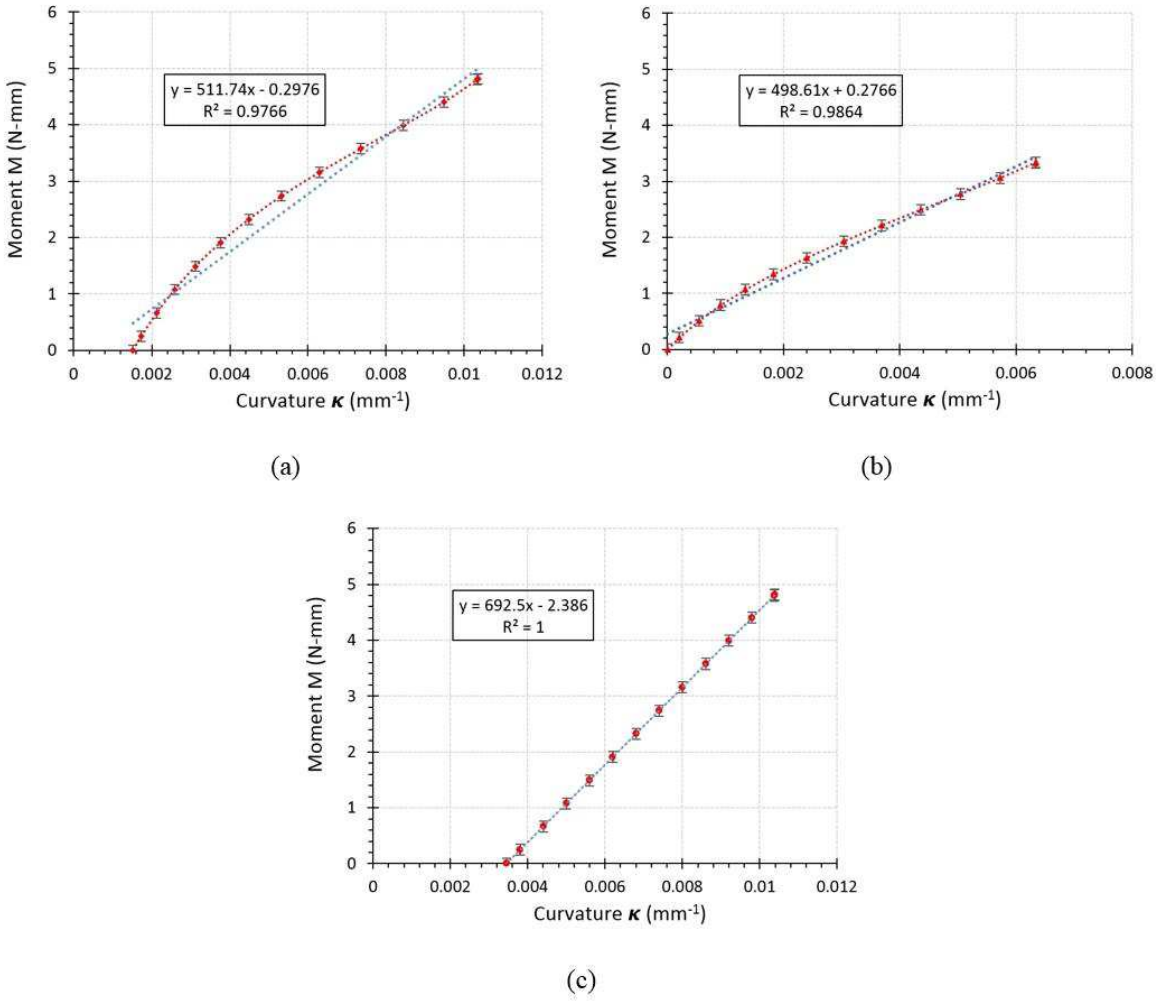

Figure 2.19: Bending moment versus curvature with linear fit for warp (face1) (a) up to 50 mm tip displacement, (b) up to 30 mm tip displacement, and (c) based on calculating the curvature as the second derivative (up to 50 mm).

Table 2.2: Results of calculated bending stiffness at selected test conditions.

Sample	**Tip displacement (mm)**	**Testing temperature (°C)**	**Testing rate (mm/s)**	**Bending stiffness Bs (N-mm^2)**	**Standard deviation of Bs**
5HS prepreg (warp-face 1)	50	RT	3	518.47	
5HS prepreg (warp-face 2)	50	RT	3	449.46	
5HS prepreg (weft-face 1)	50	RT	3	430.50	
5HS prepreg (weft-face 2)	50	RT	3	494.93	
5HS dry (warp-face 1)	50	RT	3	191.89	
5HS dry (weft-face 1)	50	RT	3	143.88	
5HS prepreg (warp-face 1)	50	50	3	399.30	
5HS prepreg (warp-face 1)	50	70	3	171.20	
5HS prepreg (warp-face 1)	50	90	3	139.75	
5HS prepreg (warp-face 1)	50	RT	6	577.74	
5HS prepreg (warp-face 1)	50	RT	9	604.07	
5HS prepreg (warp-face 1)	30	RT	3	510.46	
5HS consolidated prepreg (warp-face 1)	50	RT	3	599.83	178.116

Table 2.3: A comparison between the calculated bending stiffness and the slope of the linear fit.

Bending stiffness (N-mm^2)	
Calculated Eq. 2.7	**Slope of the linear fit**
518.47	511.74
449.46	439.92
430.50	421.36
494.93	466.88
191.89	171.73
143.88	128.77
399.30	387.7
171.20	166.23
139.75	135.65
577.74	560.95
604.07	586.52
510.46	498.61
599.83	590.51

2.6 Conclusion

Given the important role of out-of-plane bending in determining wrinkle formation during composite forming, demand for efficient and robust forming simulations for prepreg materials is increasing. To provide accurate simulation input, a suitable prepreg bending test that offer good control of the testing parameters (including both rate and temperature dependencies) is necessary. To meet this need, the present study reports on a new test method based on a vertical cantilever test associated with a linear actuator and load cell.

Investigations of out-of-plane bending behavior of satin woven carbon/epoxy prepregs were assessed across different sample configurations, processing temperatures, and rates. The results revealed that bending stiffness is approximately 20% higher in the warp direction than in the weft direction. This distinction should be considered during future forming simulation inputs. Bending stiffness was found to decrease significantly with increasing temperature. This decrease is strongly correlated with resin viscosity reduction: higher temperatures reduce the load required to achieve the same tip displacement. Moreover, the experiments showed that bending behavior is rate-dependent, due to the viscoelastic behavior of the prepreg. A good agreement between the calculated bending stiffness based on suggested method and the slope of the linear fit was observed for all results. Although the application of higher temperatures (over 120 °C) during the new test method was difficult due to reliance on a non-contact heater facility, the new method allowed for sufficient control of deflection shape, testing rates, and processing temperatures within the range of thermosetting resin. An investigation of viscoelastic behavior was also undertaken. Overall, the new test method demonstrated good reproducibility of results.

Future work is needed to address the viscoelastic behavior at different temperatures. Once this investigation is complete, a mathematical model describing the real viscoelastic response of the materials associated with the bending model may be developed.

Chapter 3

A theoretical model with experimental verification for bending stiffness of thermosetting prepreg during forming process*

Abstract

Capturing the out-of-plane properties using a suitable experimental method and combination of constitutive models and modeling techniques is required to improve forming simulation outcomes for composite prepregs, with the ultimate aim of predicting and optimizing forming processes. This paper proposes a theoretical model for bending behavior of woven fabric-based out-of-autoclave prepregs under conditions relevant to forming process. Time and temperature dependencies are considered by means of time–temperature superposition in a linear viscoelastic material model. A new approach for considering the testing rate and temperature with respect to a reference value is also established. Experimental tests are carried out for estimation of the model parameters and validation of the proposed model. A special bending test setup is utilized to allow for adequate control of testing rates and temperatures as well as viscoelastic investigations. A good agreement between the predicted bending stiffness and the experimental values was observed. The model and experimental results reveal that the processing temperature has the strongest influence on the bending property results.

*Reproduced from: Hassan Alshahrani, Mehdi Hojjati. A theoretical model with experimental verification for bending stiffness of thermosetting prepreg during forming process. Composite Structures, 166 (2017), pp. 136–145. http://dx.doi.org/10.1016/j.compstruct.2017.01.030

3.1 Introduction

Use of automated technologies such as Automated Tape Laying (ATL) or Automated Fiber Placement (AFP) to produce composite parts offers great promise to meet the growing need for composite materials in the aerospace and automotive industries due to low manufacturing times and concomitant lower costs [33]. However, in order to improve the productively of complex composite components used in aerospace applications, flat laminates are laid down by automated machines and then subjected to a forming process. Several deformation mechanisms come into play during the forming of composite prepregs to a desired shape, including intra-ply shear, inter-ply friction, and out-of-plane bending [6]. In order to accurately predict defects, such as wrinkling, that may arise during composite material forming processes, a considerable amount of knowledge of the deformation mechanisms of prepreg ply under forming conditions is necessary. The bending properties of the prepreg, including their temperature and rate dependencies, must be known and properly represented in the finite element model to achieve useful simulation results [11, 24, 34, 35]. However, the bending characterization and modeling of composite prepreg have received little attention in the literature compared to intra-ply shear and inter-ply friction. Some test methods have developed to measure the out-of-plane bending properties of prepreg composites [24, 40, 47, 56]. For a comprehensive review of proposed bending tests towards prepreg composites, the reader is referred to [47, 56].

The bending behavior of dry textiles has been subjected to theoretical modeling under a number of different approaches, including energy methods [57] and linear elastic beam theory [58]; a recent review on this topic was presented by Syerko et al. [59]. However, these models are unsuitable for describing the bending behavior of composite prepregs, due to their resin existence. At present, a notable lack of research exists on bending models for prepreg composites. One relevant study was conducted by Martin et al. [43], who developed a viscous fluid beam bending model that relied on a plane strain assumption. This model was based on the 'Ideal fiber-reinforced model' (IFRM) developed by Spencer [60]. Wang et al. [44] proposed a model for predicting buckling test results that combines both the

'elastic' buckling model and the 'plastic' buckling model. The modeling of 'elastic' buckling was based on classical elastic laminate beam theory, while the modeling of plastic buckling was based on the uniaxial continuum theory for ideal fiber-reinforced fluids. Recently, Sachs [30] developed a viscoelastic bending model that differentiates between elastic fiber and the highly viscous thermoplastic matrix. In this approach, the fiber is subjected to bending under the Euler-Bernoulli beam theory; the matrix is assumed to be Newtonian and is subjected to shear. However, the model fit parameters (such as viscosity and Young's modulus) were much higher than the actual material properties. Currently, there are at present no accurate theoretical models available to predict bending stiffness of prepregs at processing parameters. Thus, this paper is developed a theoretical model for bending behavior of thermosetting prepreg under conditions relevant to forming process.

3.2 Motivation

This work is motivated by the increased demand for more efficient and robust forming simulations, as bending stiffness plays an important role in determining wrinkle formation [24,35]. Wrinkling is caused by out-of-plane deformation due to compressive loading in the plane of the material during the forming process. Consequently, capturing the out-of-plane properties using a suitable experimental method and combination of constitutive models and modeling techniques is required, with the ultimate aim of predicting and optimizing forming processes.

Whereas continuous materials (such as sheet metals and composite plates with hardened matrix) show a relatively high bending stiffness, prepreg sheets are inherently much more flexible. This can cause problems for the calculation of bending stiffness for prepreg materials; reliance on the tensile modulus to assess bending stiffness tends to produce an unrealistically elevated stiffness assessment that is not representative of the true property [11,61]. Thus, it is necessary to develop an equivalent bending stiffness model that accurately captures the bending stiffness of prepreg materials as a function of its temperature-time dependencies in order to precisely compute out-of-plane wrinkle formation in the finite

element forming simulations.

3.3 Theoretical formulation

Cantilever beam theory presents a possible solution with some adoptions to predict the bending stiffness of prepreg materials. The prepreg yarn is composed of two external viscoelastic polymer plies with a linear elastic ply of thickness *h/2* in between, as shown in Figure 3.1, and assumed to deform as an Euler-Bernoulli beam. In order to assist in measuring bending stiffness, the cantilever is clamped at one end; a load P is then placed on its free end and perpendicular to the bar axis. Small deformation theory is used to analyze the cantilever, based on the following assumptions: the influence of shear is neglected, and a uniaxial state of stress is considered. Assuming that the neutral axis does not coincide with the geometric axis as shown in Figure 3.1, the total strain, based on the Euler-Bernoulli assumption, can be defined as

$$\epsilon_x = \frac{-(y + y_0)}{R} \tag{3.1}$$

where y_0 is the position of the neutral axis *(n.a.)* relative to the geometric axis where the total strain is zero, R is the radius of curvature. A beam with rectangular cross-section *(height = h, width = b)* is considered. Equations for the axial force acting on the cross section and the bending moment are as follows:

$$F_x = \left[\int_{-\frac{h}{2}}^{-\frac{h}{4}} \sigma(t)\, b dy + \int_{-\frac{h}{4}}^{-y_0} \sigma_t b dy + \int_{-y_0}^{\frac{h}{4}} \sigma_c b dy + \int_{\frac{h}{4}}^{\frac{h}{2}} \sigma(t)\, b dy \right] = 0 \tag{3.2}$$

$$M = -\left[\int_{-\frac{h}{2}}^{-\frac{h}{4}} \sigma(t)\, by dy + \int_{-\frac{h}{4}}^{-y_0} \sigma_t y b dy + \int_{-y_0}^{\frac{h}{4}} \sigma_c y b dy + \int_{\frac{h}{4}}^{\frac{h}{2}} \sigma(t)\, y b dy \right] \tag{3.3}$$

Here $\sigma(t)$ is the time-dependent stresses in viscoelastic plies, σ_c and σ_t are the compressive stresses and tensile stresses in elastic ply through the thickness, respectively, and $M = P(l - x)$ is the resulting bending moment at coordinate x due to the applied load P. Because no axial load was assumed, the integral of all stresses through the cantilever cross section must be equal to zero. Heretofore, the cantilever beam theory is established without taking into account the constitutive equations that describe the stress-strain relation. Therefore, we only need to solve the constitutive model to estimate the stress and calculate the bending stiffness.

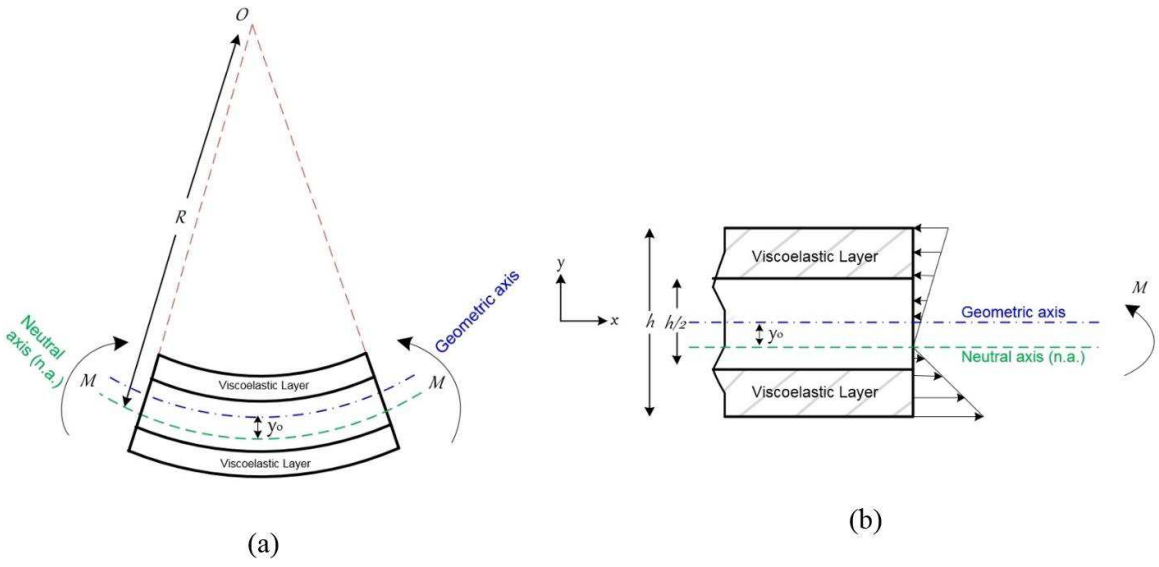

Figure 3.1: (a) Prepreg yarn deformation under pure bending and (b) stress distribution in the beam cross section.

3.3.1 Constitutive models

A compressive modulus (E_c) and a tensile modulus (E_t) are introduced to calculate results for the negative and positive strains within the elastic ply, respectively [27]. Based on Hooke's law, compressive stresses and tensile stresses become as follows:

$$\sigma_c = E_c \, \epsilon \tag{3.4}$$

$$\sigma_t = E_t\ \epsilon \tag{3.5}$$

The most general model for linear viscoelasticity is the generalized Maxwell or Wiechert model [54], schematically represented in Figure 3.2, which consists in parallel a series of Maxwell spring–dashpot units and a Hookean spring. The stress can be expressed in the integral form as

$$\{\sigma(t)\} = \int_0^t Y\left[t-\tau\right] \frac{\partial\left\{\epsilon(\tau)\right\}}{\partial\tau} d\tau \tag{3.6}$$

where *Y(t)* is the relaxation modulus. When the strain is constant in time *(ϵ = constant)*, the resulting stress equation (Eq. 3.6) reduces to [62]

$$\sigma\left(t\right) = Y\left(t\right)\ \epsilon \tag{3.7}$$

Note that, the latter equation is the uniaxial stress-strain relation for a polymer analogous to Hooke's law, however, it is valid only for the case of a constant input of strain. The constant input of strain (strain not vary with time) can be attained through the relaxation test that employed in this study. Based on the superposition principle, the total stress in the element is the sum of the elemental stresses and can be described by Prony series, which provides a convenient representation of the stress relaxation as follows [54]:

$$\sigma\left(t\right) = \epsilon_0 \left(E_\infty + \sum_{i=1}^{N} E_i e^{-\frac{t}{\tau_i}}\right), \qquad with \quad \tau_i = \frac{\eta_i}{E_i} \tag{3.8}$$

where E_∞ is the equilibrium modulus, t is the time, E_i and τ_i are the elastic components and relaxation time in the Maxwell component. The relaxation modulus of a generalized Maxwell model is given by

$$Y(t) = E_\infty + \sum_{i=1}^{N} E_i e^{-\frac{t}{\tau_i}} \tag{3.9}$$

Substituting Eq. 3.1 into Eqs. 3.4, 3.5, and 3.7, the bending moment (Eq. 3.3) at time t becomes

$$M(t) = -\left[\int_{-\frac{h}{2}}^{-\frac{h}{4}} Y(t)\left(\frac{-y-y_0}{R}\right) b y dy + \int_{-\frac{h}{4}}^{-y_0} E_t\left(\frac{-y-y_0}{R}\right) y b dy + \int_{-y_0}^{\frac{h}{4}} E_c\left(\frac{-y-y_0}{R}\right) y b dy + \int_{\frac{h}{4}}^{\frac{h}{2}} Y(t)\left(\frac{-y-y_0}{R}\right) y b dy\right] \tag{3.10}$$

Solving Eq. (3.10) leads to

$$M(t) = \frac{E_t}{R}\left(\frac{bh^3}{12}\right)\left\{\frac{7}{8}\left(\frac{Y(t)}{E_t}\right) + \frac{1}{16}\left[\left(\frac{4y_0}{h}-1\right)^2\left(\frac{2y_0}{h}+1\right)\right] - \frac{E_c}{16E_t}\left[\left(\frac{4y_0}{h}+1\right)^2\left(\frac{2y_0}{h}-1\right)\right]\right\} \tag{3.11}$$

The curvature (κ) is *1/R*; the equivalent bending stiffness (B_s) can be written as

$$B_s(t) = E_t\left(\frac{bh^3}{12}\right)\left\{\frac{7}{8}\left(\frac{Y(t)}{E_t}\right) + \frac{1}{16}\left[\left(\frac{4y_0}{h}-1\right)^2\left(\frac{2y_0}{h}+1\right)\right] - \frac{E_c}{16E_t}\left[\left(\frac{4y_0}{h}+1\right)^2\left(\frac{2y_0}{h}-1\right)\right]\right\} \tag{3.12}$$

The distance of the neutral axis *(n.a.)* from the geometric axis y_0 can be obtained from the axial force equilibrium equation as

$$F_x = \left[\int_{-\frac{h}{2}}^{-\frac{h}{4}} Y(t)\left(\frac{-y-y_0}{R}\right) b dy + \int_{-\frac{h}{4}}^{-y_0} E_t\left(\frac{-y-y_0}{R}\right) b dy + \int_{-y_0}^{\frac{h}{4}} E_c\left(\frac{-y-y_0}{R}\right) b dy + \int_{\frac{h}{4}}^{\frac{h}{2}} Y(t)\left(\frac{-y-y_0}{R}\right) b dy\right] = 0 \tag{3.13}$$

Eq. (3.13) results in

$$F_x = 16\ {y_0}^2 - 8\ h\left(\frac{E_t + E_c + Y(t)}{E_t - E_c}\right) y_0 + h^2 = 0 \tag{3.14}$$

Using the general quadratic equation, the y_0 can be expressed with a, b, and c constants as

$$y_0 = \frac{-b \pm \sqrt{b^2 - 4ac}}{2a} \tag{3.15}$$

where

$$\begin{aligned} a &= 16 \\ b &= -8\ h \left(\frac{E_t + E_c + Y\left(t\right)}{E_t - E_c} \right) \\ c &= \ h^2 \end{aligned} \tag{3.16}$$

Substituting Eq. 3.16 into Eq. 3.15, the y_0 can be written as

$$y_0 = \frac{8h \left(\frac{E_t + E_c + 2Y(t)}{E_t - E_c} \right) \pm \sqrt{64h^2 \left[\left(\frac{E_t + E_c + 2Y(t)}{E_t - E_c} \right) + 1 \right] \left[\left(\frac{E_t + E_c + 2Y(t)}{E_t - E_c} \right) - 1 \right]}}{32} \tag{3.17}$$

Notice that the preceding equation has two solutions, but the equilibrium equation Eq. (3.14) is satisfied more accurately with negative sign solution. Thus, the negative sign in y_0 equation (Eq. 3.17) is used in this study rather than the positive sign solution.

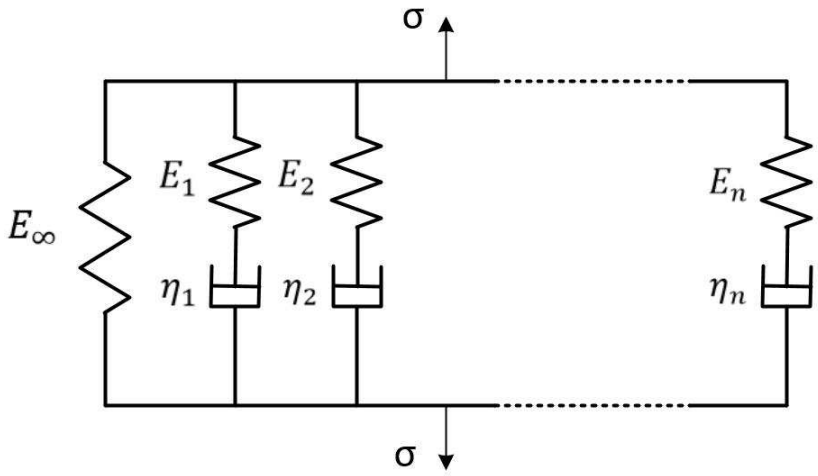

Figure 3.2: Representation of the generalized Maxwell model.

3.3.2 Model parameters determination

Eqs. (3.11) and (3.12) for bending moment and stiffness include material parameters of the prepreg and the relaxation modulus (E_t, E_c, and $Y(t)$). Since the tensile rigidities are large compared to the compressive rigidities, the tensile modulus (E_t) of prepreg is quoted from the data sheet provided by the supplier [63] as the young modulus of the fabrics in both directions. While, the compressive modulus (E_c) and relaxation modulus ($Y(t)$) are determined in the following subsection (3.3.2.1) and (3.3.2.2), respectively.

3.3.2.1 Compressive modulus E_c

The compressive modulus is determined by performing a compression test (buckling test) using a HOSKIN machine of 5 kN capacity, see Figure 3.3 (a). According to [44, 64], and the experimental observations of buckling test results, a buckling curve can be divided into three regions: elastic, plastic buckling and a transition region, as illustrated in Figure 3.3 (b). From the elastic buckling where the prepreg samples behave like a spring (straight line in buckling curve), the compressive modulus can be obtained by the slope of stress-strain curve for this region. The compressive modulus can be predicted following the formulations described by Wang et al. [44], who predict the compression force required for elastic buckling of UD prepreg using the strain energy. However, this is beyond the scope for the presented modeling approach.

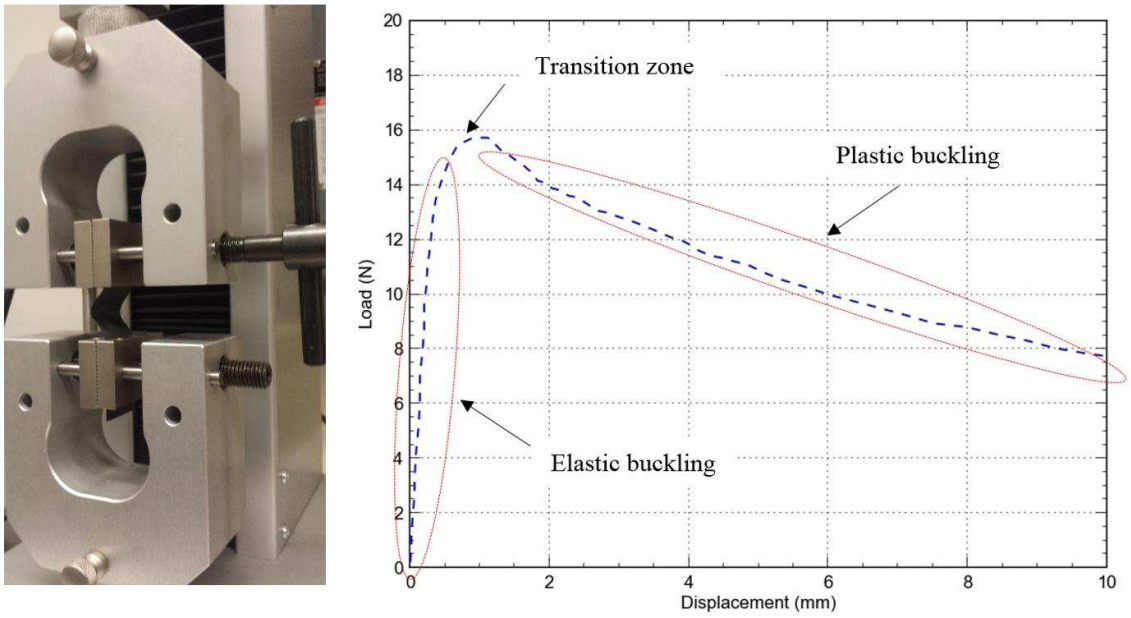

(a) (b)

Figure 3.3: (a) Buckling test on prepreg sample and (b) obtained buckling test result.

3.3.2.2 Relaxation modulus $Y(t)$

The proposed bending test for prepreg materials at forming conditions, detailed in Section 3.4, can be used to measure the stress–relaxation response of the cantilever. The sample can be loaded to a specific tip displacement and then held in that position as shown in Figure 3.4 (a), thus ensuring that the strain remains constant for the duration of the test. Load versus time curve at that displacement position can then be recorded via the load cell to represent the stress–relaxation response. This load is multiplied by the sample's length to plot the bending moment against time; the relaxation curve is exhibited in Figure 3.4 (b). The initial value of the load at time 0 sec was the load observed when the test stopped at the desired tip displacement. The aforementioned Generalized Maxwell (Wiechert) model with three spring–dashpot elements was chosen for approximation of the experimental data; (Eq. 3.8) can be rewritten as

$$\sigma(t) = \epsilon_0 \left[E_\infty + E_1 e^{-\frac{t}{\tau_1}} + E_2 e^{-\frac{t}{\tau_2}} + E_3 e^{-\frac{t}{\tau_3}} \right] \tag{3.18}$$

Eq. (3.18) can be rearranged as

$$\sigma\left(t\right)=\frac{\sigma_0}{E_b}\left[E_\infty+E_1e^{-\frac{t}{\tau_1}}+\ E_2e^{-\frac{t}{\tau_2}}+\ E_3e^{-\frac{t}{\tau_3}}\right] \tag{3.19}$$

where σ_0 is the maximum bending stress, and E_b is the bending modulus ($\mathrm{N/mm^2}$). The bending modulus can be obtained by solving the large deflection equation for a flexible uniform cantilever beam loaded with a concentrated load at the free end. From the elastica theory [50], a large deflection equation *x (y)* can be obtained as follows:

$$x(y)=\int_0^y\frac{G(y)}{\left\{1-\left[G(y)\right]^2\right\}^{1/2}}dy \tag{3.20}$$

where

$$G(y)=\frac{P}{2EI}\left[y^2-\left(L-\Delta\right)^2\right] \tag{3.21}$$

Taking E as the bending modulus (E_b), and solving Eq. (3.20) with reference to *x'(y)* and Eq. (3.21) for (E_b), we obtain

$$E_b=\frac{6\ P\ \left[y^2-\left(L-\Delta\right)^2\right]\sqrt{1+x'(y)^2}}{x'\left(y\right)\ b\ h^3} \tag{3.22}$$

where P is the load required to achieve a certain tip displacement, y is defined as the distance to the applied load from the fixed end, L is the sample length, Δ is the vertical displacement of the free end, *x'(y)* is the first-derivative (slope), b is the width of the sample, and h is the thickness of the sample.

The maximum bending stress can be calculated using the following equation [65]:

$$\sigma_0=\frac{M_{max}\ y}{I}=\ \frac{\left(M_{max}\right)h/2}{b\ h^3/12}=\ \frac{6M_{max}}{b\ h^2} \tag{3.23}$$

Since the maximum stress is at the cantilever beam clamp and the minimum stress at the free-end, the average stress for the entire beam is then half the maximum stress [65]. Consequently, Eq. (3.19) becomes as follows:

$$M(t) = \frac{M_{max}}{E_b}\left[E_\infty + E_1 e^{-\frac{t}{\tau_1}} + E_2 e^{-\frac{t}{\tau_2}} + E_3 e^{-\frac{t}{\tau_3}}\right] \tag{3.24}$$

Using the data analysis software (Curve-Expert) with the customized model based on Eq. (3.24), fits to the experimental relaxation data can be obtained. Thereafter, the parameters obtained from the curve-fitting approach are used in the subsequent equation (Eq. 3.25) to calculate the relaxation modulus.

$$Y(t) = \left[E_\infty + E_1 e^{-\frac{t}{\tau_1}} + E_2 e^{-\frac{t}{\tau_2}} + E_3 e^{-\frac{t}{\tau_3}}\right] \tag{3.25}$$

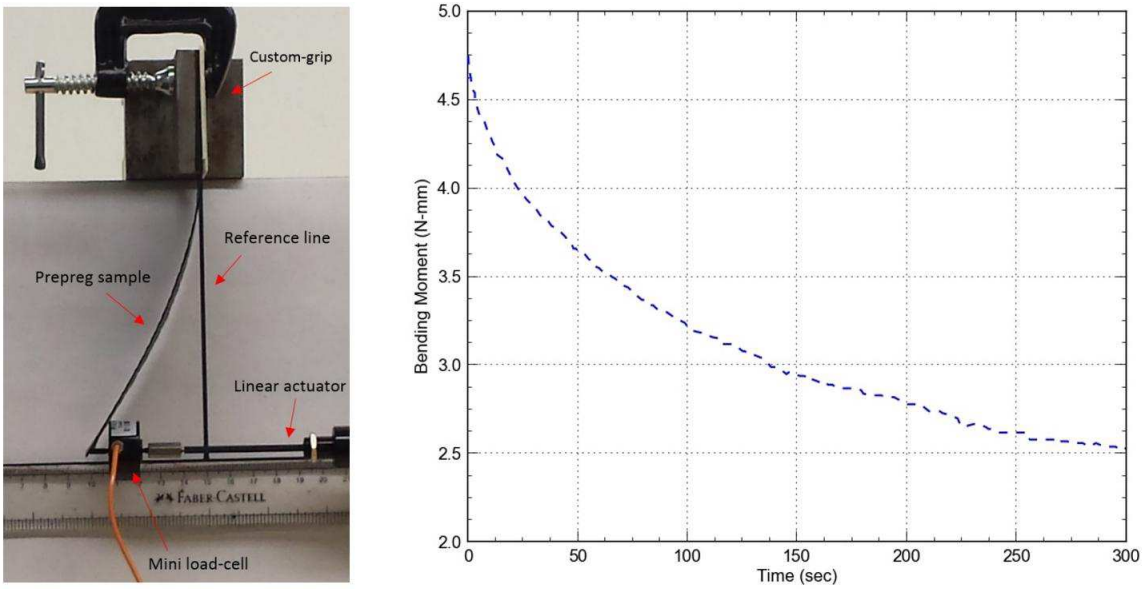

(a) (b)

Figure 3.4: (a) Proposed bending test for measuring the stress-relaxation response and (b) relaxation curve recorded at room temperature.

3.3.3 Time–Temperature dependencies

In the forming process, the sample is heated and then formed at certain rates. The effect of processing temperature and rate on bending stiffness calculation must therefore be taken into consideration. The rate in this case is correlated to the testing time and ultimately to the forming time. The testing time (t_s) can be defined as

$$t_s = \frac{d}{s} \tag{3.26}$$

where d is the maximum tip displacement, and s is the testing speed applied to reach this displacement. The testing time based on Eq. (3.26) is used in Eq. (3.25) to calculate the bending stiffness at a certain rate. Following this, Eq. (3.25) can be rewritten as

$$Y\left(t_s\right) = \left[E_\infty + E_1 e^{-\frac{t_s}{\tau_1}} + \ E_2 e^{-\frac{t_s}{\tau_2}} + \ E_3 e^{-\frac{t_s}{\tau_3}}\right] \tag{3.27}$$

It should be noted that the testing time varies with the speed applied during the bending test. This also can be related to the forming time during the forming process operation. At present, the moment and bending stiffness equations (Eqs. (3.11) and (3.12)) do not consider the influence of temperature on bending behavior. To meet this need, the shift factor (α_T) and its dependency on the bending stiffness are introduced using time-temperature superposition. The reduced time τ and the actual time t are related by the following equation [54]:

$$\tau = \int_0^t \frac{dt}{\alpha_T(T\left(t\right))} \tag{3.28}$$

If the temperature (T) is constant, α_T is also constant and therefore, the reduced time can be defined as

$$\tau = \frac{t}{\alpha_T} \tag{3.29}$$

Accordingly, the relaxation modulus (Eq. 3.9) becomes

$$Y(t) = E_\infty + \sum_{i=1}^{N} E_i e^{-\frac{t}{\alpha_T \tau_i}} \tag{3.30}$$

The shift factor (α_T) can be obtained by Williams, Landel, and Ferry [66], which is accepted for temperatures above the glass transition temperature T_g or by Arrhenius form [67] for temperatures below the T_g. However, the bending properties at forming temperature are significantly decreased due to a reduction in viscosity of uncured prepreg plies. Therefore, the shift factors for each temperature respect to a chosen reference temperature can be determined by [68]

$$\alpha_T = \frac{\eta(T)}{\eta(T_{ref})} \tag{3.31}$$

where $\eta(T)$ and $\eta(T_{ref})$ are the steady-state viscosity at temperature T and reference temperature T_{ref}, respectively. The variation of viscosity with temperature in prepreg sample was investigated by performing rheological tests using a MCR 500 Rheometer (see Ref. [16]). Note that this shift factor will be applied in the relaxation modulus equation (Eq. 3.30), during calculation of bending moment and bending stiffness at processing temperature using Eqs. (3.11) and (3.12). A MATLAB program was written for these equations in order to facilitate the calculation of bending stiffness at given forming temperatures and rates.

3.4 Experimental verification

In this section, an experimental study for bending behavior of prepreg at forming conditions is carried out in order to verify the results obtained from the theoretical model. The experimental approach and the materials used are briefly presented below, see [56] for further details.

3.4.1 Materials and test setup

The out-of-autoclave (OOA) prepreg chosen for this study consist of a 5-harness (5HS) satin weave (6 K carbon fiber tows) impregnated with an epoxy resin (Cycom 5320). The fabric's areal weight is 380 g/m^2 and the resin content is 36% by weight. The measured thickness of uncured one-ply is approximately 0.55 mm.

In the proposed test, the sample is clamped vertically (vertical cantilever), while deflection shape and applied load are controlled by a linear actuator and a miniature-load cell, respectively, see Figure 3.5. Direct commands and change settings (such as required travel displacements, speeds, or current position) can be sent via the controller connected to the actuator, while the force required to achieve tip displacement is subsequently recorded by the load cell software. The temperature throughout the sample is monitored by an infrared camera (FLIR) to ensure uniform heating during the elevated temperature tests (using a non-contact radiant heater). The rate-dependent effect can be measured by adjusting the testing speed using the actuator's controller.

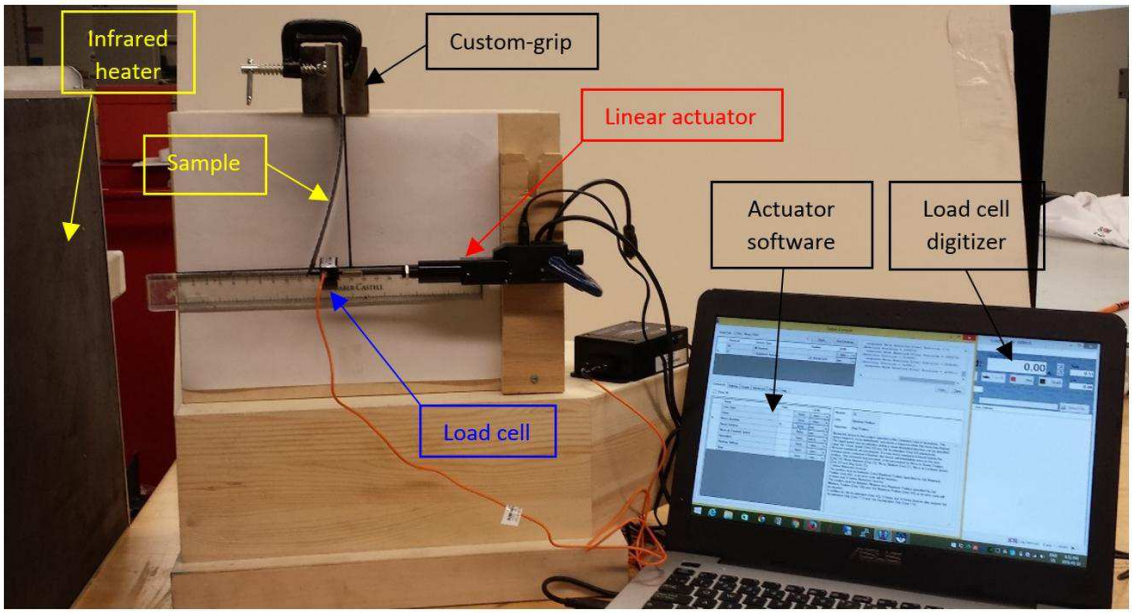

Figure 3.5: Proposed bending test setup for prepreg characterization purposes at processing conditions.

3.4.2 Samples and test procedure

The samples selected for the bending experiments were 150 mm long by 50 mm wide, with an un-gripped length of 120 mm. The samples were cut so that their warp and weft directions were perpendicular to the applied load as shown in Figure 3.6. The satin fabric is an asymmetrical style about its middle plane; however, face 1 in Figure 3.6 was selected to be in tension during bending experiment within this study to avoid complexity. The analysis of the bending behavior during composite forming process requires high curvature (higher displacement) to accurately simulate the process. Therefore, tip displacement of 30 mm was used. Images of the bent shape are captured by a digital camera and processed in ImageJ software to extract the data points. Data points on the deflection profile are subsequently fitted using a proper polynomial function. The curvature of the profile is then calculated from the obtained polynomial fit according to Euler-Bernoulli's law for large deformation produced by bending. The value of the recorded load can be used to calculate the moment at each selected point. Finally, the moments at each point can be plotted against the corresponding curvature values. The slope of moment-curvature curve gives

a convenient assessment of bending stiffness. Tests were conducted on samples at room temperature (RT), and 70 °C, i.e. below cure reaction temperature. Two test speeds were applied at room temperature: 3 mm/s, and 9 mm/s. At least three trials were conducted under each condition to ensure that the results are repeatable.

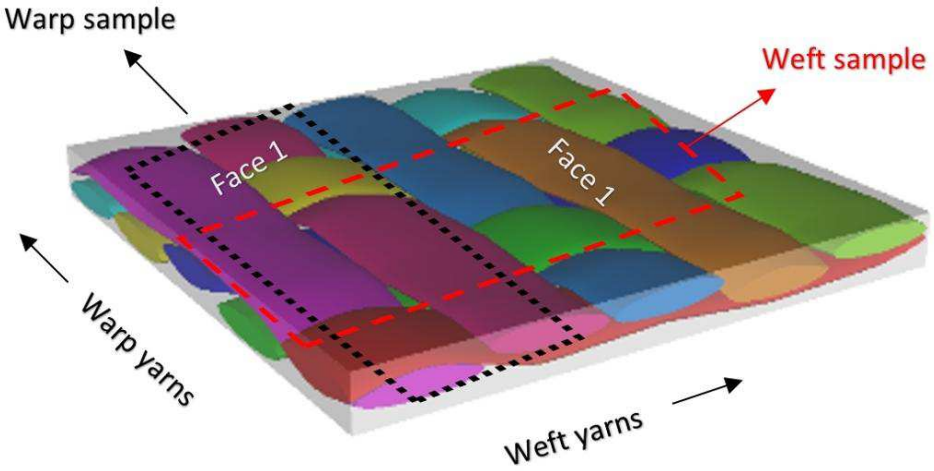

Figure 3.6: 5HS prepreg samples and yarn direction to the applied load.

3.5 Results and discussion

3.5.1 Model parameters

As previously mentioned, the compressive modulus is determined by the slope of the stress-strain curve of elastic buckling. The stress versus strain values for 5HS (warp) and 5HS (weft) samples at room temperature were plotted and fitted by a linear trend, as shown in Figure 3.7 (a) and (b), respectively. The slope of this linear trend represents the compressive modulus value. The compressive modulus in warp sample (see Figure 3.7 (a)) is relatively higher than the one in the weft direction.

A generalized Maxwell model based on Eq. (3.24) was used to fit the experimental relaxation data as shown in Figure 3.8 (a) and (b) for warp and weft, respectively. In the experimental curves, the initial value of the load at time 0 sec was the load observed when the test stopped at the 30-mm tip displacement. Although the overall result was a gradual decrease (relaxation), the rate of relaxation varied across time, becoming slower over the

course of the experiment. Note, furthermore, that a zero load value was never attained; cross-linked polymers are expected to decrease to a constant value over time. Two different trials were made for each sample, and the average among these values was presented. Parameters for the relaxation modulus Eq. (3.27) are listed in Table 3.1. All remaining parameters including viscosity values at reference (23 °C) and processing (70 °C) temperatures are tabulated in Table 3.2.

Table 3.1: Generalized Maxwell model parameters extracted from averaged relaxation curves.

Sample	E_∞ (MPa)	E_1 (MPa)	E_2 (MPa)	E_3 (MPa)	τ_1 (s)	τ_2 (s)	τ_3 (s)	R^2
Warp	180.27	27.07	66.43	427.79	1.26	12.13	126.57	0.999
Weft	180.44	187.18	186.64	44.88	84.61	84.60	4.11	0.998

Table 3.2: Required model parameters of selected material.

	Warp	**Weft**
E_t (GPa) [63]	69.08	68.25
$\eta((T_{ref}) = 23)$ (Pa.s) [16]	2.3e+5 (extrapolated)	
$\eta(T = 70)$ (Pa.s) [16]	9e+4	

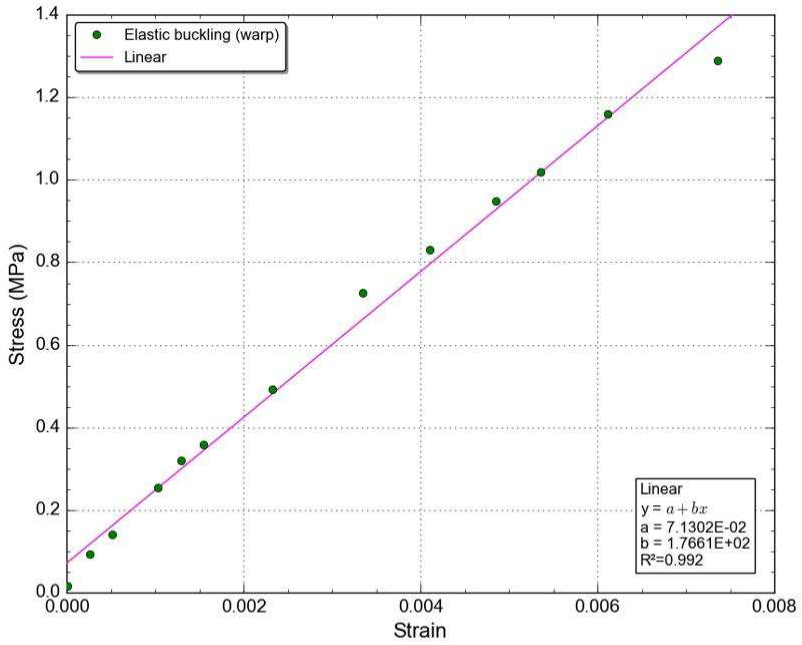

(a)

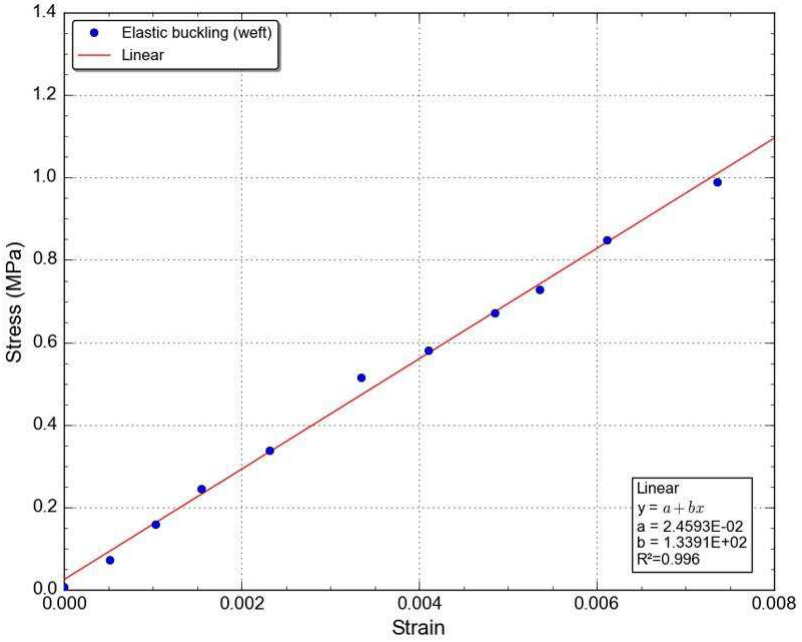

(b)

Figure 3.7: Stress-strain curve of elastic buckling with linear fit (a) warp sample and (b) weft sample.

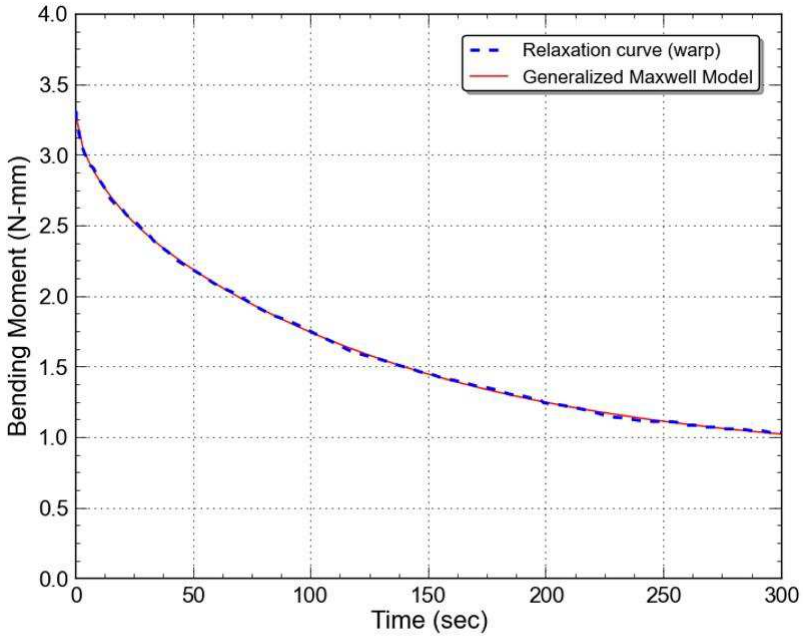

(a)

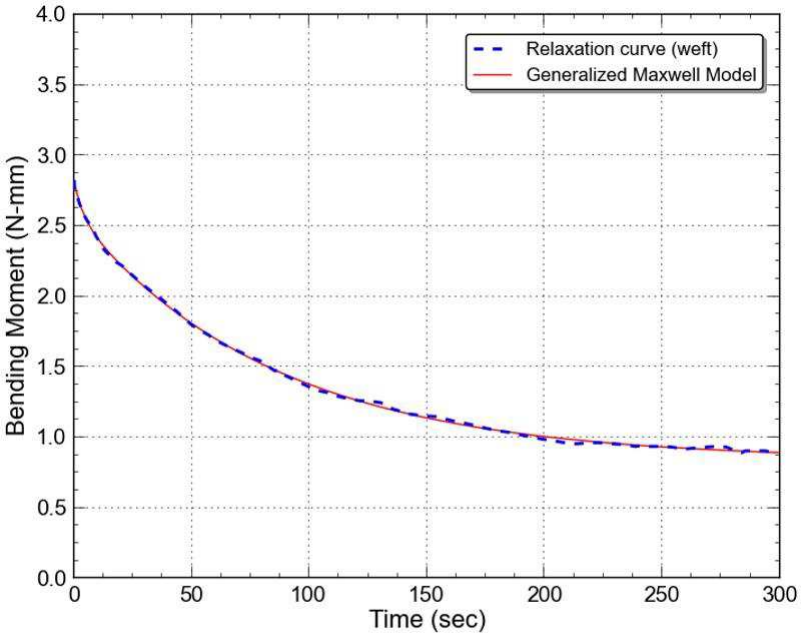

(b)

Figure 3.8: Comparison between relaxation tests and generalized Maxwell model (a) warp sample and (b) weft sample.

3.5.2 Experimental results in comparison with proposed model

3.5.2.1 Warp vs. weft samples

Model predications and experimental results of bending moment with the parameters from Table 3.1 and 3.2 for both warp and weft samples tested at room temperature with a speed of 3 mm/s, are given in Figure 3.9 (a) and (b), respectively. Recall that the testing time was calculated according to Eq. (3.26). The experimental results in Figure 3.9 (a) and (b) show a relatively nonlinear relationship between the bending moment and curvature. This is due to the utilization of a second-order nonlinear differential equation, based on Euler-Bernoulli's law for large deformation, during curvature calculation as long as the slope of the deflection curve is significant [50]. Note that describing the beam's curvature using the second derivative gives a linear relationship between the bending moment and curvature; however, this may yield a calculation error if a forming simulation is the objective. The obtained polynomial fit is a third-order equation for all samples tested up to a 30-mm tip displacement. A slight difference in the curvature values among the tested samples was observed, while the load required to achieve the same tip displacement for warp and weft samples was totally different. The experimental results show that the bending moment in the warp direction is approximately 20% higher than the bending moment in the weft direction. This is because the warp sample has a lower number of crimps.

According to Figure 3.9 (a) and (b), the predicted bending moments using Eq. (3.11) is in a good agreement with the experimental results, especially at higher curvature values. The trends of predicted curves demonstrate a linear relationship between moment and curvature that is related to the linear elastic and viscoelastic assumptions outlined in Section 3.3. Table 3.3 showed minor error percentages between the experimental bending stiffness value (slope) and the prediction value by means of Eq. (3.12) for both warp and weft samples. This discrepancy is attributed to the fact that the bending behavior of woven fabric structure is more complex due to the inherent undulation between yarns. At the same time, the proposed model is based on a single prepreg yarn; however, it can predict an acceptable value of bending stiffness for woven fabric prepregs to be the first input in

forming simulation. It is also possible that the area moment of inertia *(I)* of a prepreg sheet does not bend like a solid beam due to the possible relative slip of fibers [44]. This implies that not all fibers bend about the same neutral axis. The accuracy of the linear fit in Figure 3.9 (a) and (b) may also contribute to the difference between the prediction and experimental results.

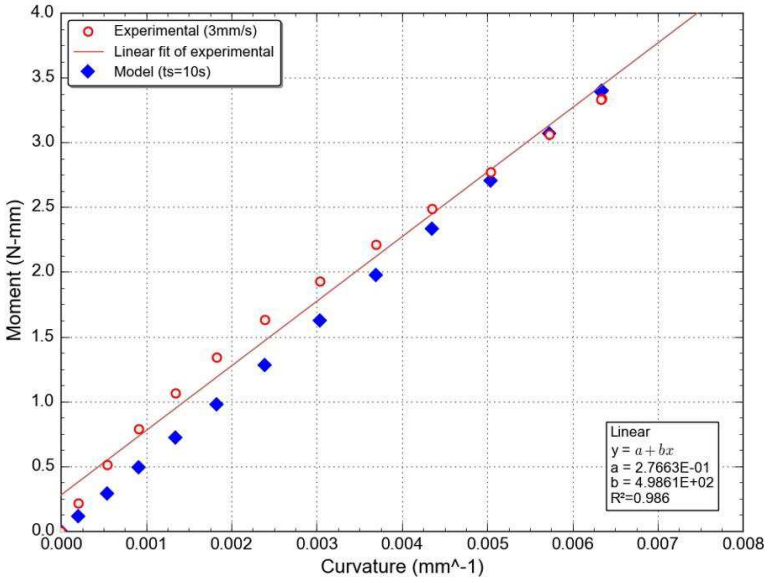

(a)

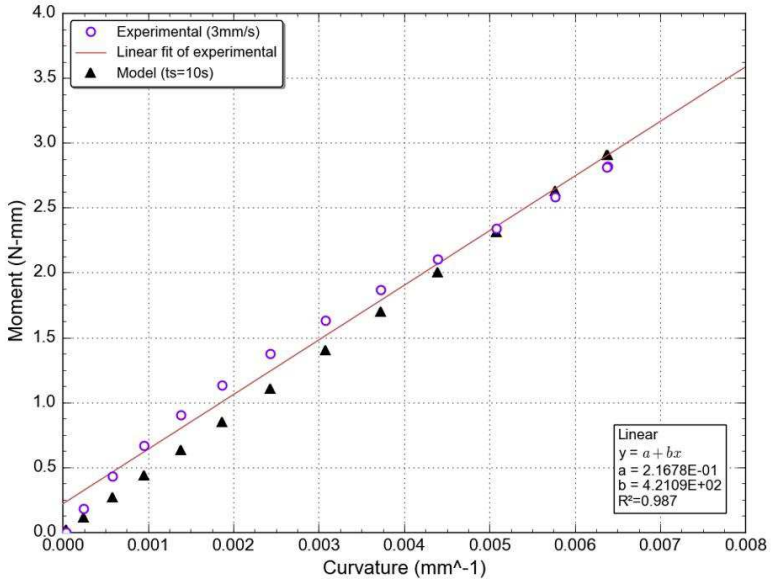

(b)

Figure 3.9: Model predications and experimental results at room temperature with a speed of 3 mm/s (a) warp sample and (b) weft sample.

3.5.2.2 Rate–Temperature dependencies

Processing temperature and forming rate are known to be important parameters during the forming of prepreg materials. For simplicity, only warp-direction sample results are presented in this section. The experiments reveal that bending behavior is rate dependent because of the viscoelastic behavior of the prepreg. Figure 3.10 shows that higher rates resulted in a higher load requirement in order to bend the sample to the desired tip displacement (30 mm). Over a rate increase from 3 to 9 mm/sec as shown in Figure 3.9 (a) and Figure 3.10 respectively, the maximum bending moment increased by approximately 16%. Figure 3.10 shows the corresponding predicted bending moment with a testing time of 3.33 sec. As seen, Eq. (3.11) with different testing time that corresponds to the chosen rate can reasonably capture the trend of the rate dependence of selected materials. Moreover, it can be seen that decreasing the testing time, t_s, increases the bending stiffness (see Table 3.3), which was also observed during the bending experiment. However, the increase in absolute values is relatively small when compared with the increase in experimental value.

A 2.53% error between predicted bending stiffness and the experimental value that tested with a rate of 9 mm/sec was observed (see Table 3.3). Hence, utilization of testing time approach respect to the reference rate gives confidence to the proposed model to predict a viscoelastic bending stiffness at any given rates without performing extensive experiments for relaxation test at the desired rates. It is worth noting that the time used in the proposed model could be related to the forming experiment time as any parts are formed at certain rates. This finding needs further investigation, particularly at different forming rates during prepreg forming simulation.

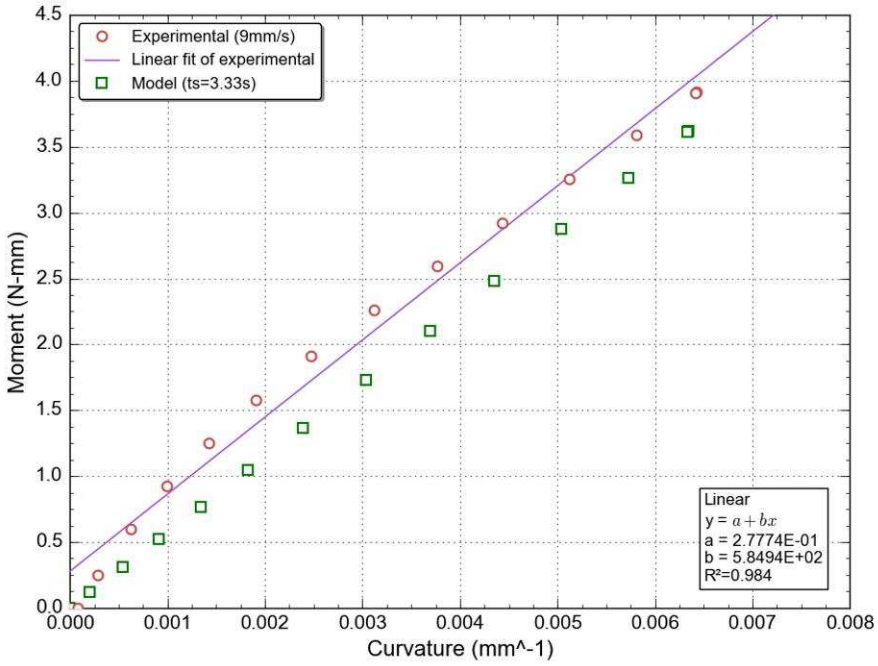

Figure 3.10: Model predications and experimental results of warp sample at a speed of 9 mm/s.

To investigate the effect of temperature on bending behavior, tests were performed at a consistent rate (3 mm/sec) and various temperatures: room temperature (RT), and 70 °C. The experimental results, shown in Figure 3.11, reveal that bending moment decreased significantly with increasing temperature. For instance, the maximum moment at room temperature was 3.336 N-mm, versus 1.226 N-mm at 70 °C, a reduction of 63%. This drop in maximum moment is strongly correlated with a reduction in resin viscosity: higher temperatures reduce the load required to achieve the same tip displacement.

Figure 3.11 shows the predicted as well as the experimentally-measured bending moment of the warp sample when the temperature is set at 70 °C. In Figure 3.11, the time–temperature superposition TTS Eq. (3.30) with a shift factor Eq. (3.31) was used during calculation of bending moment and bending stiffness at processing temperature using Eqs. (3.11) and (3.12), respectively. Model predictions based on (TTS) gave overestimation bending moment values compared to the experimental results (see Figure 3.11). The reason behind this could be that the processing temperature has a significant impact as well on

other material parameters such as compressive and tensile moduli. Moreover, the time–temperature superposition (TTS) may not well-applicable for uncured prepreg materials as the master curves used to be driven from cured sample during rheological tests. However, using the same shift factor Eq. (3.31) in the final value of relaxation modulus at reference temperature as well as in compressive and tensile moduli showed a good agreement between experimental and model as illustrated with purple rhombuses in Figure 3.11. A comparison between bending stiffness values are shown in Table 3.3 for both experimental and shifted values. These findings suggest that an investigation of the viscoelastic behavior at different temperatures should be compared with the shifted value obtained from this study. Note that the viscosities used in Eq. (3.31) are the viscosity of selected prepreg sample not the neat resin, reported in an earlier study [16]. Moreover, the proposed setup was found to allow for adequate control of testing rates as well as processing temperatures within the range of thermosetting resin. The model and experimental results showed that the bending stiffness values are sensitive to the applied forming conditions such as rates and temperatures. However, the temperature influence on bending outcomes tends to be more than the rate effect for this materials. Therefore, in order to improve the forming simulation to predict the wrinkling, bending behavior at these conditions must be correctly represented in the finite element simulation.

Table 3.3: Results of predicted and experimental bending stiffness at selected test conditions.

Sample	**Tip displacement (mm)**	**Testing temperature (°C)**	**Testing rate (mm/s)**	**Bending stiffness Bs(N-mm^2)**		
				Experimental	Model (Eq.(3.12))	Error%
Warp	30	RT	3	498.61	535.83	6.94
Weft	30	RT	3	421.09	455.81	7.61
Warp	30	RT	9	584.94	570.46	2.53
Warp	30	70	3	176.19	210.12 (shifted)	16.14

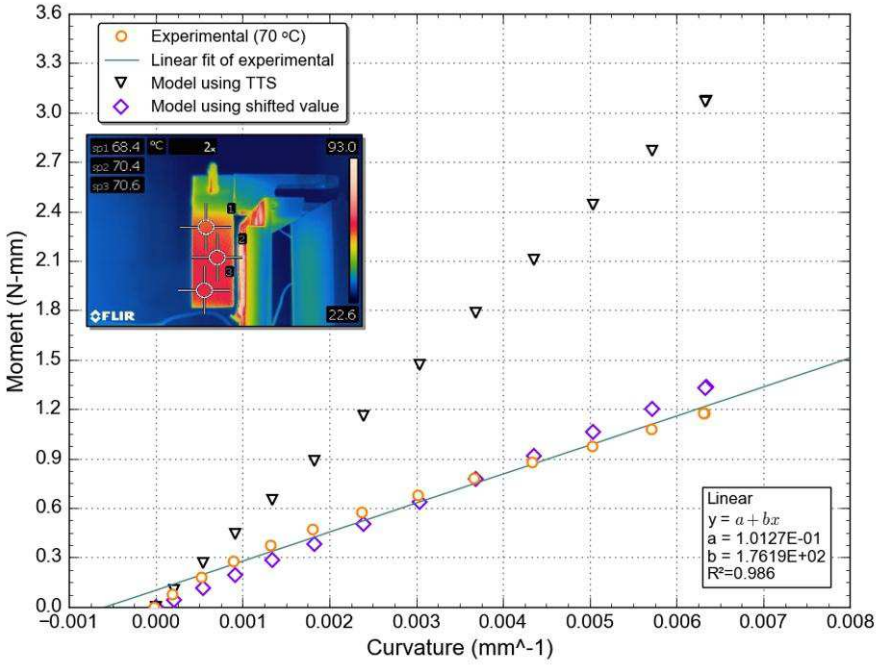

Figure 3.11: Comparison between experimental results and model predications using TTS and shifted value for warp sample at 70 °C.

3.6 Conclusion

A theoretical model was presented that can be applied for a wide range of processing conditions to predict the bending behavior of thermosetting composite perpreg during forming process. The model was included the processing temperature and rate and was validated with a set of experimental tests. The predicted bending stiffness was found to be in a good agreement with experimental values at selected conditions. However, there was slight differences due to the complexity of undulation in woven fabric structure as well as the outlined assumptions. A new approach for considering the testing rate and temperature with respect to a reference value was also developed. The proposed approach can reasonably captured the trend of the rate and temperature dependencies of selected materials without performing extensive experiments for relaxation test at the desired rates and temperatures. It was found that processing temperature has the strongest influence on the bending stiffness results. Therefore, further work is needed to investigate the viscoelastic behavior at

different temperatures in order to compare with the shifted value presented in the current study. Overall, the bending properties obtained by the proposed model can be used as an initial input in finite element model which reduces the effort required by experimental investigations.

Chapter 4

Bending behavior of multilayered textile composite prepregs: Experiment and finite element modeling*

Abstract

An accurate model and assessment of out-of-plane bending properties can improve the forming predictions of multilayered textile prepregs using a suitable modeling technique. This paper aims to investigate the bending properties of multilayered textile thermosetting composite prepregs under conditions relevant to the forming process. A finite element model based on a viscoelastic approach has been developed to predict the bending behavior of different stacking sequences at different processing parameters, including temperature and rate. The effect of stacking sequences on out-of-plane bending deformation was studied experimentally and numerically through the developed modeling methodology. Furthermore, the paper analyzes the feasibility of using a viscoelastic material model to model the bending behavior of rate-dependent material and its application in forming simulation. A comparison between elastic and viscoelastic material models showed the importance of considering the rate dependency to describe the bending behavior of prepreg materials. The experimental and numerical results show that the bending properties strongly depend on the fabric lay-up inside multiple stacked plies. Bending and friction properties were also found to significantly influence the occurrence of wrinkles during the forming simulation.

*Reproduced from: Hassan Alshahrani, Mehdi Hojjati. Bending behavior of multilayered textile composite prepregs: Experiment and finite element modeling. Materials & Design, 124 (2017), pp. 211–224. http://dx.doi.org/10.1016/j.matdes.2017.03.077

4.1 Introduction

Composite materials can be produced through an assortment of manufacturing techniques. Conventional composite manufacturing techniques such as hand lay-ups are labor intensive, time–consuming, costly, and less productive. Moreover, increased demand for many modern structures together with an increase in their size and complexity showed the need for fast, and cost-effective manufacturing alternatives. Automated technologies such as Automated Tape Laying (ATL) or Automated Fiber Placement (AFP) offer great promise to meet the growing need for composite materials in the aerospace and automotive industries, mainly due to their short manufacturing times and resulting lower costs [33]. However, to produce high-complexity and high-volume output, a forming step associated with automated machines is required. This involves automated machines laying down flat laminates and then transforming them into three-dimensional shapes by forming processes using the application of heat and pressure.

Various deformation mechanisms come into play during the process of forming composite prepregs into a desired shape, including intra-ply shear, inter-ply friction, and out-of-plane bending [6]. Haanappel et al. [7] showed that the formability of a composite laminate is determined by a delicate balance between these basic deformation mechanisms. In order to accurately predict defects such as wrinkling that may arise during composite material forming processes, out-of-plane bending behavior must be incorporated into the composite forming model [11,24,29,35,69]. Therefore, the bending properties of the prepregs, including their temperature and rate dependencies, must be known and properly represented in the finite element (FE) model to achieve useful simulation results. Since this cannot be achieved using the membrane approaches [70–72] that are common in textile sheet forming simulations, it is necessary to adopt an alternative modeling strategy. Moreover, prepreg sheets are inherently much more flexible than continuous materials; thus, using a conventional shell element in forming simulation is no longer applicable because the bending stiffness is derived from in-plane material response [6, 11]. Some models are presented in the literature, where bending behavior is de–coupled from in-plane by using specialized shell element

in finite element forming simulation based on elastic [7, 25–27], elastic with temperature-dependent [13, 28], or viscoelastic approaches [29]. The latter research [29] showed that modeling rate-dependent bending behavior using a viscoelastic approach is crucial to predict wrinkling in FE forming simulation of thermoplastic pre–impregnated tapes. In their study, the bending characterization was based on isothermal investigations using the rheometer bending setup presented by Sachs [30]. A rate-control test setup was developed in an earlier study [56], because the viscous effect of the resin may introduce a rate dependency. The bending results of single ply of woven fabric-based out-of-autoclave thermoset prepregs showed that the bending behavior is rate-dependent and it is significantly influenced by processing temperatures [56, 73].

Although several studies have been conducted towards the characterization of bending behavior of prepregs (see Refs. [47, 56] for a comprehensive review), there is still lack in prediction analysis through modeling that considered the actual bending behavior and its dependencies. Some commercial software tools, such as PAM-FORM [31] and AniForm [32], offer the possibility of modeling a number of features of composite forming. However, no details or application of out-of-plane bending behavior of prepreg composites based on viscoelastic material models are available in the literature using these commercial software tools. Therefore, this paper aims to develop a FE model based on a Kelvin-Voigt approach using AniForm software [32], for bending behavior of multilayer textile thermoset prepregs at conditions relevant to the forming process. Bending behavior of different stacking sequences of selected materials are examined experimentally and numerically. Validation of the proposed model is made using the rate-control bending test developed in [56]. Moreover, this paper analyzes the feasibility of using a viscoelastic material model to model the bending behavior of selected material and its application in forming simulation. This includes the relationship between the bending and friction mechanisms during the bending experiments and its influence on defect formations in the forming simulation.

Intra-ply shear, inter-ply friction, and out-of-plane bending properties are required to accurately model the out-of-plane bending behavior for multilayers. To this end, the material characterization tests were conducted to obtain the required properties for the material

models in the FE simulation, as described in the following section.

4.2 Characterization of material properties

4.2.1 Materials

This study tested a 5-harness (5HS) satin weave (6k carbon fiber tows) impregnated with an epoxy resin (Cycom 5320) designed for out-of-autoclave manufacturing applications. The fabric's areal weight is 380 g/m^2 and the resin content is 36% by weight. The measured thickness of uncured one-ply is approximately 0.55 mm. Using out-of-autoclave (OOA) prepreg materials in the forming processes provides a great cost savings opportunity by allowing the use of low-cost tooling due to the lower cure temperatures.

4.2.2 Out-of-plane bending properties

An experimental study of the bending behavior of selected material at forming conditions was carried out using a special setup allowing for investigation into rate and viscoelastic effects. The experimental approach is concisely described below; the reader is referred to [56] for further details.

4.2.2.1 Bending test setup and procedure

In this test setup, as shown in Figure 4.1 (a), the sample is clamped vertically (vertical cantilever) [39], while deflection shape and applied load are controlled by a linear actuator and a miniature-load cell, respectively. Direct commands and change settings (such as required travel displacements, speeds, or current position) can be sent via the controller connected to the actuator, while the force required to achieve tip displacement is subsequently recorded by the load cell software. The temperature throughout the sample is monitored by an infrared camera (FLIR) to ensure uniform heating during the elevated temperature tests (using a non-contact radiant heater). The rate-dependent effect can be measured by adjusting the testing speed using the actuator's controller.

The analysis of the bending behavior during the composite forming process requires high curvature (higher displacement) to accurately simulate the process. Therefore, tip displacement of 30 mm was used. Figure 4.1 (b) summarizes the bending test procedure. Note that ImageJ software was used to extract the data and these points are subsequently fitted using a proper polynomial function to calculate the curvature. The value of the recorded load was used to calculate the moment at each selected point.

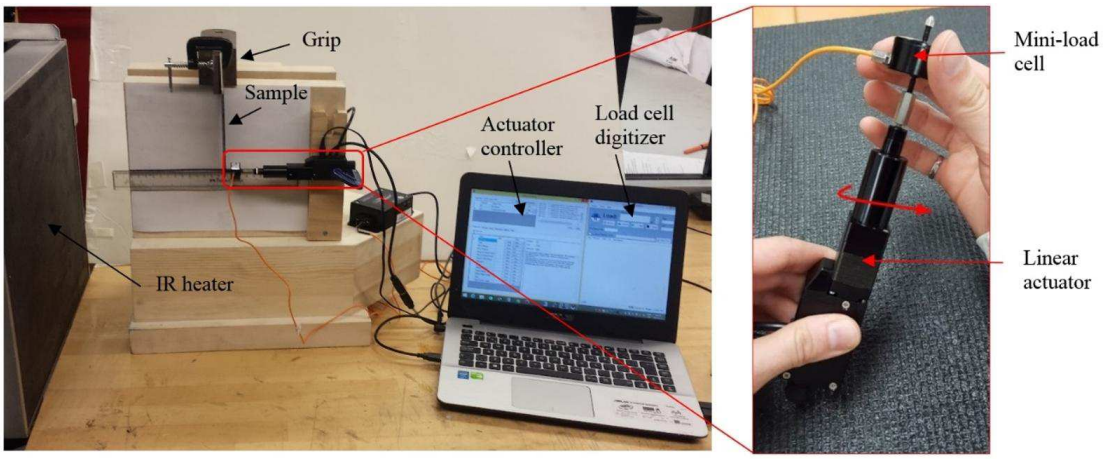

(a)

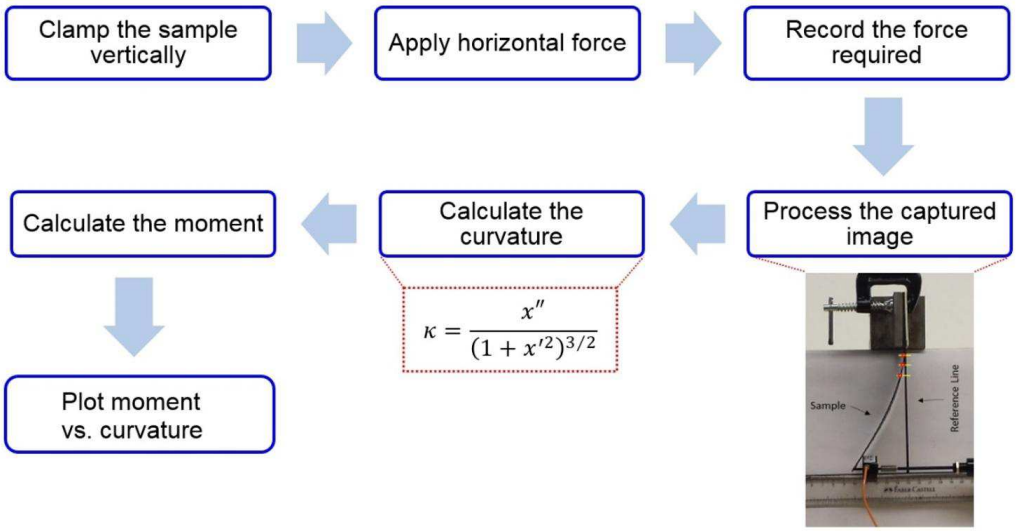

(b)

Figure 4.1: (a) Bending test setup including heat source, and (b) steps followed to extract the bending properties.

4.2.2.2 Fabric lay-up configuration

The samples selected for the bending experiments were 150 mm long by 50 mm wide, with an ungripped length of 120 mm (see selected sample in Figure 4.2). In a 5HS-woven fabric, 80% of the fibers on one face are in the strip-long direction, whereas 80% of the fibers on the other face are perpendicular to that direction. Therefore, face 1 in Figure 4.2 was selected to be in tension during the bending experiments. Three layers of textile composite with different ply orientations, specified with respect to warp yarns as shown in Figure 4.2, were considered. Note that the 0° axis was always parallel to the warp yarn direction based on the ply 1. Prior to testing, multilayered samples were preconsolidated at 70 °C with a pressure of 0.1 MPa using vacuum bagging for 30 minutes. All four stacking sequences, shown in Figure 4.2, were tested under the conditions relevant to the forming process.

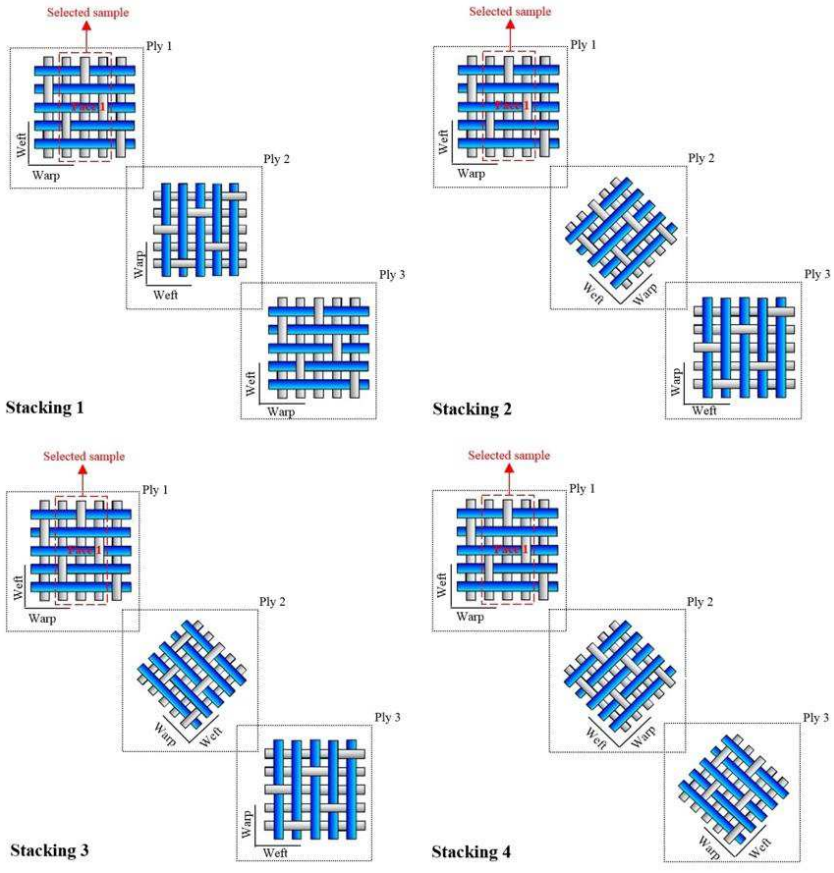

Figure 4.2: Stacking sequences of three layers of textile composite with selected samples for bending experiments.

4.2.3 Intra-ply shear properties

In an earlier study, the intra-ply shear properties at forming conditions for 5HS satin weave impregnated with an epoxy resin (Cycom 5320) were characterized over a range of processing temperatures using a bias extension test and a non-contacted infrared heater [15, 74]. In a bias extension test, the material is extended along the bias, beginning at ($\pm 45°$) to the direction of applied tensile force. The bias extension test has the advantage of being able to be performed on any tensile machine. The test sample must be divided into three zones. The change in fiber angle (2θ) can be measured from the images taken of each test, as depicted in Figure 4.3 (a). Accordingly, the corresponding shear angle γ between the weft and warp yarns in Zone A can be obtained by:

$$\gamma = 90 - 2\theta \tag{4.1}$$

The tests were carried out on two layers at [$\pm 45°$] with a sample size of 100 mm x 50 mm. Figure 4.3 (b) shows the typical load-displacement response at 70 °C with a displacement rate of 20 mm/min. Three samples were tested and the average was plotted with the vertical bars, which represent one standard deviation. These results will be used to calibrate the intra-ply shear model as shown in Section 4.3.1.

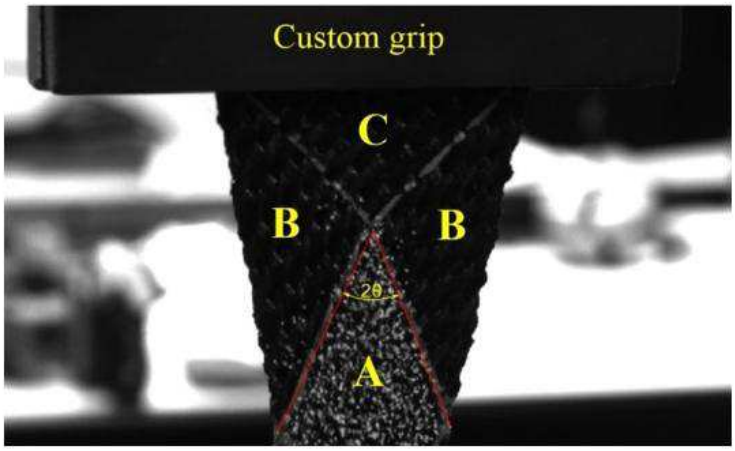

(a)

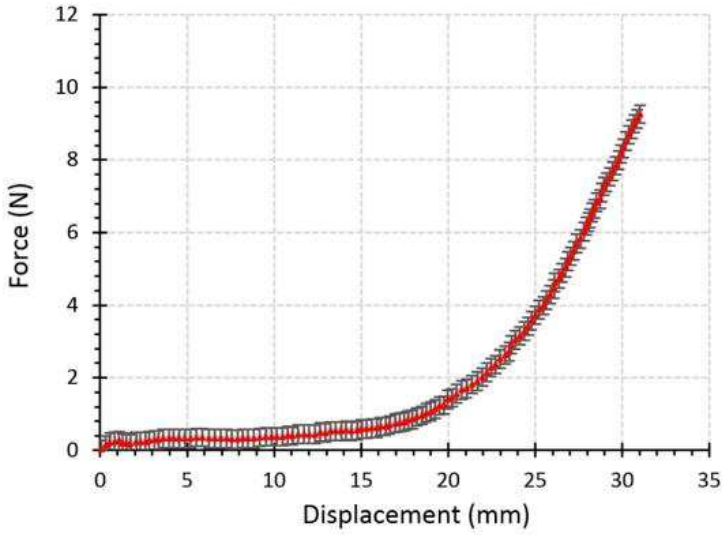

(b)

Figure 4.3: (a) Bias extension test with the measurement of the material angles at Zone A, and (b) load-displacement response at 70 °C with a displacement rate of 20 mm/min.

4.2.4 Inter-ply friction properties

The inter-ply friction properties of the materials were measured using the same method as described previously in [18]. The friction test rig was designed and constructed so that different temperatures and different normal pressures could be applied to the prepreg sample during testing, as shown in Figure 4.4 (a). This test rig was installed on a tensile testing machine that can provide different pulling rates and measure the frictional resistance between

prepreg layers. The tests were performed at different pulling rates with 70 °C and a normal pressure of 0.5 atmosphere. The results of friction coefficients for selected material can be seen in Figure 4.4 (b). Three samples were tested for these conditions and the error bar represents the standard deviation.

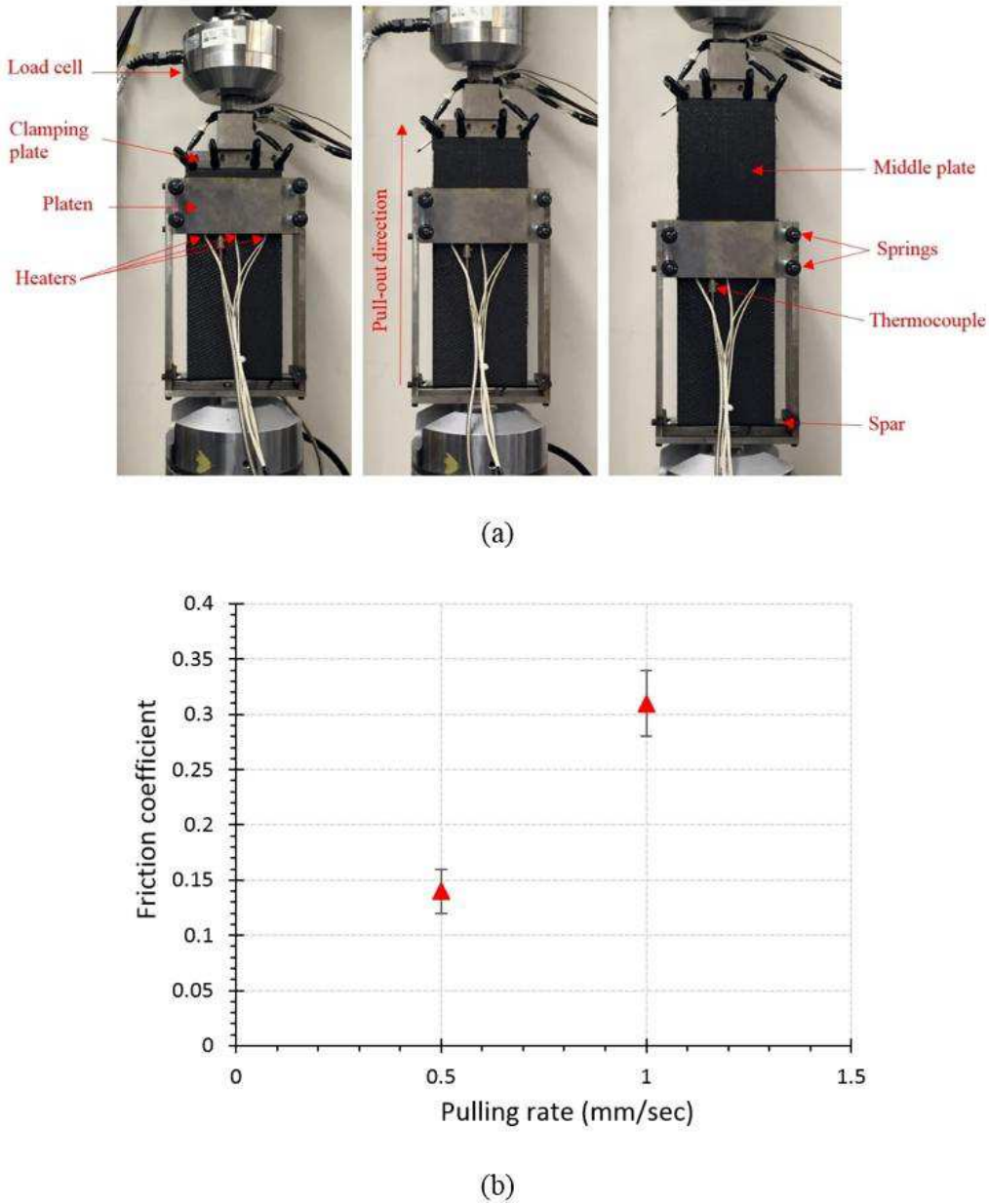

Figure 4.4: (a) The friction test rig installed on a tensile testing machine, and (b) friction coefficients at different pulling rates.

4.3 Finite element modeling

AniForm Finite Element software [32], which is designed for use in composite forming, is particularly useful for predicting the behavior of anisotropy of uncured prepregs. This study used the AniForm software to predict out-of-plane bending deformation of textile thermoset prepregs. AniForm adopts a continuum mechanical approach solved by an implicit FE approach: by modeling the prepreg plies as de–coupled shells allows the bending properties to be described in continuum shell elements. An AniForm shell element is created by combining an LTR3D membrane element with a Discrete Kirchhoff Triangle (DKT) element using the same nodes as shown in Figure 4.5 (a). Accordingly, the resulting shell element is able to capture realistic behavioral properties for both in- and out-of-plane materials using different constitutive models (see Figure 4.5 (b)). Results from material characterization procedures and the observed behavior can be used to assign proper constitutive material models that can correctly describe the response of deformation mechanisms.

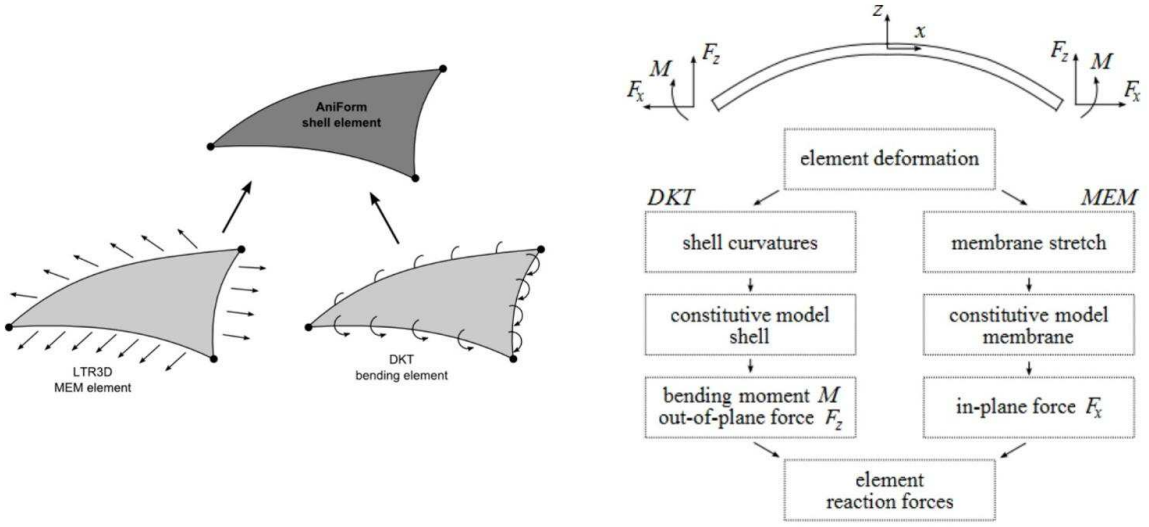

(a) (b)

Figure 4.5: (a) AniForm shell element, and (b) the de-coupled shell approach [32].

4.3.1 Material models

To model the membrane behavior, the Ideal Fiber-Reinforced Model (IFRM) developed by Spencer [60] and applied to viscous media [75] was applied. The stresses in the membrane element for 5HS prepreg plies is given by [7]:

$$\sigma = -pI + T_a aa + \ T_b bb + \tau \tag{4.2}$$

where T_a is the fiber tension along the fiber direction a, T_b is the fiber tension along the fiber direction b, aa and bb are the second-order tensor with cartesian components $a_i a_j$ and $b_i b_j$, and $-pI$ is the hydrostatic pressure term. τ is the matrix-related extra stress tensor, which can be modeled using a two parameter elastic Mooney–Rivlin and a Cross-viscosity fluid model connected in parallel [7]:

$$\tau = \left[2C_{10}\left(\mathbf{B} - \mathbf{I}\right) - 2C_{01}(\mathbf{B^{-1}} - \mathbf{I})\right] + 2\eta(\dot{\gamma})\mathbf{D} \tag{4.3}$$

Here, C_{10} and C_{01} are the Mooney–Rivlin material constants, $\boldsymbol{B}$ and is the left Cauchy-Green strain tensor, $\boldsymbol{D}$ is the rate of deformation tensor. The viscosity η depends on the deformation rate $\dot{\gamma}$ and is described with the Cross model according to [76]:

$$\eta(\dot{\gamma}) = \frac{\eta_0 - \eta_\infty}{1 + m\dot{\gamma}^{(1-n)}} + \eta_\infty \tag{4.4}$$

where η_0 is the viscosity at low shear rate, and η_∞ is the viscosity at high shear rates, n is the (Cross) rate constant, and m is the consistency index.

The fibers are modeled based on a linear elastic fiber model. There are significant differences in stiffness between the carbon fibers and the matrix. Thus, the stiffness of fibers is reduced so that the fibers still behave as nearly inextensible while the differences are minimized to avoid numerical instabilities [77, 78]. The bias extension test was simulated in AniForm using these material models as shown in Figure 4.6 (a). The experiment and simulation results are presented in Figure 4.6 (b), and the fitted parameters for the membrane

elements are listed in Table 4.1.

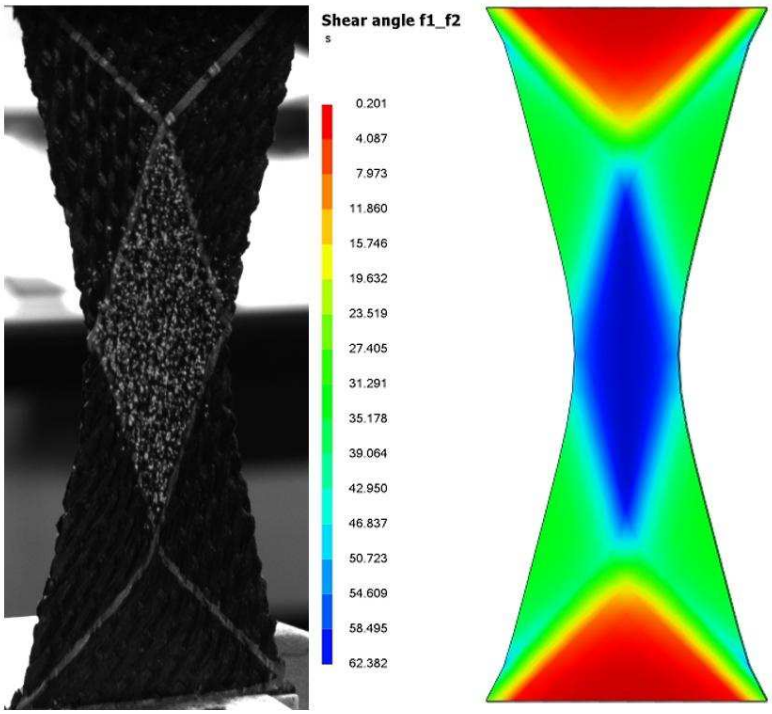

(a)

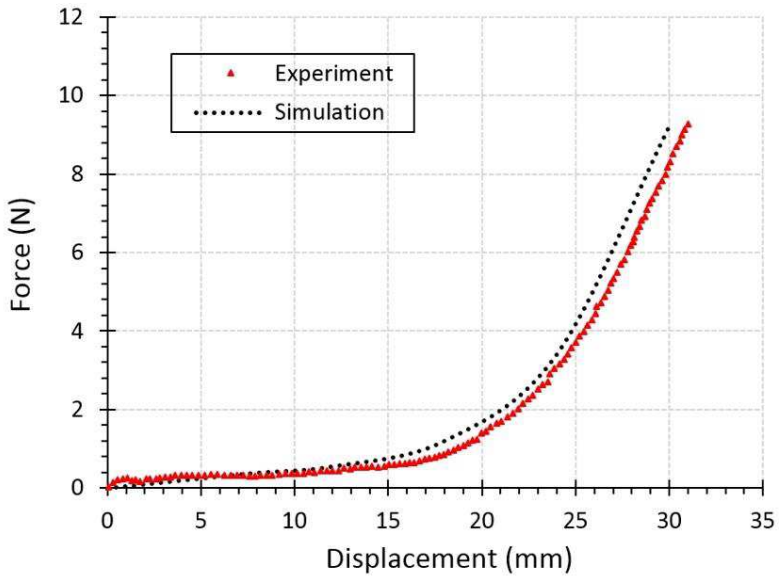

(b)

Figure 4.6: (a) Simulation of bias extension test using elastic Mooney–Rivlin and a cross-viscosity fluid model, and (b) bias extension response and simulation fit.

The bending characterization experiment was used to determine the initial bending properties of one-ply, as shown in the previous section. Moreover, the ply bending stiffness can be calculated as a function of rate and temperature using a thermo–viscoelastic model developed in a previous study [73]. A viscoelastic approach (Kelvin–Voigt) was used to model the out-of-plane bending behavior, which encompasses both an elastic spring and viscous damper connected in parallel. An isotropic elastic model was used to model the spring part, whereas the damper was modeled using a Newtonian viscous fluid model. Table 4.2 represents constitutive models and parameter values used for out-of-plane bending elements. Note that the input data in Table 4.2 was based on the bending experiment of single ply at 70 °C and the corresponding prepreg sample viscosity according to [73] and [16], respectively.

The inter-ply friction was modeled as a combination of Coulomb friction, viscous friction and adhesion. These basic material models are connected in parallel generating a mixed model (combined models) to correctly describe the interface properties. Coulomb friction is governed by a friction coefficient independent of pressure and speed. The viscous friction is based on the presence of fluid film between the contact surfaces. It can be defined as

$$\tau_{xy} = \eta\dot{\gamma} \tag{4.5}$$

where τ_{xy} is the in-plane surface traction, η is the viscosity, and $\dot{\gamma}$ is the shear rate in the fluid film. The shear rate can be determined according to the following relation [32]:

$$\dot{\gamma} = \frac{V_{xy}}{h} \tag{4.6}$$

where V_{xy} is slip velocity and h is film thickness. Note that from the preceding equations, the viscous friction is dependent of both speed and temperature (viscosity). The viscosity value at processing temperatures was based on the measured neat resin viscosity of epoxy resin (Cycom 5320) according to [79]. Besides this form of friction, a material model known as adhesion was used to model the tacky properties between surfaces. However, the adhesive tension was set based on the value provided by Haanappel et al. [7]. A penalty stiffness

model that facilitates the contact condition during the numerical simulation, thereby inhibiting surfaces in contact from penetration was also applied. All required parameters for inter-ply friction models (contact element), including friction coefficients μ determined in Section 4.2.4, are listed in Table 4.3.

Table 4.1: Material model and fitted parameters for the membrane elements (in-plane).

Model assigned	**Parameter**	**Input data**
Elastic fiber model	E_f (MPa)	1000
Mooney–Rivlin	C_{01} (MPa)	0.00328
	C_{10} (MPa)	0.12
Cross–viscosity model	η_0 (MPa s)	0.403
	η_∞ (MPa s)	0.0004
	n	0.81
	m	2.87

Table 4.2: Viscoelastic material model and properties for the DKT elements (bending).

Model assigned	**Parameter**	**Input data**
Isotropic Hooke	E (MPa)	275
	ν (-)	0.33
Viscous model	η (MPa s)	0.09

Table 4.3: Ply-ply material properties for contact elements.

Model assigned	**Parameter**	**Input data**
Coulomb–viscous friction	μ (-)	0.14
	η (MPa s)	0.0003
	h (mm)	0.0011
Adhesion	Tension (MPa)	0.1
Penalty model	Penalty stiffness (N/mm^3)	1.0

4.3.2 Modeling of bending test

The bending test is modeled in AniForm to predict the bending behavior and validate the selected material models. This software is tailored to setting up a real forming process, rather than making it easy to model characterization experiments, thus some modifications are needed to model this bending experiment. Each ply is modeled using an experimental sample size (120 mm long by 50 mm wide) and meshed with a structured mesh of 960 three–node triangular shell elements, as shown in Figure 4.7 (a), which consist of a membrane element and a DKT. To model the top edge to behave as fully clamped, the rotations and translations of this edge nodes were secured. Note that line grippers can rotate axially; therefore, the nodes along this line must be secured completely in all translational degrees of freedom. A tip displacement of 30 mm along the x axis was applied on the lower gripper (see Figure 4.7 (b)) and the model was created in which the reaction force and moment can be extracted. All selected fiber orientations are represented in the model.

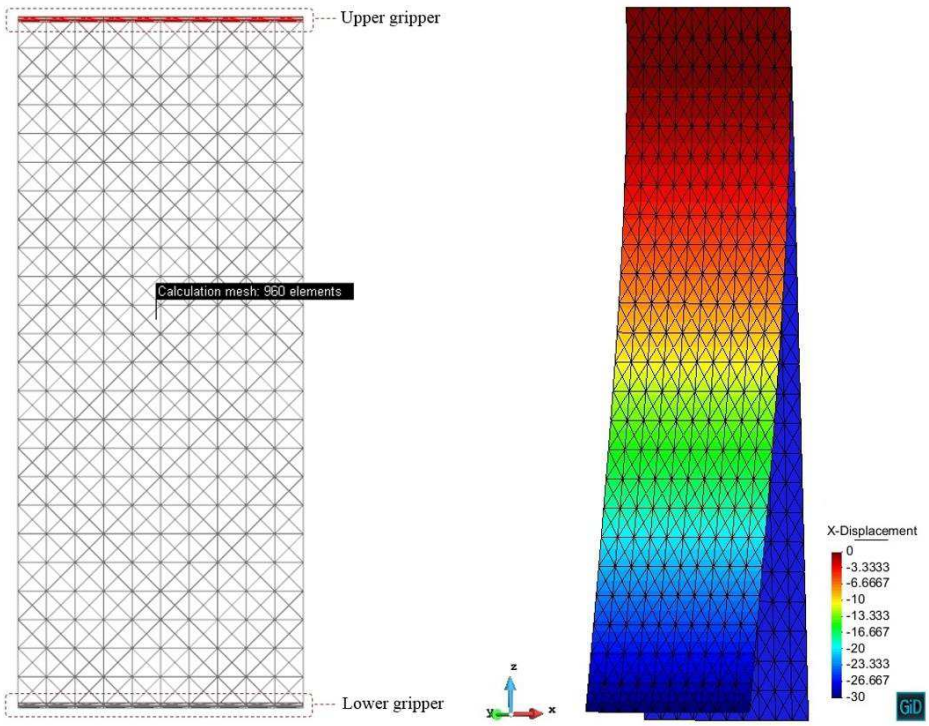

Figure 4.7: (a) Ply mesh with element numbers, and (b) bending test modeling in AniForm.

4.4 Results and discussion

Experimental tests were conducted on samples at room temperature, and 70 °C, i.e. below cure reaction temperature [16]. Two test speeds were applied at room temperature–3 mm/s and 9 mm/s–to investigate the effect of testing rate. This section presents the results from both experimental tests and numerical simulations. First, the experimental results for selected sequences of multilayered samples are evaluated. Then, in Section 4.4.2, a numerical outcome is compared with the experimental results by using the developed FE model with the parameters from Tables 4.1, 4.2, and 4.3. Note that the results of multilayered samples are presented by the stacking number (stacking 1, 2, 3, and 4) as described in Section 4.2.2.2.

4.4.1 Experimental results

The image analysis of the samples during the bending experiments shows that all stacking sequences bend together with no observed separation between the plies. This is due to the pre-consolidation process before testing and the tacky effect between layers. The test results are based on the average of three trials conducted at each condition. Figure 4.8 (a) shows the load required to reach a tip displacement of 30 mm for all selected stacking sequences at 70 °C, and the vertical error bars represent the standard deviation. These loads were used to calculate the bending moment in order to generate moment versus curvature curves, as shown in Figure 4.8 (b). As can be seen, stacking 1, [0, 90, 0] with respect to warp direction, required the highest load to bend the sample to the desired displacement. The results of stacking 1 were expected since the applied load was perpendicular to weft yarns in plies 1 and 3 and warp yarns in ply 2. However, the previous findings in [56] for single ply show that the bending stiffness is higher when the load is applied perpendicularly to the warp yarns direction than when applied to the weft direction.

Figure 4.8 (b) also shows that rotating ply 2 and ply 3 by 45° and 90°, respectively, decreased the bending stiffness by approximately 21% compared to stacking 1. The reduction in load is attributed to middle–ply orientation (45°), which requires the lowest load to

deform the sample compared to 0° and 90° orientations. However, changing the orientation of the middle–ply from 45° (stacking 2) to – 45° (stacking 3) shows different bending stiffness responses (see Figure 4.8 (a) and (b)). A significant decrease in bending properties was observed in stacking 4. This decrease is caused by the orientation of the second and third plies. It is worth noting that besides the effect of fabric style and orientation, the friction between plies plays an important role in terms of facilitating the through thickness shear during the bending experiments at elevated temperatures. Thus, the friction also contributes to the observed difference between tested stacking sequences. Moreover, as previously investigated in [18], the angle between the fibers and the pulling direction during ply-ply friction experiments affects the friction resistance. The results show that frictional resistance decreases as the angle of warp yarn changes from 0° to 45° with respect to the pulling direction. Accordingly, the coefficient of friction decreases by approximately 22% when the angle is set to 45°.

Figure 4.9 (a) shows the maximum bending moment for stacking 1 at room temperature (23 °C) and processing temperature (70 °C) with a constant speed (3 mm/s). Since matrix viscosity decreases with increasing temperature, higher temperatures are expected to reduce load and thus reduce the effect of friction between layers. The results at elevated temperatures from single ply [56] and multilayered samples presented in this paper have borne out this expectation; higher temperatures do indeed result in a load reduction, and consequently a significant decrease in bending stiffness. The effect of testing rate, which simulates the forming rate required during the actual forming process, was investigated at room temperature. The results are presented in Figure 4.9 (b). There is a clear correlation between testing rate and the load required to bend the sample, as can be seen by the obtained maximum bending moment values for two selected rates. This implies that a higher testing rate results in a higher load required to bend the sample to the desired tip displacement.

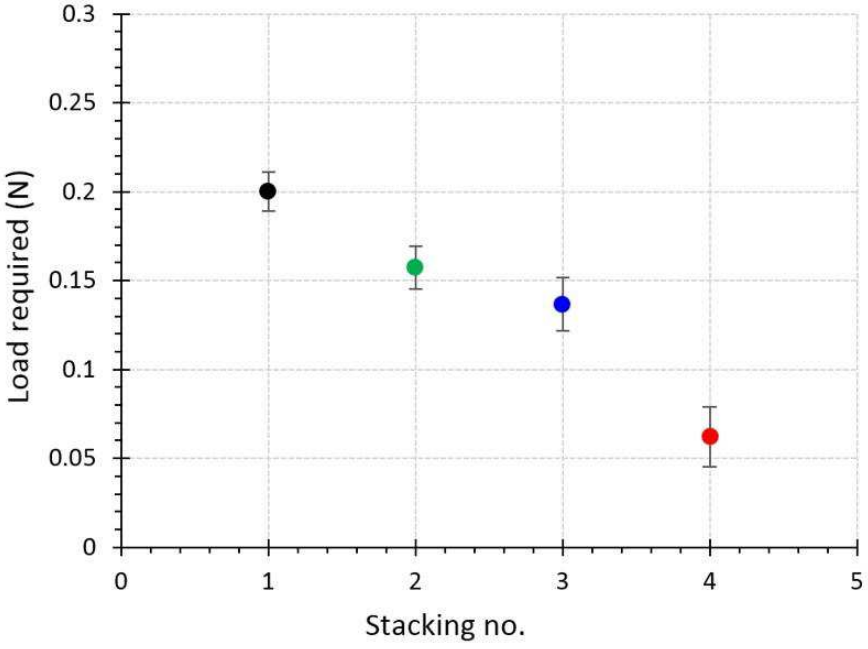

(a)

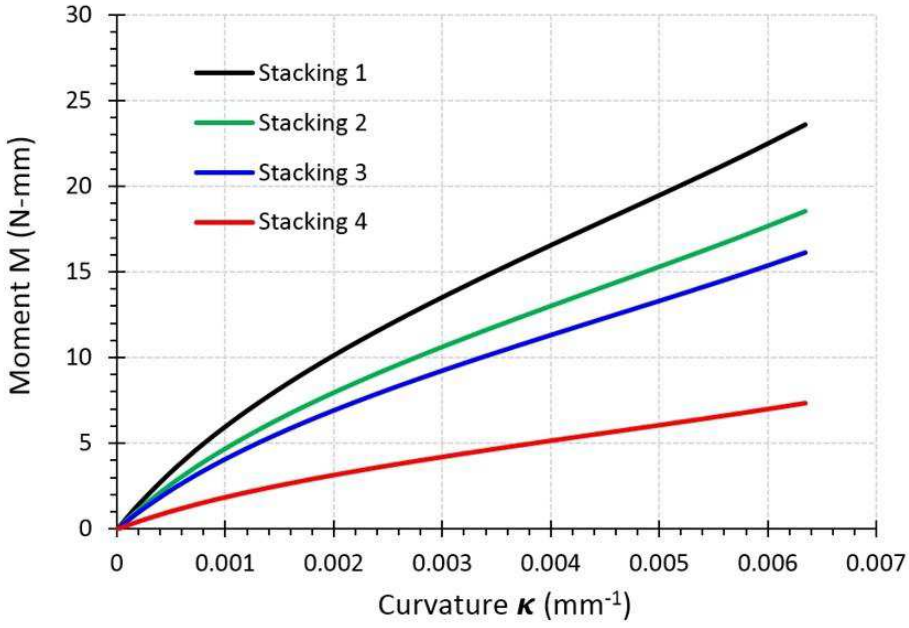

(b)

Figure 4.8: (a) Load required to reach a tip displacement of 30 mm, and (b) moment vs. curvature curves for all selected stacking sequences at 70 °C.

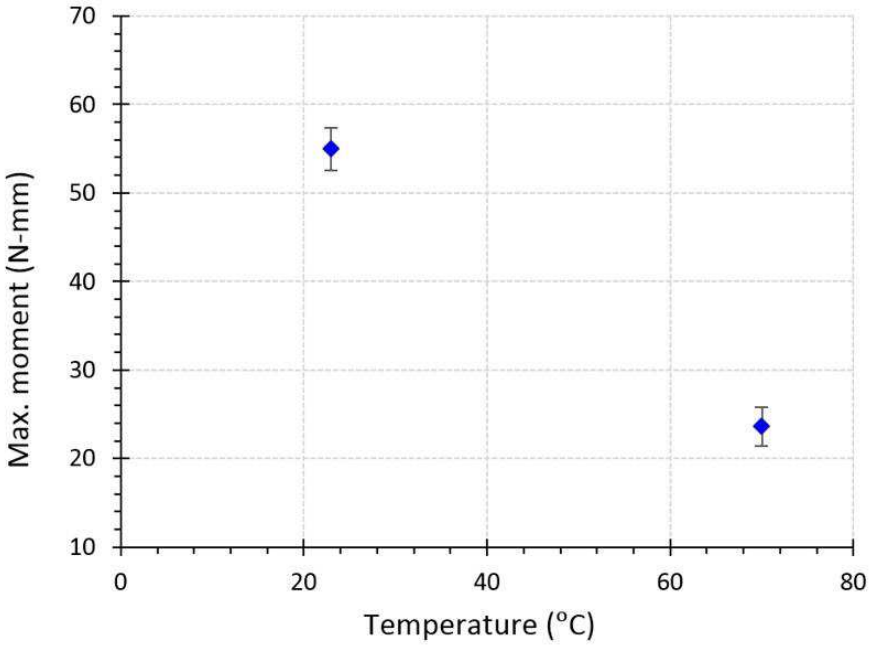

(a)

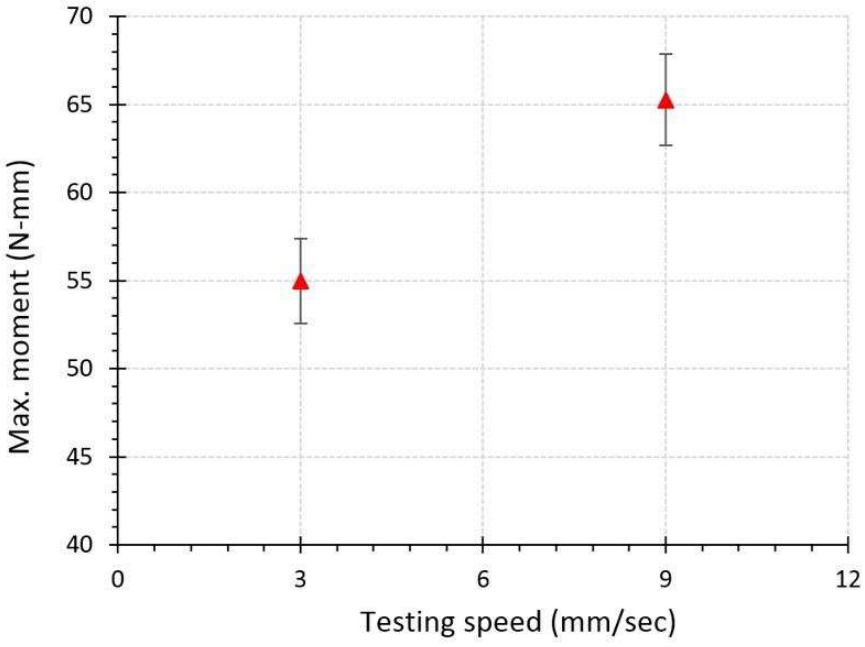

(b)

Figure 4.9: (a) Maximum bending moment for stacking 1 at different temperatures with a constant speed of 3 mm/s, and (b) effect of testing rate at room temperature.

4.4.2 Numerical results with experimental verification

The simulation results are based on reaction forces and moments extracted from the model at each selected condition. Figure 4.10 (a) shows the predicted curvature–moment curve against the experimental measurements for stacking 1 and 4. The results from the FE model show a good agreement with the experimental results. However, the predicted values of stacking 4 are relatively lower than the experimental values by approximately 14%. Note the slight difference in curvature value between all tested stacking sequences; the curvature values along the sample, shown in Figure 4.10 (a), were used to plot the present results. Moreover, as discussed previously, the friction coefficients when the angle was set to 45° to the pulling direction were used for stacking sequences 2, 3, and 4. Although the experimental measurements show notable differences between 45° (stacking 2) and –45° (stacking 3), Figure 4.10 (b) reveals that the reaction results from simulations for both stacking 2 and 3 are quite similar. This similarity may be due to the lack of consideration of the inherent undulation between yarns in woven–fabric structures. It should also be noted that scaling of the material models of selected lay-ups for bending does not correspond to the number of plies as in the case for in-plane models [32]. In this model, the scaling for bending was set to 2 in the Weights setting, which was found to be more convenient to the experimental calibration.

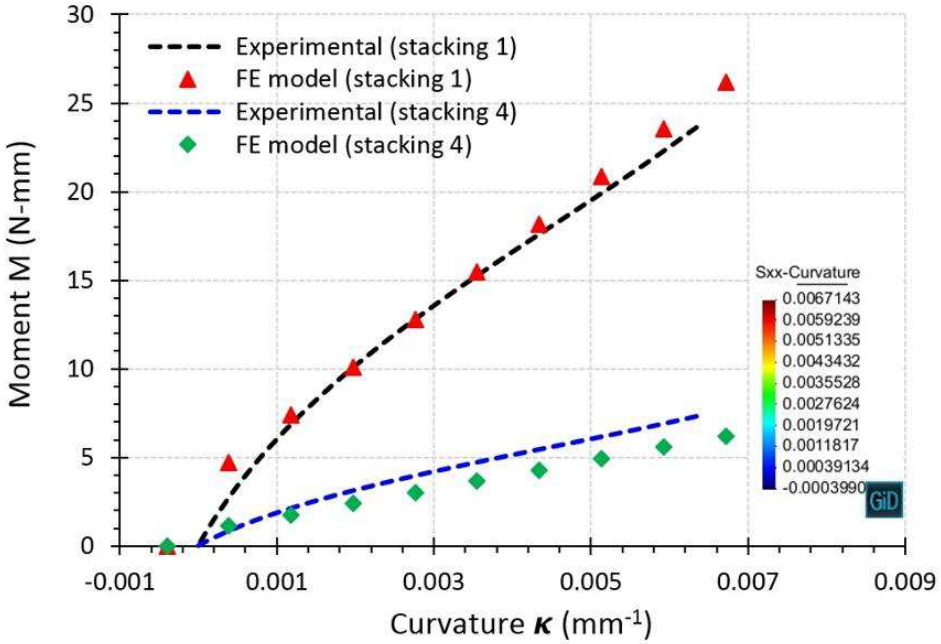

(a)

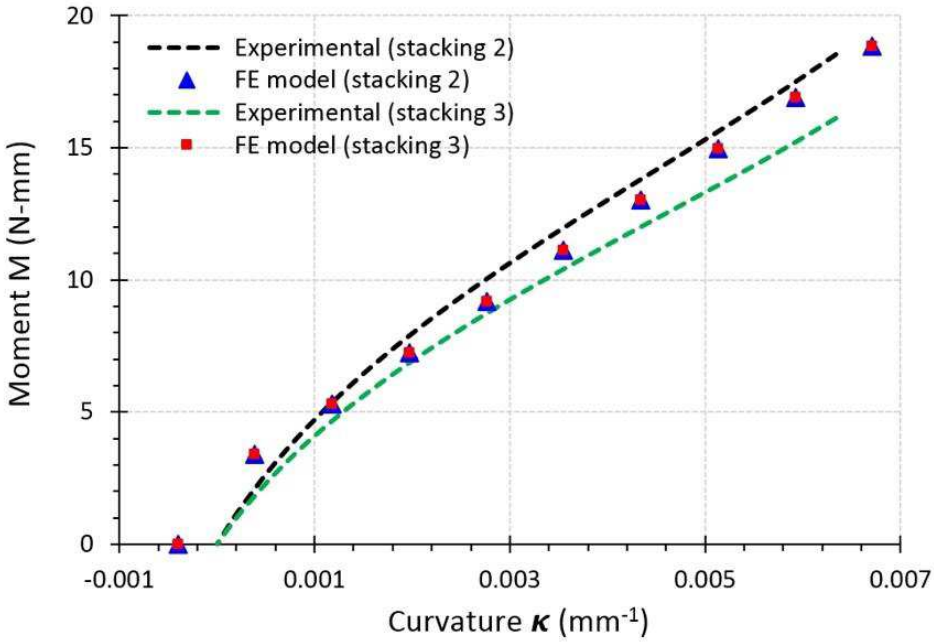

(b)

Figure 4.10: Predicted curvature–moment curve against the experimental measurements at 70 °C (a) for stacking 1 and 4, and (b) for stacking 2 and 3.

Figure 4.11 (a) depicts the maximum bending moment (moment in the clamp) obtained at 70 °C and at room temperature. As can be seen, the FE model predicts the reaction moment at the clamp with acceptable correlation for both temperatures. Further, these results show that the predicted values at room temperature are lower than the experimental values, unlike at 70 °C. This is because the model only considered bending and ply-ply properties at room temperature, according to the obtained results in [56] and [18] respectively.

Figure 4.11 (b) shows the effect of testing rates conducted at room temperature on the maximum bending moment. It was found that a decrease in time span in the AniForm model can increase the reaction moment; higher rates entail lower time spans. Thus, this time in the model should be related to the actual testing time, and ultimately to the forming time. In this case, the testing time during the experiment was calculated as the tip displacement over the selected testing speed. Accordingly, for a testing rate of 3 and 9 mm/s, the testing time was 10 and 3.33 sec, respectively. The FE model can predict the bending properties at the desired rate as long as the time span in the model is set according to the testing time values. Therefore, the bending properties at the rate of 9 mm/s can be predicted by using the properties obtained at 3 mm/s with a time span of 3.33 sec instead of 10 sec. This procedure reduces the effort required for experimental investigations at different rates. However, minor errors still exist following this procedure (see Figure 4.11 (b)). Introducing the fiber stiffness of warp and weft yarns separately in the FE modeling approach in future investigations will improve prediction capabilities.

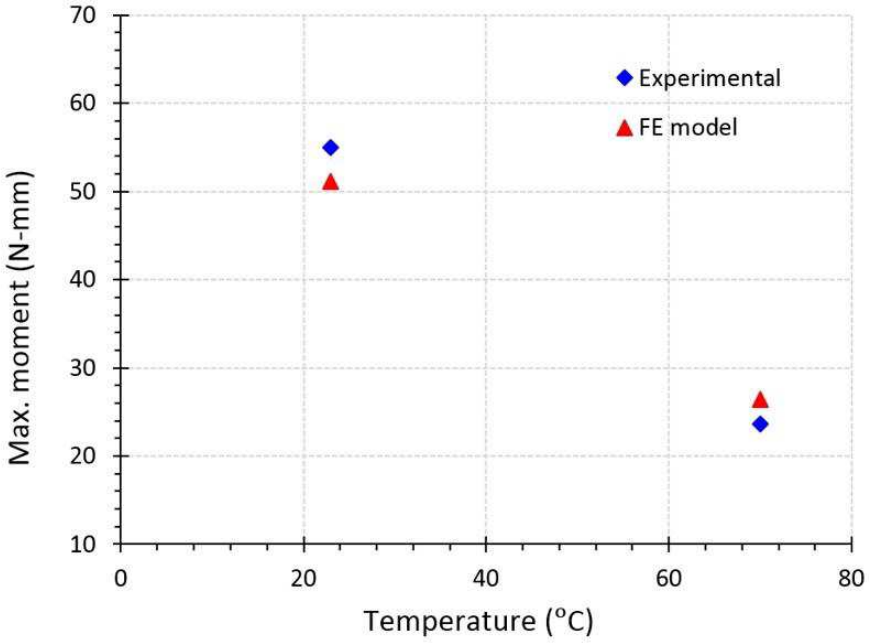

(a)

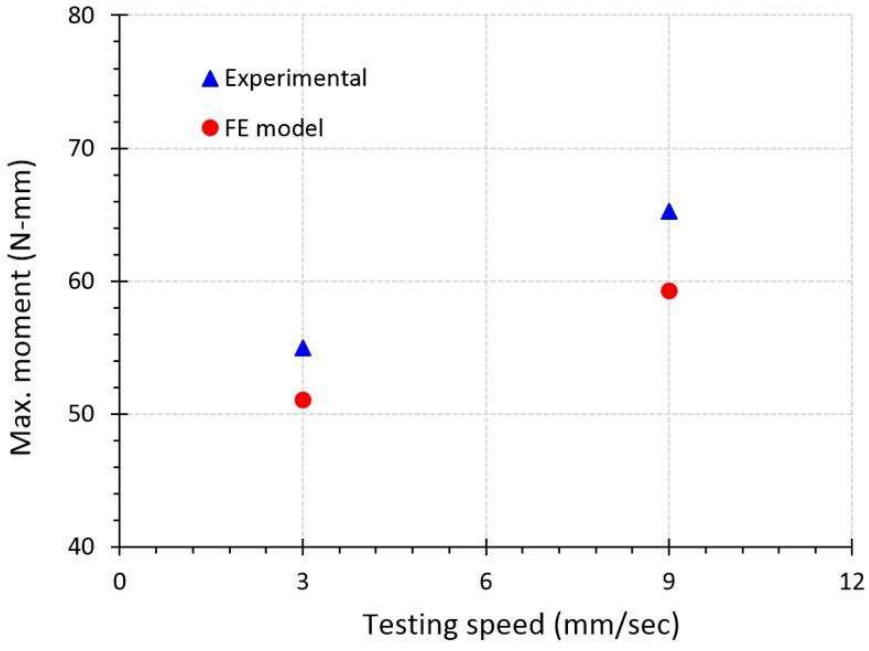

(b)

Figure 4.11: Experimental and FE-model results of maximum bending moment for stacking 1 (a) at different temperatures with a constant speed of 3 mm/s, and (b) at different testing rates.

4.4.3 Influence of alteration of bending material model

The Kelvin–Voigt approach used in this study was compared to an elastic approach in order to study the effect of the material model on the bending behavior. Stacking 1 at a temperature of 70 °C was modeled using an elastic bending model (Isotropic Hooke) with parameters presented in Table 4.2. It was found that the maximum bending moment at the clamp using the elastic model was around 33.27 N-mm. The bending moment was overestimated compared to experimental data (23.62 N-mm) and numerical outcome using the viscoelastic approach (26.4 N-mm). The difference between the values from the elastic vs. the viscoelastic approach is about 23%. Although considering other viscoelastic models, such as generalized Maxwell, may help to improve prediction of the bending behavior, as documented by [29], the Kelvin–Voigt model in AniForm is reasonably sufficient to predict the bending behavior of multilayered textile prepregs. However, the simulation outcomes are highly dependent on the input data. This can be seen by the different results obtained at 70 °C and room temperature as well as in the forming simulation presented below.

4.5 Application in forming simulation

The forming simulation was conducted over a geometry provided by AniForm software [32]. The boundary conditions considered in this simulation are related to the stamp forming process. Thus, the female tool was fixed, while the male tool was moved downwards. Note that no blank holder boundaries were used in this simulations run. The aforementioned material models were used with the same parameters presented in Tables 4.1, 4.2, and 4.3. Note that the ply–tool properties in this simulation was set as half of the inter-ply friction properties. Two different cases were considered. First, the effect of bending parameters on forming results was studied using a single ply with fine mesh in order to capture wrinkle formations. Second, the forming simulation process was performed for all four stacking sequences. Each ply in multiple stacked plies was meshed with 10206 elements and grid size of 6.1 mm to reduce the simulation time.

4.5.1 Case 1

To investigate the effect of bending stiffness on out-of-plane wrinkles, two different values of bending stiffness were selected: experimental value (see Table 4.2) and a factor of 0.3. Initially, Figure 4.12 (a) shows the forming simulation results with experimental bending parameters. The simulation results with bending stiffness multiplied by 0.3 are depicted in Figure 4.12 (b). Two different forming results were observed in terms of wrinkle formations simply by changing the bending parameters. The forming simulation with low bending stiffness resulted in a high number of wrinkles. Reduction in bending stiffness decreases the resistance to compressive loading in the material plane, which may cause out-of-plane deformation (wrinkling). When the compressive stress exceeds a critical limit, wrinkling occurs [17]. In contrast, an increase in bending stiffness exhibited a lower number of wrinkles. These findings are also reported in the literature for different forming geometries [7,11,24]. Therefore, to obtain useful results, the true experimental bending stiffness rather than an estimated guess must be used in the forming simulation.

It is shown that the shear angle distributions within the formed part are also influenced by the bending stiffness values (see Figure 4.13 (a) and (b)). Although the contour plots of lower and experimental bending stiffness showed similar maximum shear angle locations, the magnitude of shear angles was smaller for cases of lower bending stiffness. One possible reason for this deviation is that an increase in bending stiffness can prevent the ply from out-of-plane deformation, thereby transferring this deformation into in-plane shear within the ply. This may indicate that a higher bending stiffness can increase the limit of shear deformation, ultimately providing a reduction in wrinkling. However, use of too high bending stiffness during forming simulation may prevent the material to accommodate correctly the required shape. Moreover, it should be noticed that the maximum shear angles obtained are lower than the locking angle investigated by the authors in [15, 80]. Thus, the locking angle alone is not sufficient to be a wrinkling indicator. These findings strongly suggest that the relationship between the bending properties and other deformations (intra-ply and inter-ply friction) should be explored, as the wrinkle prediction is highly dependent on these

combined properties, particularly for multilayered textile prepregs. Consequently, in case 2 presented below, an attempt is made to draw attention to the relation between the observed defects and those combined properties for selected stacked plies.

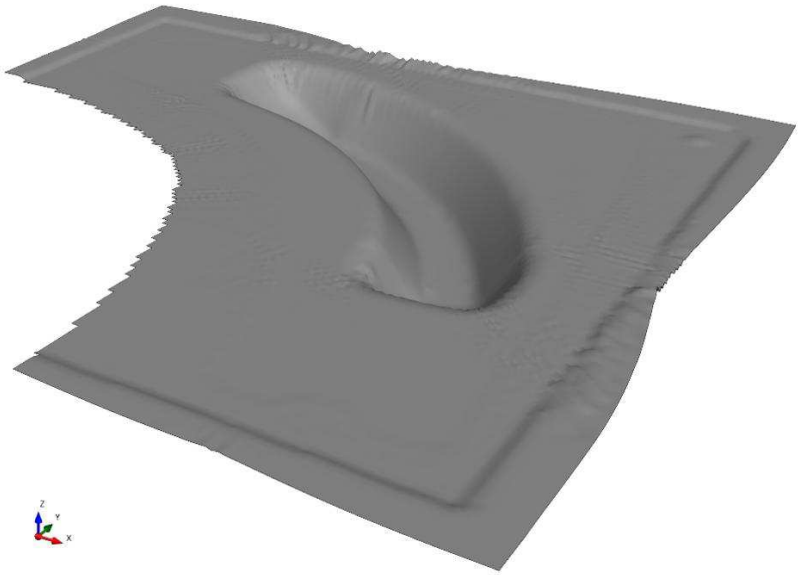

(a) Experimental bending stiffness value

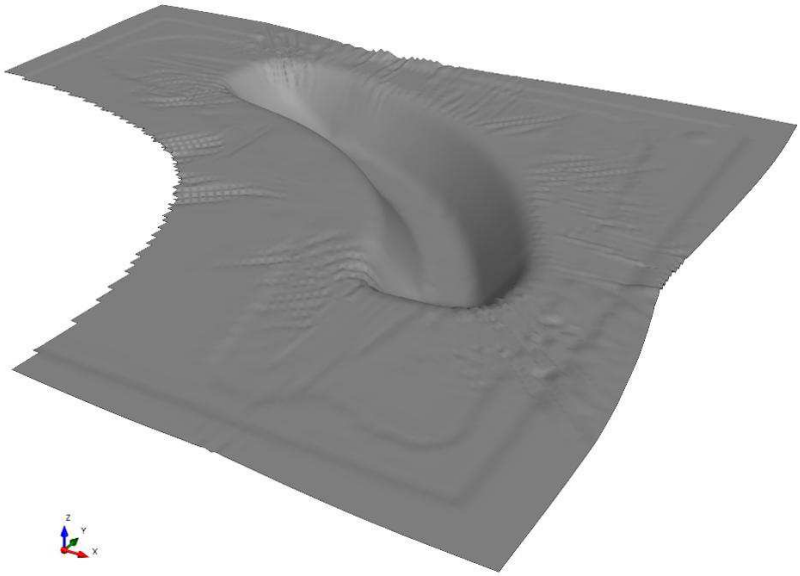

(b) Experimental value multiplied by 0.3

Figure 4.12: Sensitivity of bending stiffness on forming simulation results (a) experimental bending stiffness, and (b) experimental bending stiffness multiplied by 0.3.

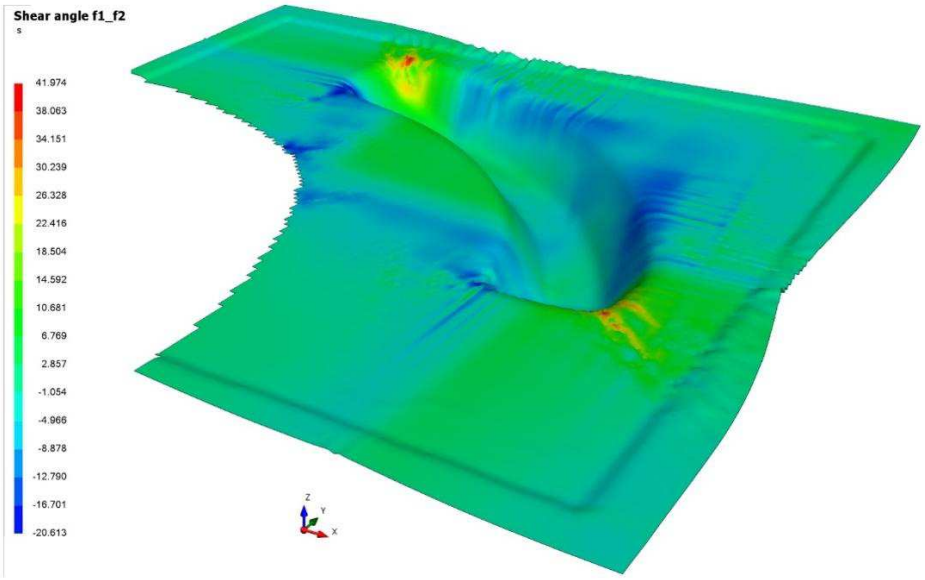

(a) Experimental bending stiffness value

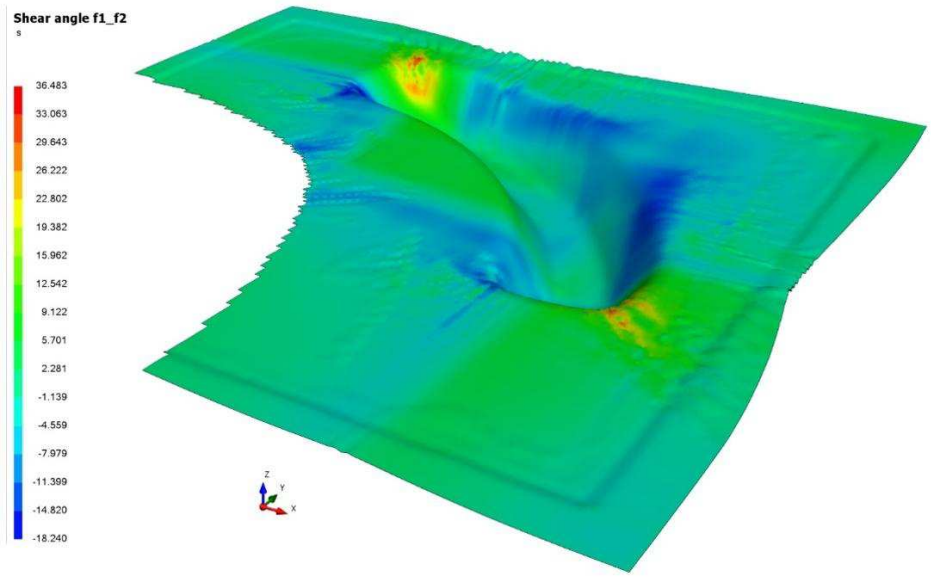

(b) Experimental value multiplied by 0.3

Figure 4.13: Intra-ply shear angles within the formed part (a) experimental bending stiffness, and (b) experimental bending stiffness multiplied by 0.3.

4.5.2 Case 2

The forming predictions for all four stacking sequences over selected geometry are shown in Figure 4.14. Only small wrinkles and waviness are found in stacking 1 [0, 90, 0], as can be seen in Figure 4.14 (a). Although stacking 2 and 3 showed similar amounts of wrinkle formations, as well as their locations, the size of wrinkles differs, especially in the wrinkles positioned in the right and top flanges. This can be interpreted as the relative orientations between neighboring plies in stacking 2 and 3 are similar, i.e., the difference in the amount of inter-ply friction between + 45° and – 45° with respect to 0° is quite small. Moreover, the bending properties of these two stacked plies using the FE model are in the same amount of magnitude (see Section 4.4.2). Figure 4.14 (d) visualizes the simulation results for stacking 4; more wrinkles and other defects, such as delamination between the plies, were observed. Note that ply 2 and ply 3 in stacking 4 are stacked opposite each other.

In order to further point out the effect of ply orientations on forming outcomes, Figure 4.15 illustrates the distribution of shear angles in each ply. Different responses between selected stacking sequences as well as the plies within each sequence were observed. Figure 4.15 (a) shows the shear angles of stacking 1. A slight difference in in-plane deformation was found between the plies that oriented in the same direction (see ply 1 and 3 in Figure 4.15 (a)). Ply 2 shows the inverse value of shear angles with relatively similar order of magnitude. This is expected as the second ply is oriented by 90° with respect to first and third plies. The contour plots of plies for stacking 2 and 3 are shown in Figure 4.15 (b) and (c). The results show that the maximum obtained shear angles and their locations are close to each other. This observation is probably related to the fact that the bending and friction properties of stacking 2 and 3 are comparatively identical. However, the bending experimental results showed minor differences between them. Figure 4.15 (d) visualizes the shear angles in plies within stacking 4. The resulting plots of ply 1 and 2 do follow the results obtained for stacking 2 and 3. However, ply 3 shows different results in terms of value of maximum shear angles and the final shape, as seen in the top and right flanges of Figure 4.15 (d).

In all cases, high bending stiffness along with low friction between the plies reduce the risk of wrinkling. In addition, as shown in cases 1 and 2, the limit of shear deformation (shear angles) tends to increase as the bending stiffness increases, which ultimately provides a reduction in wrinkling. This finding is in accordance with the experimental observations for all four stacking sequences. For example, stacking 1 had the highest bending stiffness compared to other stacking sequences and resulted in less wrinkling. The orientation between the plies, which plays an important role in terms of frictional resistance as shown in [18], also contributed to the wrinkle formations. As the plies are oriented in the same direction of sliding, which slides along the yarns, a higher force of friction is expected. Consequently, the rotation of fibers inside the laminate eased the sliding and thus decreased the frictional resistance. Murtagh et al. [81] reported that the resin flow across the fibers is easier than flow along the fiber direction due to the higher apparent viscosity of the resin in the fiber direction, compared with the transverse direction. However, this effect needs to be explored through microscope investigations; it will be considered in a future study. In woven fabric prepregs, the space between yarns is filled with the resin, which facilitates the intra-ply shear and ply-ply friction. On the contrary, for UD prepregs, many fibers are in contact, inducing high resistance against these deformations [7]. Note that to produce free-defect parts, a balance between these deformation modes during the forming is required, as indicated in [7]. Also, the boundary conditions in the forming process, such as tool geometry, processing parameters, and process type, impact the forming results. Therefore, further investigations using different tool geometries and different stacking sequences will allow for clearer conclusions to be drawn about the balance between these important deformation modes as well as their influences on the observed defects.

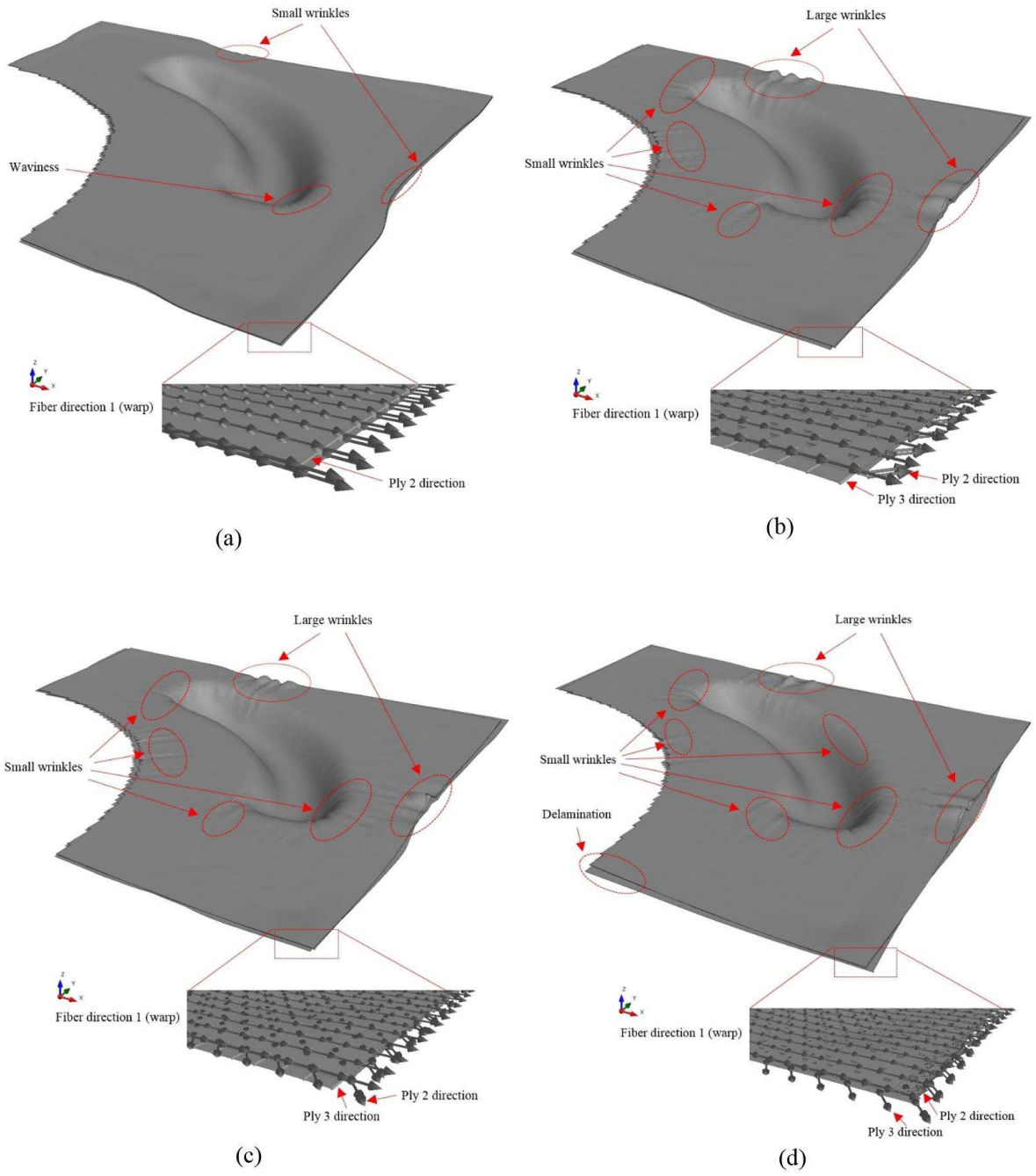

Figure 4.14: Forming simulation results with observed defects (a) stacking 1, (b) stacking 2, (c) stacking 3, and (d) stacking 4.

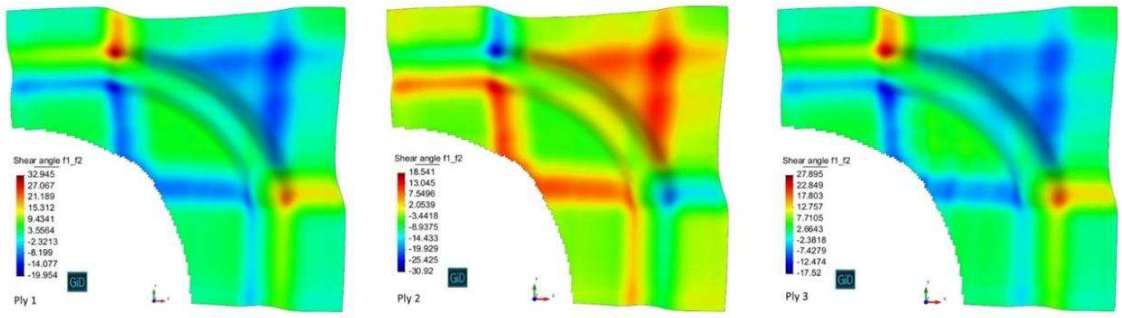

(a) Stacking 1

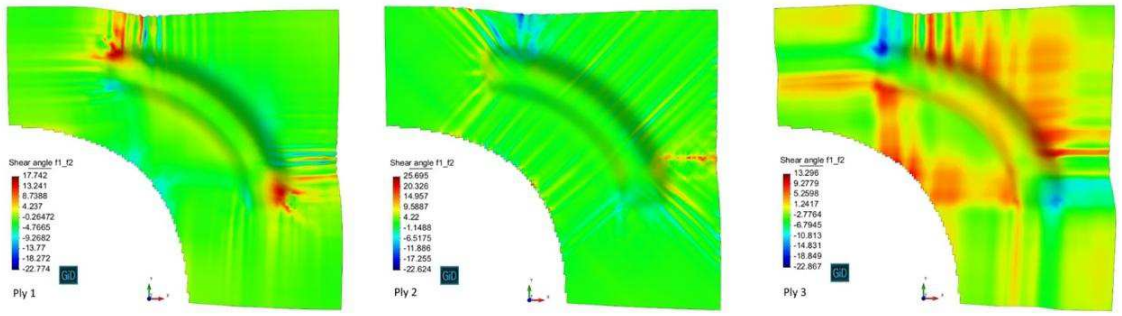

(b) Stacking 2

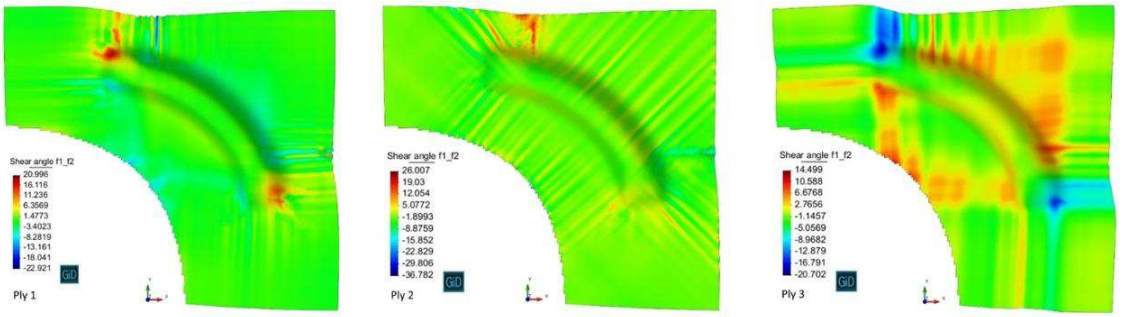

(c) Stacking 3

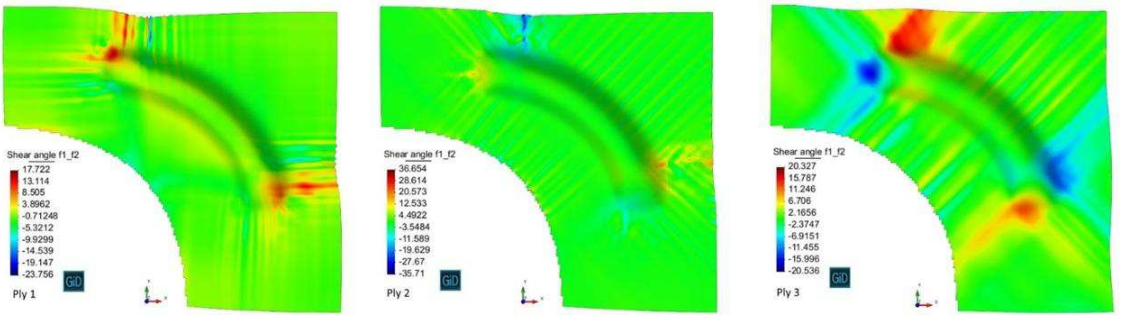

(d) Stacking 4

Figure 4.15: Intra-ply shear angles in each ply (a) stacking 1, (b) stacking 2, (c) stacking 3, and (d) stacking 4.

4.6 Conclusion

A finite element model based on a viscoelastic approach was developed to predict the bending behavior of multilayered textile thermosetting composite prepregs at different processing parameters, including temperature and rate. The experimental and numerical results revealed that the bending properties strongly depend on the fabric lay-up inside multiple stacked plies. The predicted bending properties were found to be in good agreement with the experimental results for selected stacking sequences. However, the FE model gave the same results for stacking 2 [0, + 45, 90] and stacking 3 [0, – 45, 90], while the experimental measurements showed some differences. This difference may be due to the inherent undulation between yarns in woven-fabric structures. A notable difference in bending behavior was observed after comparing Kelvin–Voigt and elastic material models. Moreover, bending behavior is also influenced by the friction between plies, which plays an important role in terms of facilitating the through thickness shearing during the bending experiments at processing temperature.

The forming simulation outcomes showed that high bending stiffness along with low friction between the plies may help to increase the limit of shear deformation (shear angles), ultimately providing a reduction in wrinkling. However, future work needs to be conducted using different tool geometries and different stacking sequences to verify the relation between the observed defects and those combined properties for multiple stacked plies.

Chapter 5

Experimental and numerical investigations on formability of out-of-autoclave thermoset prepreg using a double diaphragm process*

Abstract

The formability of textile out-of-autoclave thermoset prepreg using double diaphragm forming has been investigated to produce a component for aerospace applications. A one-step procedure has been used for both the forming and curing processes using the same experimental set-up. A finite element model has been developed to simulate the double diaphragm forming process, with consideration for the diaphragm material properties at forming conditions. To identify potential causes for wrinkle development, important considerations, such as local fiber compressive stresses, shear angle distributions, and stacking lay-up sequences, have been analyzed. Furthermore, different forming simulation scenarios were applied to reduce the wrinkle defects. Results indicate that a change in lay-up sequences significantly affects the formability; thus, wrinkle formations cannot be avoided at challenging locations for some lay-up arrangements. The forming simulations are in agreement with the experimental results in terms of prediction of large wrinkles and intra-ply shear. Meanwhile, high local compressive stress regions provide a good indication for where the critical areas appear, which can be considered when the small wrinkles cannot be predicted with the element size used.

*Reproduced from: Hassan Alshahrani, Mehdi Hojjati. Experimental and numerical investigations on formability of out-of-autoclave thermoset prepreg using a double diaphragm process. Composites Part A: Applied Science and Manufacturing, 101 (2017), pp. 199–214. https://doi.org/10.1016/j.compositesa.2017.06.021

5.1 Introduction

Composite materials can be produced by applying different manufacturing techniques. Conventional composite manufacturing techniques, such as hand lay-up, are labor-intensive, time-consuming, costly, and less productive than other techniques [6]. Automated manufacturing processes are promising methods in aerospace and automotive industries because of their low manufacturing time and lower cost [33]. However, due to geometric limitations of automated tape laying (ATL) and automated fiber placement (AFP), an additional step is required to form complex shapes. This forming step involves the application of heat and pressure to transform flat laminates into the desired shape prior to curing [6, 82]. The most important sheet-forming processes for composite materials are the diaphragm (single or double) and stamp forming methods [3, 4]. Both processes exhibit high efficiency and high productivity during formation. However, the stamp forming process is very expensive due to its need for two close-tolerance dies for each shape. Krebs et al. [83] conducted a direct comparison between matched-die press and diaphragm forming using thermoplastic composite. They found that matched-die forming produces a better surface finish and the flange thickness variation is slightly less severe compared to diaphragm forming. At the same time, however, the matched-die forming restricts the material movement, which may lead to out-of-plane buckling.

Double–Diaphragm Forming (DDF) is a thermoforming process that was initially applied to thermoplastic matrix composites [84]. In the DDF process, composite prepreg plies are placed between two deformable sheets known as diaphragms. The diaphragms are then clamped, heated with the laminate to the processing temperature, and formed to the mold by applying vacuum pressure from beneath the lower diaphragm and/or positive pressure on the top [85]. Vacuum pressure is generally used for forming thermosets [86]. During the initial step of the forming process, the laminate must be in a flat and tension state to avoid any compression that may lead to wrinkling [11]. Hence, the vacuum pressure is applied between two diaphragms, inducing the clamping force during the pre–heating process. This clamping force plays an important role in avoiding wrinkle formations as shown in [87].

Polymeric diaphragms are most commonly used because of their ability to deform without rupturing under high processing temperatures [88]. As recently was reported in [86], the deformation modes and the defects raised during the forming process are also dependent on the diaphragm material type. However, the choice of diaphragm materials is limited by the commercial availability of the desired properties.

Most previous research [88–92] has focused on diaphragm forming processes that use thermoplastic prepregs. These studies have shown that forming the thermoplastic prepreg can be influenced by processing parameters, tool geometries, and diaphragm materials. Recently, this process has been used in forming thermoset prepregs [19, 52, 80, 93]. In the diaphragm forming of thermosetting prepregs, the matrix is only heated enough to decrease its viscosity to the point where the prepreg can be formed readily. Thereafter, the curing process usually takes place in an oven or autoclave.

A forming simulation based on Finite Element (FE) methods allows for determination of suitable process parameters without the requirement of expensive trial and error tests. Moreover, potential material defects during forming can be predicted, which assist designers in reliably choosing appropriate material types and processing parameters for complex structure. However, a considerable amount of knowledge of the mechanical behavior of prepreg ply and accurate material properties inputs are required to obtain precise forming predictions [47, 94]. In the diaphragm forming simulation, the diaphragm material was modeled in the literature based on the Mooney-Rivlin model [77], plastic model [95], or Ogden model [86]. However, an important challenge is to capture the behavior and forming properties of the diaphragms and the prepreg sheets, including their out-of-plane bending properties. Currently, the bending properties of diaphragm materials that can be used in DDF process simulation are unavailable. Furthermore, as shown in an earlier study [80], the diaphragm material stiffness decreases as temperature increases, allowing for better tool conformity. Thus, besides the prepreg material models and properties, the diaphragm properties at forming conditions must be accurately represented in the FE model.

The current work aims to experimentally and numerically investigate the formability of out-of-autoclave thermoset prepreg over a complex geometry for aerospace applications

using a DDF process. An evaluation of the DDF process in terms of observed defects, stacking sequences, and pre-forming state is carried out. In the present study, out-of-autoclave (OOA) prepregs are used to reduce overall processing time and cost. Therefore, the proposed double-diaphragm setup can fully accommodate the forming and curing steps of the process, thus bypassing the need for an oven. The diaphragm and prepreg material properties at forming conditions, including their out-of-plane bending properties, are considered in the FE model.

5.2 Forming experiment methodology

5.2.1 Double-Diaphragm Forming (DDF) setup

A custom-built DDF setup was developed, which consists of three main parts: DD tool, vacuum system, and heating system, as shown in Figure 5.1 (a) and (b). DD tool involves two deformable silicone rubber diaphragms, manufactured by Torr Technologies Inc., with a thickness of 1.6 mm. The vacuum pressure between the two diaphragms was applied within DD tool using secured frames with a vacuum port connected to the vacuum pump, as shown in Figure 5.1 (c). Note that a control valve and vacuum gage were used to monitor the pressure that is applied between the diaphragms. Figure 5.1 (d) shows the vacuum box with a movable plate inside designed to control the height of the tool with respect to the lower diaphragm. To achieve the necessary processing temperatures, a radiant heater from WATLOW and thermocouples were used, as seen in Figure 5.1 (e). Moreover, the DD setup has an additional feature where the vacuum box can be adjusted using two electronic jacks to ensure a closed chamber with the heater during the curing process.

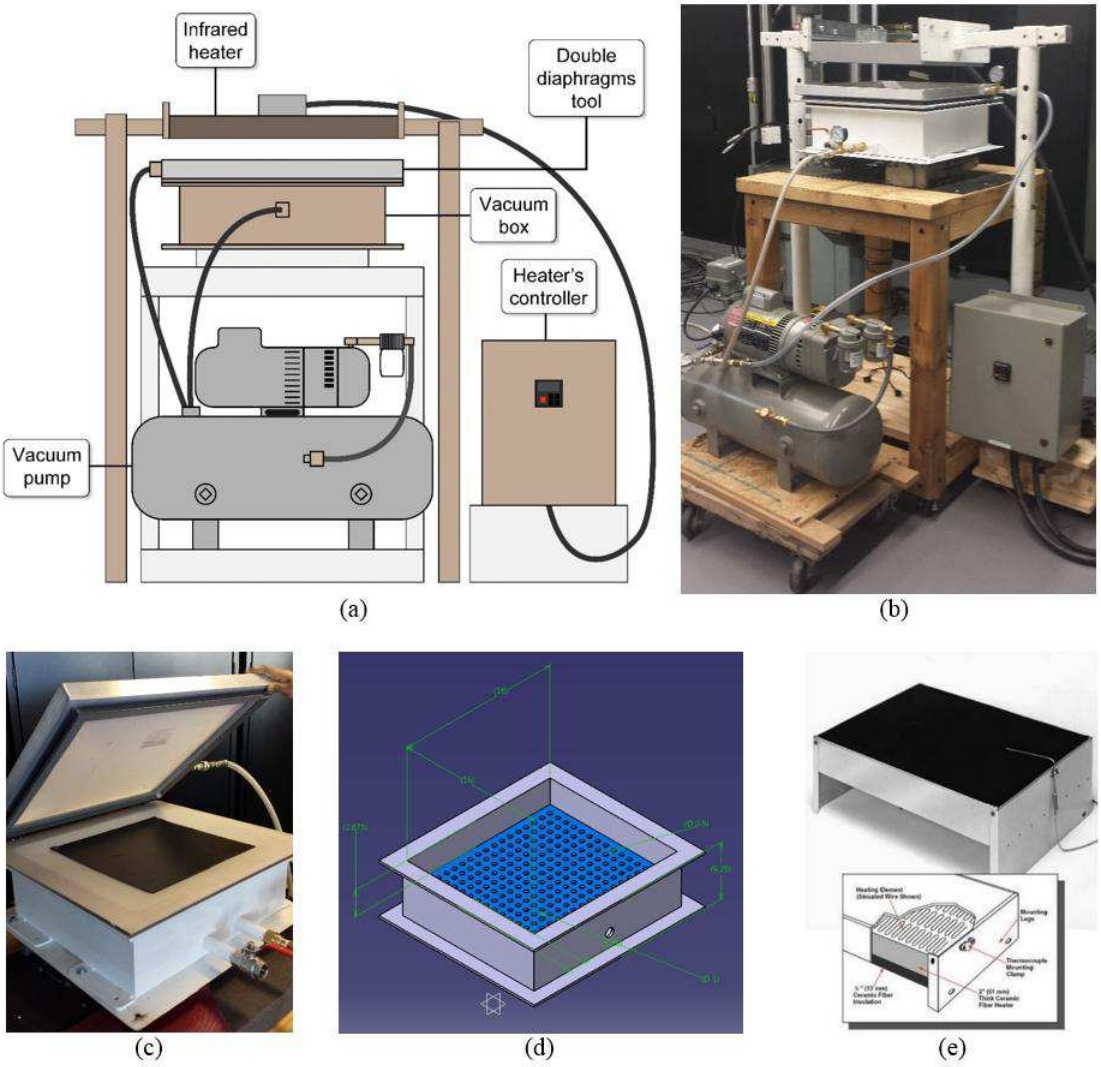

Figure 5.1: Double diaphragm forming setup: (a) schematic, (b) photograph, (c) DD tool, (d) vacuum box, and (e) radiant heater.

5.2.2 Tool geometry

In this work, a complex aerospace part (flap track fairing), as shown in Figure 5.2, was selected. The part shape includes highly-curved single and double curvature areas and asymmetric heights. Accordingly, the prepreg ply requires large shear and bending deformations to accommodate the tool shape; otherwise, wrinkles may occur. Furthermore, the capabilities of the DDF process in terms of producing high-complexity parts can be examined, particularly at the challenging curved flanges.

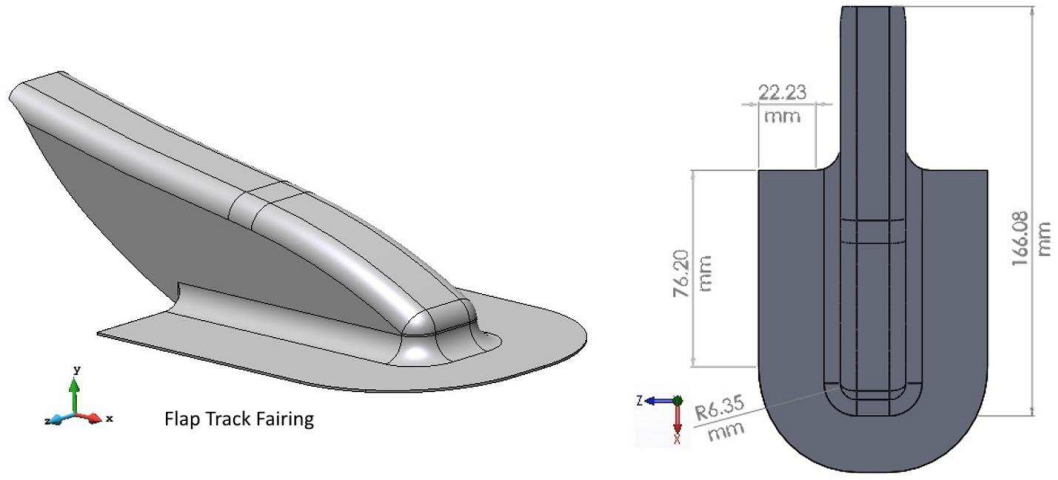

Figure 5.2: . Selected tool geometry and its dimensions.

5.2.3 Materials

The material studied in the current study is a 5-Harness Satin (5HS) carbon/epoxy OOA prepreg. The fabric has 6K fibers per tow with an areal weight of 380 g/m^2. The toughened epoxy resin (Cycom 5320) is designed for vacuum-bag-only (VBO) or OOA applications due to its lower curing temperature, which ultimately provides a reduction in manufacturing cost. The resin content is 36% by weight and the thickness of the uncured ply is approximately 0.55 mm. The stack sequences used in forming experiments were [0/0], [0/90], and [0/45] with respect to warp yarn direction. A single ply was also tested for comparison's sake.

5.2.4 DDF procedure and conditions

The tool was placed inside the vacuum box and heated for 15 minutes. Afterwards, the prepreg stacks were covered with release films and then positioned between the diaphragms. Prior to forming, the samples were clamped inside the DD tool with a pressure of 0.1 MPa and heated to the processing temperature (70 °C) for 20 minutes. Next, the forming step takes place by applying a vacuum pressure of 0.1 MPa within the box to conform the tool shape. Both forming and curing were performed sequentially using the same forming setup.

Once the forming step was done, the vacuum box was moved up to make a closed chamber with the heater, and the temperature was raised to the curing temperature (121 °C), as recommended by the manufacturer. All the formed parts were kept for 60 minutes at the same curing temperature and conditions. The temperature cycle during the forming and curing processes is shown in Figure 5.3. After the cooling process completed, the formed parts were removed and macroscopically checked for observed defects, and fiber angles.

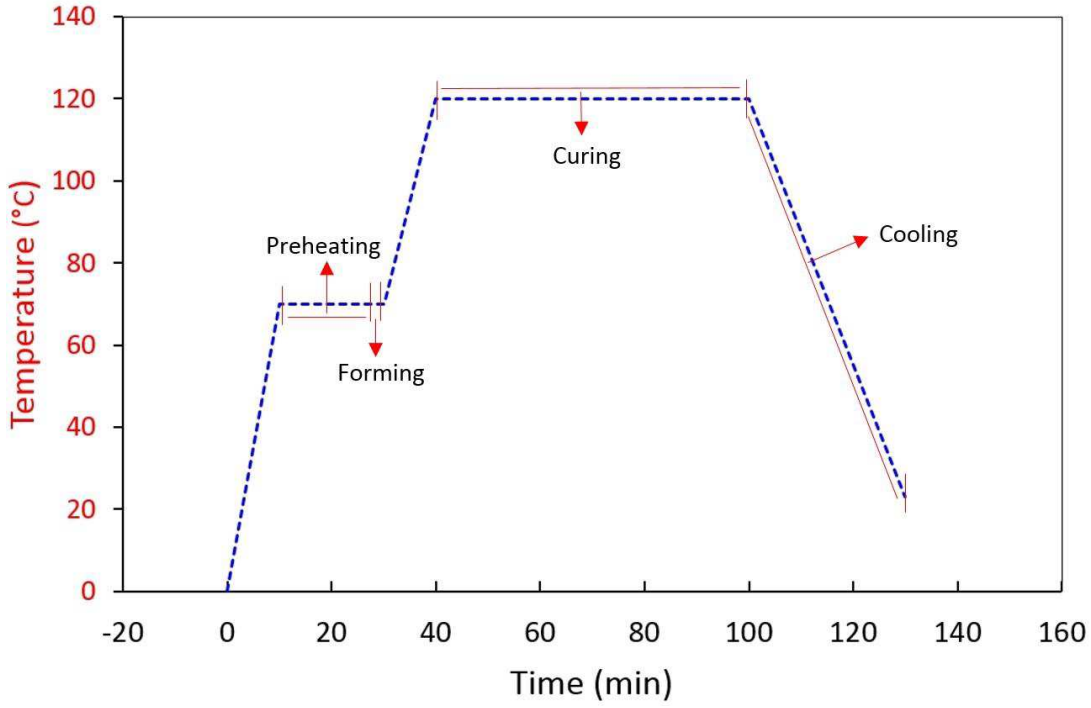

Figure 5.3: Applied temperature cycle during forming and curing processes.

5.3 Material characterization

5.3.1 Prepreg forming properties

The intra-ply shear properties of the selected materials have been characterized over a range of processing temperatures by the authors in [15, 74] using a bias extension test and a non-contacted infrared heater. The results of the bias extension test at 70 °C with a displacement rate of 20 mm/min are presented in Figure 5.4. The initial stiffness variation

is very low, particularly up to a displacement of 15 mm. The in-plane shear deformation continues until the shear angle between weft and warp becomes locked. The shear stiffness increases rapidly as the adjacent yarns start to compress each other (locking angle). According to the measured shear angles during the test, the locking angle of the tested material was approximately 48°; however, inter-yarn slippage was observed on the sample before this angle was reached. It should be noted that the locking angle cannot be the only factor that predicts wrinkling, as shown in [11,80], but it could be one of a number of causes.

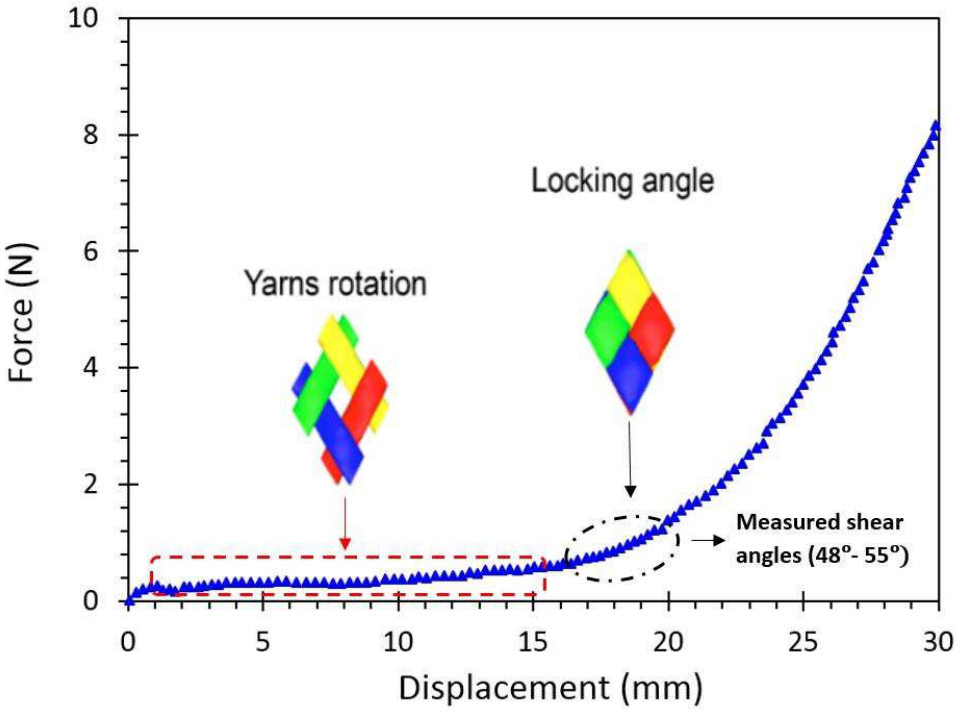

Figure 5.4: Bias extension load-displacement response at 70 °C with a displacement rate of 20 mm/min.

The bending behavior of the selected material at forming conditions was carried out using a new test method developed by the authors, see [56, 73] for more details. In this test method, the sample deflection and applied rate were controlled by a linear actuator while the load required to achieve this deflection was recorded by a miniature-load cell. Consequently, this method allows for investigation into the rate and viscoelastic effects of

time-dependent materials. A non-contact radiant heater was used during the elevated temperature tests. The bending properties of one ply tested with respect to warp yarn direction at 70 °C and a tip displacement of 30 mm are shown in Figure 5.5. Note that the samples face, where 80% of the fibers are in the strip-long direction, was in tension during the bending test. As shown in [56], the bending behavior of the selected prepregs is rate-dependent and is significantly influenced by the processing temperatures. The ply bending stiffness as a function of rate and temperature can be determined using the thermo-viscoelastic model developed in a previous study (see Ref. [73]).

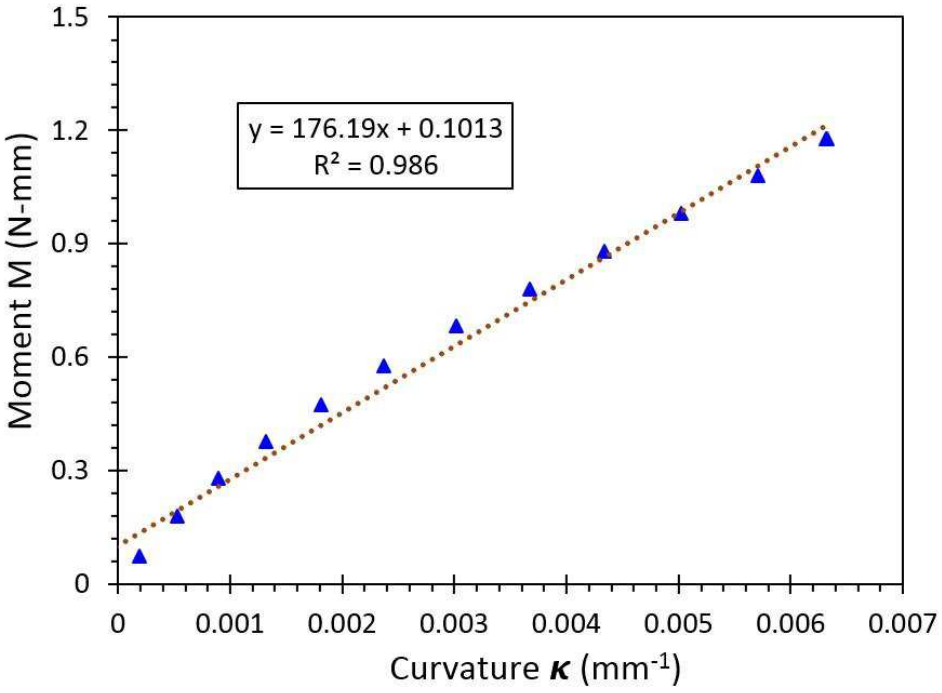

Figure 5.5: Bending properties of one ply tested with respect to warp yarn direction at 70 °C.

The ply-ply friction properties of the materials were measured using the same method as described previously in [18]. The friction setup consists of a steel middle plate and two platens that apply normal pressure to the samples. Different temperatures and different normal pressures can be applied to the prepreg sample by using three cartridge heaters and four springs, respectively. The friction setup was mounted on a tensile testing machine,

which measures the frictional resistance at different pulling rates. It was observed that frictional load reaches a maximum value, then gradually decreases to a steady state. The coefficient of friction was calculated as the ratio of the friction force to the normal force at the interface. The results of the ply-ply steady state friction coefficients at different pulling rates with 70 °C and a normal pressure of 0.5 atmosphere are shown in Figure 5.6.

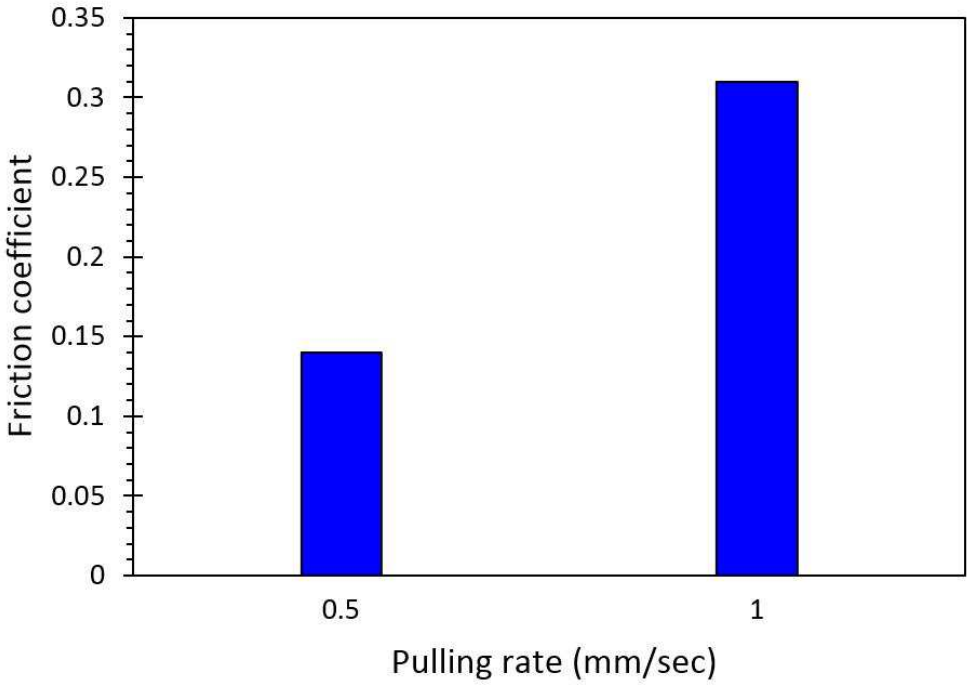

Figure 5.6: Friction coefficients at different pulling rates.

5.3.2 Diaphragm forming properties

The diaphragm material used in this study was a translucent silicone rubber (EL1040T). According to the manufacturer, this material's properties at room temperature are: tensile strength, 12.82 MPa; ultimate elongation, 1300%. A tensile test machine was used to characterize the in-plane behavior of the diaphragm. The sample dimensions were 50 mm (wide) by 100 mm (gauge length). Figure 5.7 shows the stress–strain curve of the silicone rubber material at a temperature of 70 °C, which is the processing temperature used in forming thermosetting composites according to [16, 56].

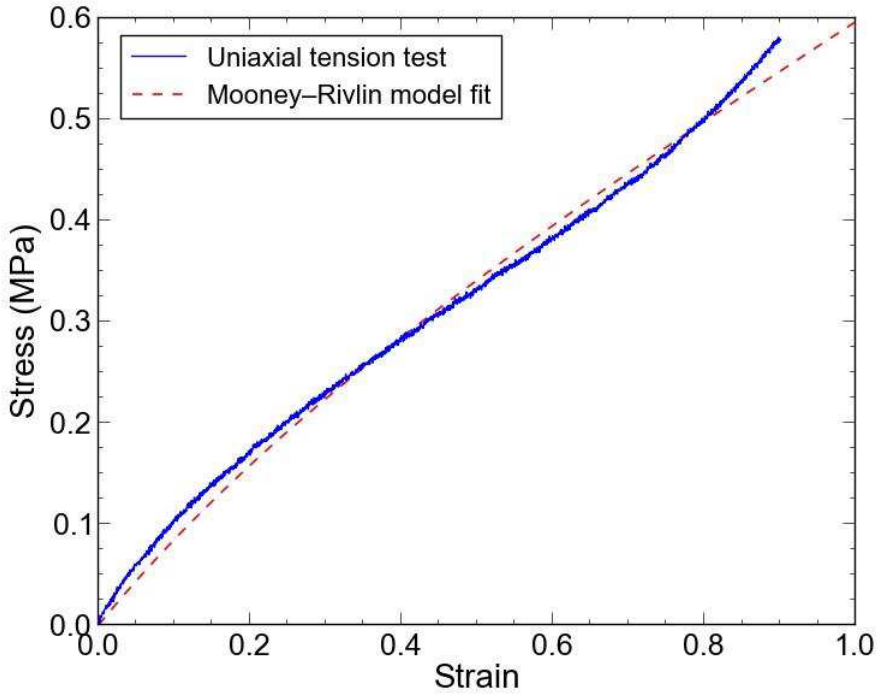

Figure 5.7: In-plane properties of the silicone rubber diaphragm material with Mooney–Rivlin model fit.

The bending properties of the diaphragm material were measured using the same setup as described previously for the bending characterization of the prepreg materials. The results are presented in Figure 5.8. As expected, the bending stiffness for the silicone rubber is very low compared to the prepreg ply. The developed bending setup enabled measurement of the bending properties for these flexible materials because the deflection shape and the small loads can be consistently controlled and recorded.

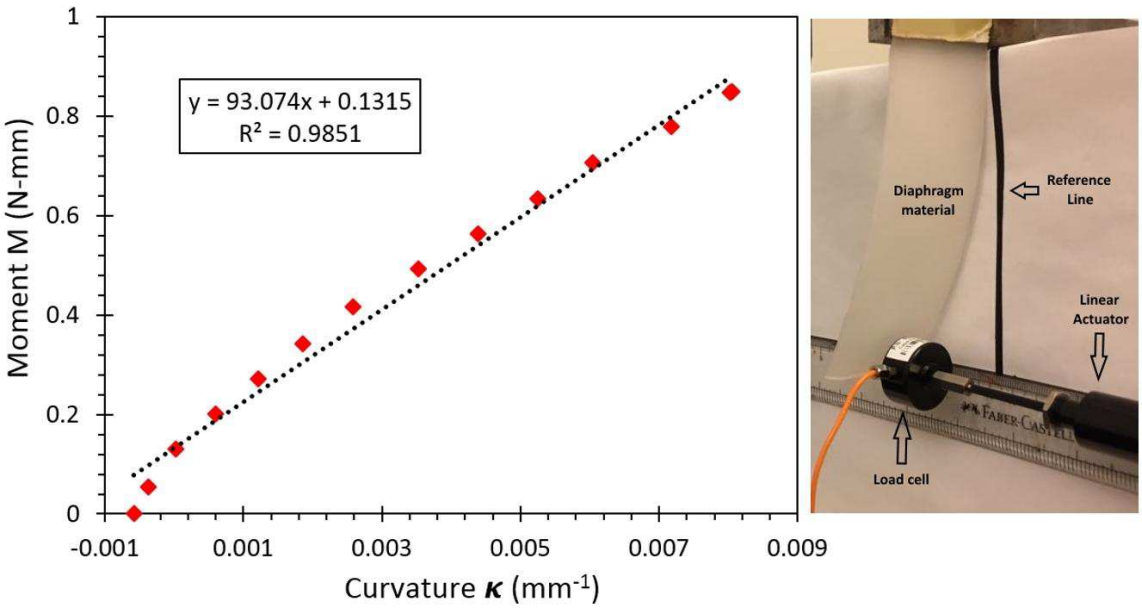

Figure 5.8: Bending properties of the silicone rubber diaphragm material.

In the DD process, the slippage also occurs between the ply-diaphragm and the tool-diaphragm interface. However, the prepreg plies during the DDF process are covered with release films; therefore, a vacuum bag is considered to be the tooling material for measuring the ply-diaphragm friction as described in [18]. The silicone rubber material was used to measure the tool-diaphragm friction. Figure 5.9 shows the load-displacement curve for the tool-diaphragm at 70 °C with a pulling rate of 0.5 mm/sec and a normal pressure of 0.5 atm. The obtained curve shows a stick-slip peak at the starting of the slippage and it significantly decreases to a minimum value before the sampling frequency of the load measurement becomes high. The noise is believed to be due to the silicone rubber elongation properties rather than any stick-slip behavior of the interface. When the normal pressure is applied to the interface area between the silicone rubber and steel middle plate, the silicone rubber elongates in different directions within the compressed interface area. This creates inconsistent pull-out slippage movement with respect to pulling direction during the friction test. Moreover, properly attaching the silicone rubber to the steel middle plate remains a challenging issue. Based on the typical raw data for the measured pulling force for ply-ply interface, the frictional load reaches a maximum value at the starting of the slippage and

it gradually decreases to a steady state value. The static friction of the respective surface interface can be calculated using the peak traction force. While, the steady state value gives the coefficient of sliding friction. However, for the tool-diaphragm interface, coefficient of sliding friction was calculated based on the friction force corresponding to the blue dashed line, shown in Figure 5.9, due to the noise in the load-displacement curve. The calculated coefficient of sliding friction at those selected conditions was 0.10 and 0.08 for the ply-diaphragm and tool-diaphragm interface, respectively.

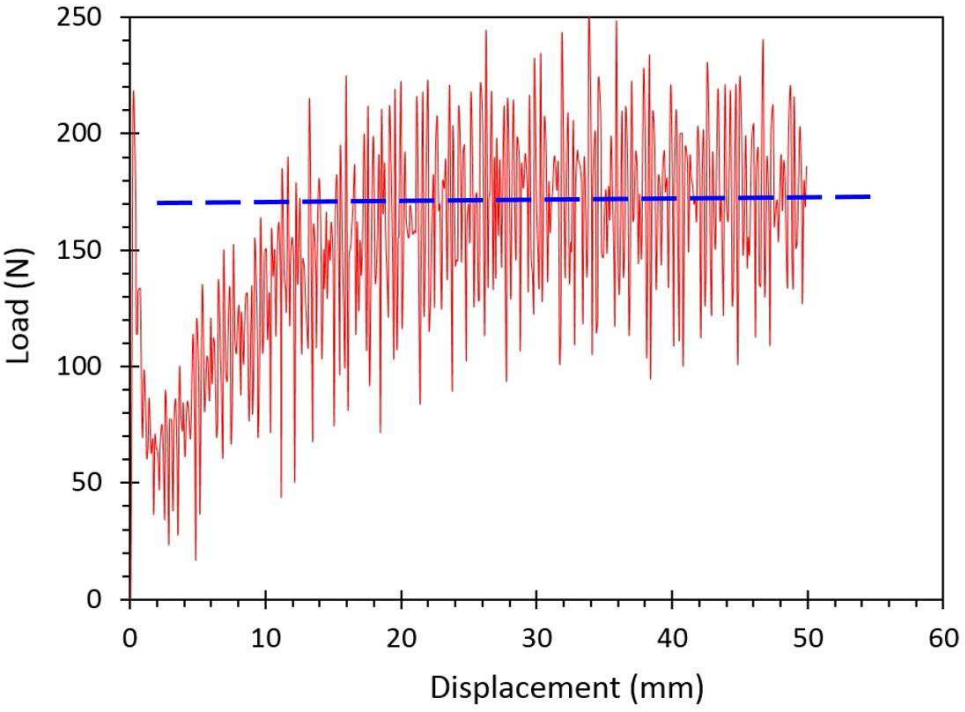

Figure 5.9: Load-displacement curve for the tool-diaphragm friction at the temperature of 70 °C.

5.4 Forming simulation methodology

5.4.1 FE model for DD process

The numerical simulations of the DDF process were conducted using the AniForm software [32]. This software was built based on a continuum mechanical formulation solved by the implicit FE approach. A schematic of the FE model is presented in Figure 5.10. In this model, the simulation geometry consists of a forming tool placed on the top of a fixed base and the DD frame including the upper and lower diaphragms. The prepreg plies were modeled using linear triangle elements coupled with Kirchoff shell elements; consequently, out-of-plane bending properties are separately defined. A mesh of 17,645 elements was utilized for each prepreg ply. Two deformable membranes that behave according to the assigned properties were used to model the upper and lower diaphragm sheets.

Four line grippers were used to secure the boundaries of each diaphragm in the x and y directions (see DD frame in Figure 5.10). The forming tool and the base were modeled as rigid bodies. Fine mesh was employed to describe those areas with higher curvatures in the tool. To model the vacuum between the diaphragms, which generates a clamping force on the prepreg stack during the DD process, equal pressures on the upper and lower diaphragms were applied as shown in the side view of Figure 5.10. After applying pressures on both sides of the diaphragms, the DD frame was moved down (-z direction) to make contact with the fixed base. Next, incremental pressure on top of the upper diaphragm was applied to simulate the vacuum pressure within the forming-box cavity. After 100 increments, a pressure of 0.1 MPa was reached. Results from the material characterization procedures, presented in Section 5.3, were used to determine the required properties for constitutive material models in the numerical simulations.

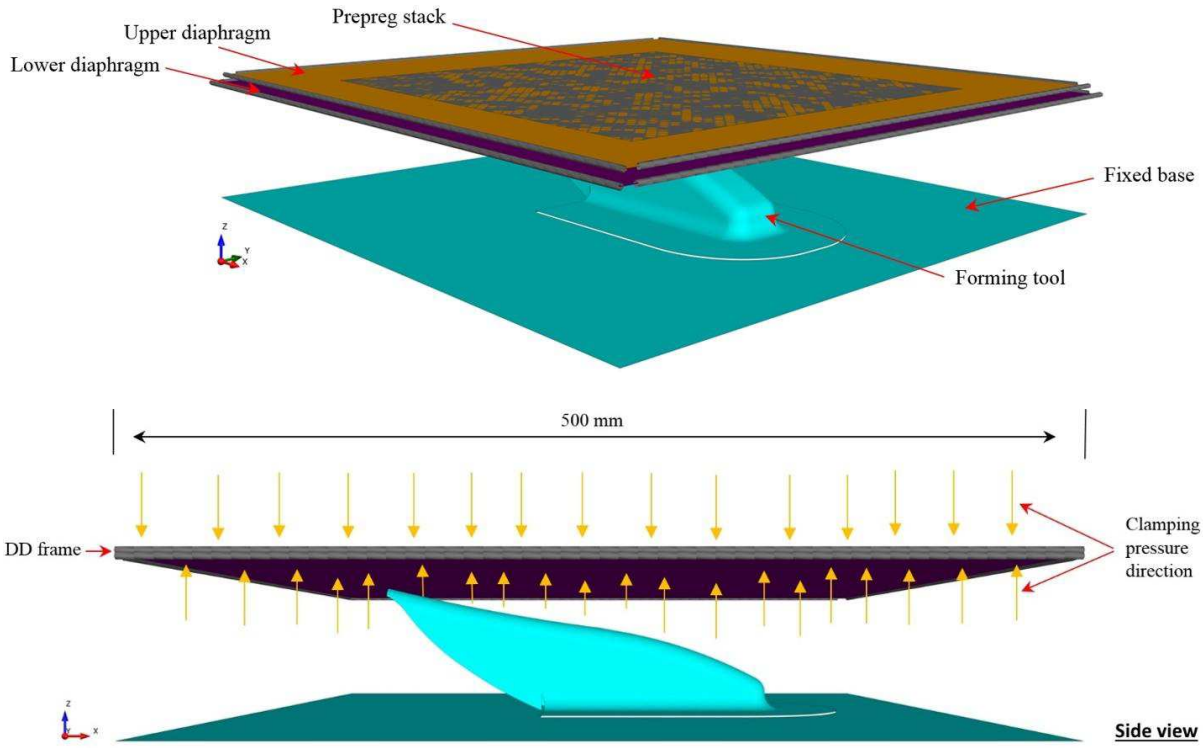

Figure 5.10: Schematic representation of the FE model for double diaphragm forming process.

5.4.2 Material models

The fibers were modeled based on a linear elastic fiber model, while the matrix was modeled using a two–parameter elastic Mooney-Rivlin and a cross viscosity fluid model [7]. Due to the significant differences in stiffness between the carbon fibers and the matrix, the fibers stiffness was downscaled to avoid numerical instabilities [77, 78]. These models were previously calibrated against bias extension test results in [96]. In-plane properties of the diaphragm material were modeled with a hyperelastic Mooney-Rivlin model and calibrated with the results from a uniaxial tensile test (see Figure 5.7). The fitted parameters for both prepreg and diaphragm materials are presented in Table 5.1.

Because the bending behavior of the selected materials was rate-dependent, the bending stiffness was modeled based on a viscoelastic approach (Kelvin–Voigt). The viscosity value was based on the measured viscosity of the prepreg sample as shown in [16]. The isotropic

formulation of Hooke's law was used to model the bending behavior of the diaphragm material. Table 5.2 represents parameter values used for out-of-plane bending elements.

A combination of Coulomb friction and viscous friction was used to model the ply-ply and ply–diaphragm frictions. The viscous friction is based on the presence of fluid film between the contact surfaces. The viscosity value of the fluid film at the processing temperature was based on the measured neat resin viscosity of the epoxy resin (Cycom 5320) according to [79]. In addition, an adhesion model was also applied to model the tackiness between surfaces. Tool–diaphragm (lower) friction properties were modeled as a penalty with Coulomb friction using the coefficient of friction presented in Section 5.3.2. All required frictional properties are given in Table 5.3.

Table 5.1: Material model and parameters for in-plane properties.

Material	**Model**	**Parameter**	**Input data**
Prepreg	Elastic fiber model	E_f (MPa)	1000
	Mooney–Rivlin	C_{01} (MPa)	0.00328
		C_{10} (MPa)	0.12
	Cross–viscosity model	η_0 (MPa s)	0.403
		η_∞ (MPa s)	0.0004
		n	0.81
		m	2.87
Diaphragm	Mooney–Rivlin	C_{01} (MPa)	0.136
		C_{10} (MPa)	0.754

Table 5.2: Material model and parameters for out-of-plane properties.

Material	**Model**	**Parameter**	**Input data**
Prepreg	Isotropic Hooke	E (MPa)	275
		ν (-)	0.33
	Viscous model	η (MPa s)	0.09
Diaphragm	Isotropic Hooke	E (MPa)	5.45
		ν (-)	0.33

Table 5.3: Material model and parameters for frictional properties.

Type	**Model**	**Parameter**	**Input data**
Ply–ply	Coulomb–viscous friction	μ (-)	0.14
		η (MPa s)	0.0003
		h (mm)	0.0011
	Adhesion	Tension (MPa)	0.1
Ply–diaphragm	Coulomb–viscous friction	μ (-)	0.10
		η (MPa s)	0.0003
		h (mm)	0.0011
Tool–diaphragm	Penalty model	Penalty stiffness (N/mm^3)	1.0
	Coulomb	μ (-)	0.08

5.5 Results and discussion

5.5.1 Forming experiment results

Selecting a higher temperature within the range of the thermosetting resin helped to increase the degree of formability over a double–curved tool as shown by the authors in an earlier study [80]. Thus, the prepreg stacks were formed over the selected tool under 70 °C as illustrated in Figure 5.11 (a). The forming rate was estimated by dividing the applied pressure in the vacuum box by the forming time [52]. Figures 5.11 (b) and (c) show, respectively, the pre–trimmed and final parts. The final part was divided into several locations, shown in Figure 5.11 (c), to analyze the observed defects.

It was difficult for both the upper and lower diaphragms to reach the exact challenging curved-flanges as shown in Figure 5.11 (a). This produced a distance between the formed surface and the tool at that location (bridging) as shown in Figure 5.11 (d). The clamping forces between the double diaphragms generated a friction force which constrains the material deformation. Also, the forming forces applied in the bridging area may induce local tensile forces in the fibers as reported in [86]. Consequently, the yarns are constrained and the deep cavity could not be reached. However, using thinner diaphragm materials may allow for better tool conformity, particularly with deep concave features. Moreover, it should be noted that when forming proceeded at a slower rate (3.3 kPa/sec), the formed piece was close to the actual shape (less bridging), while it deviated slightly in the case of a higher forming rate (10 kPa/sec). This may be attributed to the rate-dependent behavior of the prepreg, which affects the response of material deformation during the forming process at different applied rates. For example, higher rate yields higher frictional forces between all contact interfaces, so proper sliding is hard to achieve.

Note that the contact between the lower diaphragm and the tool occurs gradually as the selected tool has an irregular height. This reduces the effect that may occur due to the temperature differential between them. All forming experiments indicated that a higher applied pressure (0.1 MPa) within the vacuum box is favorable to accommodate this complex

shape.

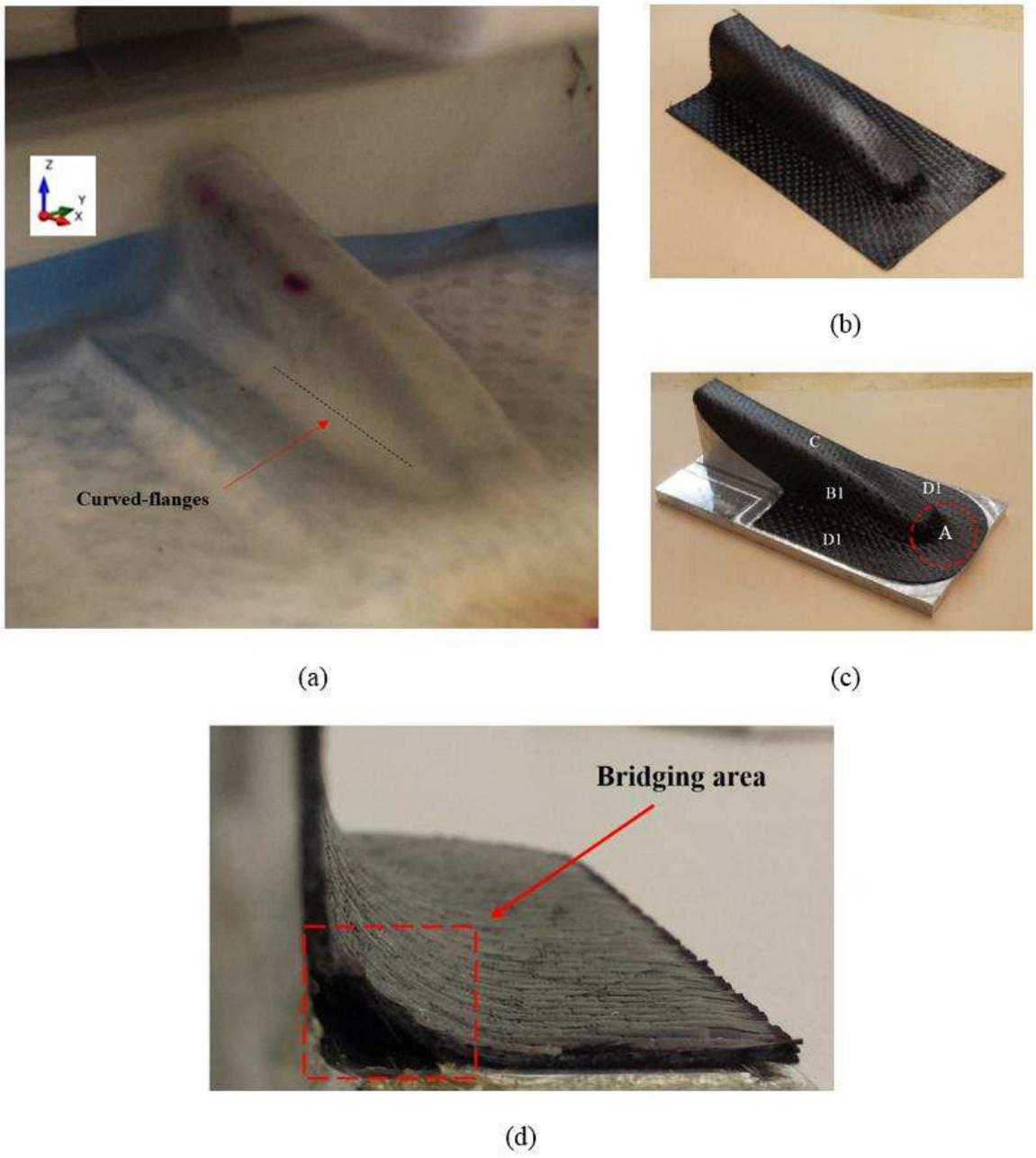

Figure 5.11: (a) Formed part during DDF process, (b) pre-trimmed part, (c) final part, and (d) bridging defect zones.

Figure 5.12 (a) shows a single-ply formed when the warp yarn direction is aligned with the x-direction. The yarns along the warp and weft directions deform largely around the double–curved regions (location A). The maximum shear angle for this sample was found to be 51° at nearby location A. Small wrinkles and waviness were observed at location A (see Figure 5.12 (a)). All other locations in the part have good surface quality. It is seen in Figure 5.12 (b) that rotating the sample by -45° with respect to the x-direction results in large wrinkles and folds throughout the part. The region of observed defects was further concentrated in location A. The magnitude and location of maximum shear angle in this case are shown in Figure 5.12 (b). Also, many yarns are bent in their own plane and are concentrated between locations A and C, unlike sample 1. The folds were also obvious in location B (see Figure 5.12 (b)).

Although the same process conditions were used in both cases, the second sample showed less surface quality and many signs of wrinkles and folds. The reason for this could be explained through results from Ref. [96], which shows that the ply bending stiffness of the [45°] sample with respect to the applied load is lower than the bending stiffness of the [0°] sample. Since the bending stiffness reduced, the compressive loading resistance of the material's plane decreases, which leads to the formation of ply wrinkles and then folds due to the vacuum pressure.

It should be noted that the angle between the warp and weft yarns where the prepreg can no longer deform without buckling is called the locking angle. This locking angle can be determined experimentally as shown in [15, 74], approximately 48° for this material, and could be one reason behind the wrinkle formations at the double-curved section (location A). However, wrinkling in some cases was evident at locations where the maximum shear angle on the formed part was much less than the locking angle. Furthermore, the location of the observed wrinkles is different than the location of the maximum shear angle as can be seen in Figure 5.12 (b). Therefore, the combined properties, including bending and friction, must be considered to understand their effect on the ply wrinkle formations.

These results suggest that the initial fabric orientation (start contact angle) in relation to the applied pressure is an important consideration to minimize the occurrence of the

defects during DDF. In this case, aligning the warp yarn direction to the x-direction gives better forming results for this geometry. However, this conclusion may not hold for other fabric architectures or other tool geometries as the formability of textile composite also depends on the internal weave architecture.

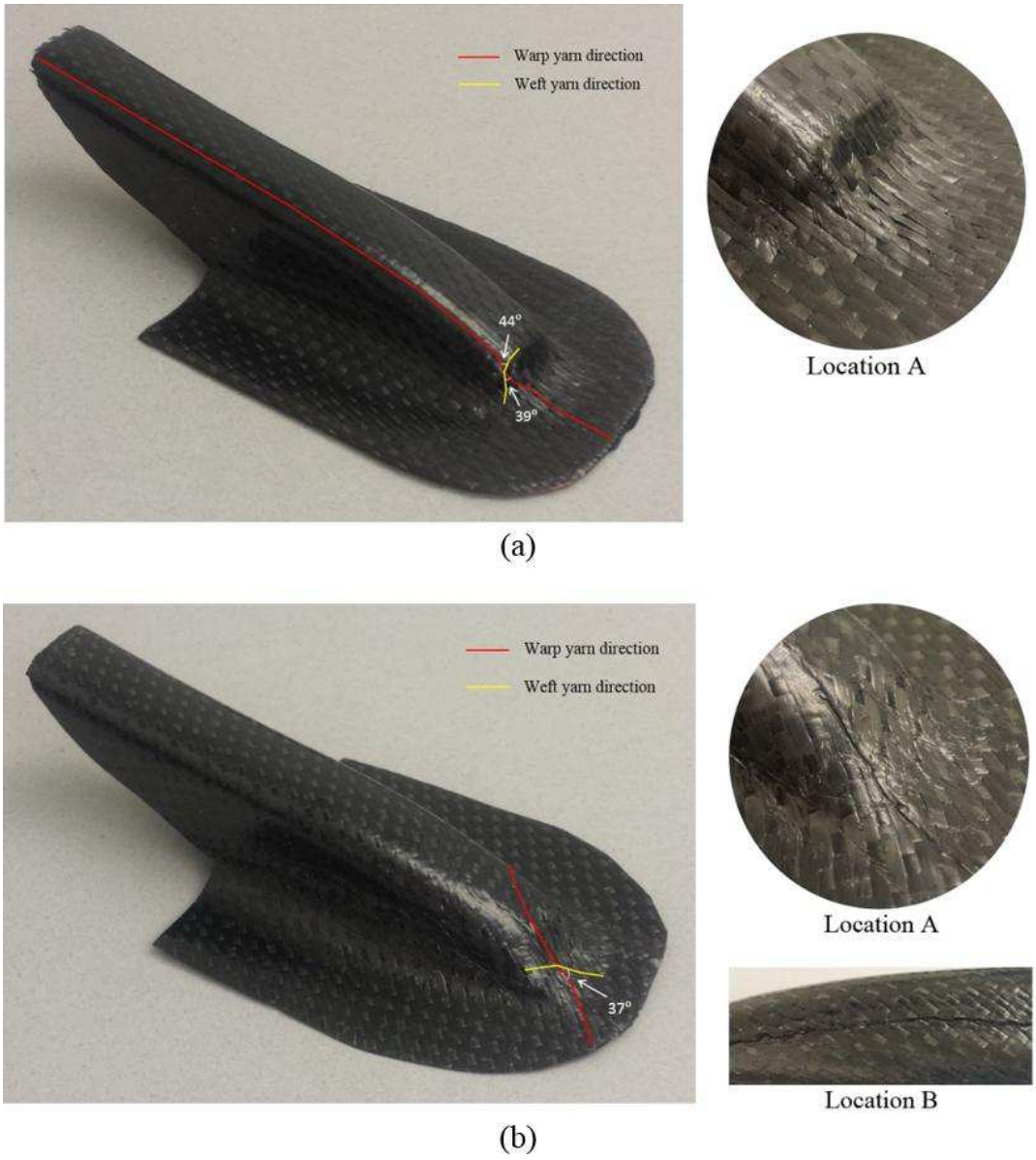

Figure 5.12: Forming results for single ply: (a) warp yarn direction is aligned with the x-direction, and (b) warp yarn direction is rotated by -45° with respect to x-direction.

In two–layered samples, the warp yarn in ply 1 (top) is aligned with the y-direction during DDF experiments. Visual inspection of all three samples formed under the same conditions shows different surface quality and size of wrinkles as shown in Figures 5.13 (a), (b), and (c) for stacking sequences [0/0], [0/90], and [0/45], respectively. Although the amount of frictional resistance is reduced as the second ply is rotated by 45° as shown in [18], due to the reduction in fiber contact compared to the [0/0] sample, stacking sequence [0/45] results in a clearly large size and number of wrinkles and less surface quality. This can be interpreted as the relative orientations between neighboring plies have a significant impact on the bending stiffness value as described in [96]. For example, the stacking [0/45] has the lowest bending stiffness compared to other stacking sequences and results in more wrinkling. A slight difference was detected between stacking sequences [0/0] and [0/90] in terms of observed defects. However, in-plane waviness was numerous in the [0/0] sample (see Figure 5.13 (a)). Over-thickness zones that were generated due to the localization buckles in yarns were also found at locations having wrinkles.

As the forming and curing steps were done at the same time, defects like resin squeeze-out were also observed, especially at the inner surfaces around the curved-flanges. The squeezing pressure at locations B and D during the curing process differs from that applied at the curved-flanges (see Figure 5.11 (a)) due to bridging defects. Thus, the resin flow occurred intensively through the fabric and concentrated in regions with insufficient pressure (the convergence areas between locations B and D). Also, there is an uneven distribution of the resin through the cross-section of OOA prepregs that may have contributed to this defect. However, extensive microscopic observations are required to deeply analyze this effect, including a resin-rich interlayer, which is beyond the scope of this paper.

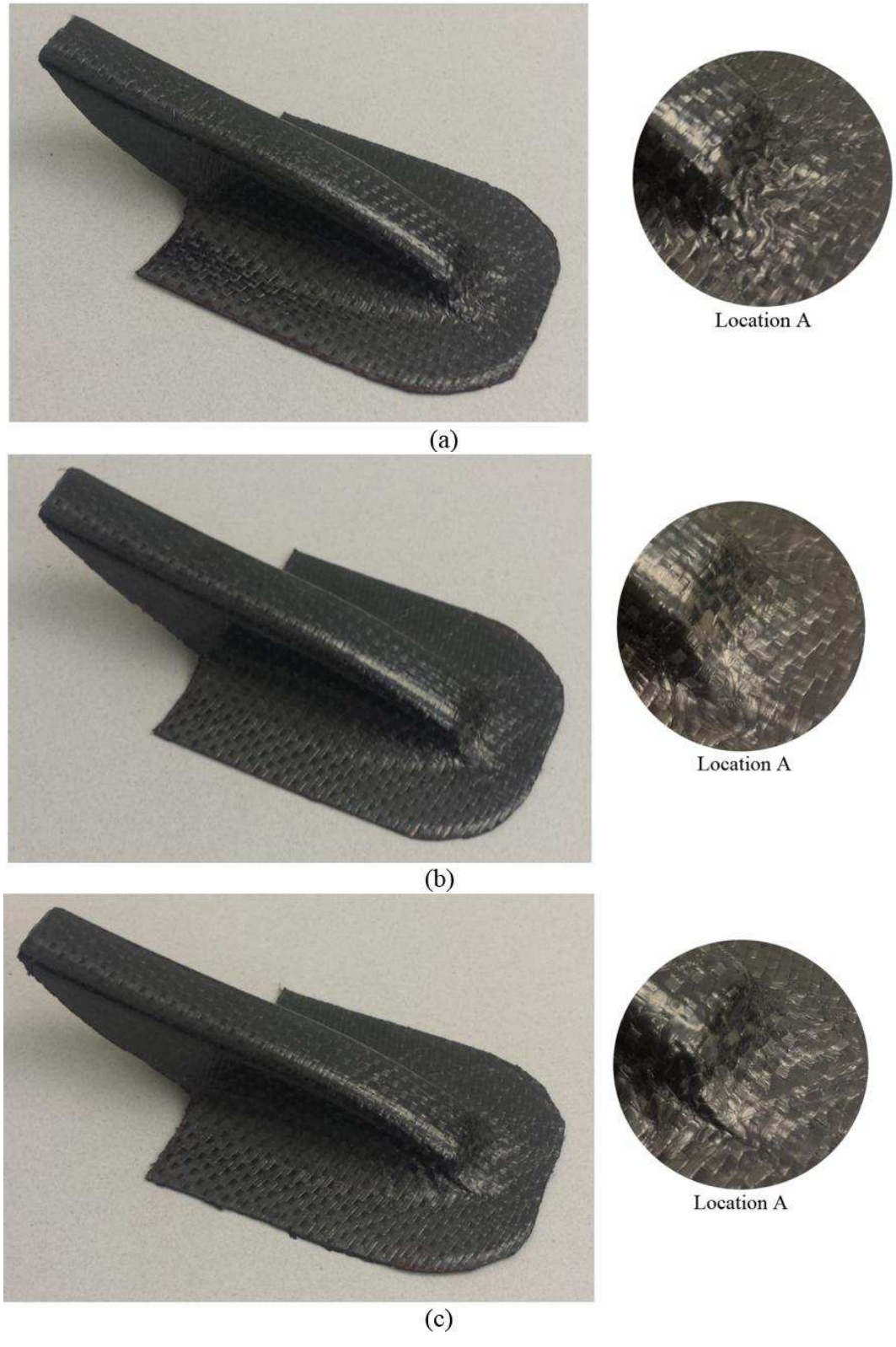

Figure 5.13: Formed part with different lay-up arrangements: (a) [0/0] sequence, (b) [0/90] sequence, and (c) [0/45] sequence.

5.5.2 Forming simulation results

To achieve a net-shape for the selected geometry during the forming simulation, the ply shape, shown in Figure 5.14 (a), was obtained after several iterations. Figure 5.14 (b) shows a near net-shaped part after applying the simulation methodology described above. There are still excessive materials in the flat zones due to the complexity of the part, selected ply orientations, and formed defects. An initial forming simulation with a rectangular ply demonstrated severe wrinkles and distortions in the undercut zones on the back. Therefore, optimizing the ply shape during the DDF simulation is required to obtain acceptable simulation outcomes. Note that the net–shaped ply was compared to a rectangular ply during the forming experiments. However, only minor differences were found between them in terms of observed defects. This occurred because the tool in the DDF process was filled in the undercut zones on the back in order to facilitate the tool machining. Thus, only rectangular plies were used in DDF experiments and then trimmed to achieve the required shape (see Figure 5.11).

Figure 5.15 (a) shows the simulation results for a single-ply where the warp yarn direction was aligned with the x-direction. Only one small wrinkle was found in location A. The shear angle distributions throughout the part and the fiber stress in direction 1 (warp in this case) are shown in Figures 5.15 (b) and (c), respectively. The higher shear angles were concentrated in the double-curved zones in location A. The results show that the maximum obtained shear angles and their locations were closed to the experimental observations. However, the magnitude of the shear angles was somewhat smaller for the experimental case due to the bridging defects that prevented the material from deforming more around the curved sections as described earlier. Further, these results are in accordance with the experimental findings in terms of formed wrinkles and overall quality (see Figure 5.12 (a)). The location of the maximum compressive stress in the fiber (blue in Figure 5.15 (c)) was found to have a similar position for the observed wrinkle.

Figure 5.16 (a) visualizes the simulation results for a single ply with a [-45°] orientation in respect to the x-direction; large wrinkles, located in the double–curved zones in location A, were observed. Although the experiment also showed large wrinkles at the same location, the fold defects at location B could not be captured by the forming prediction. The ply in this case deformed differently compared to the [0°] sample orientation. This can be seen from the formed shape and the distributions of shear angles as shown in Figure 5.16 (b). A good agreement between the measured and the predicted angles was found. Figure 5.16 (c) shows the fiber stresses in the warp direction. The results show again that the wrinkle zones have higher concentrated compressive stresses. It is worth noting that no wrinkles were found at the maximum shear angles location, although it exceed the locking angle.

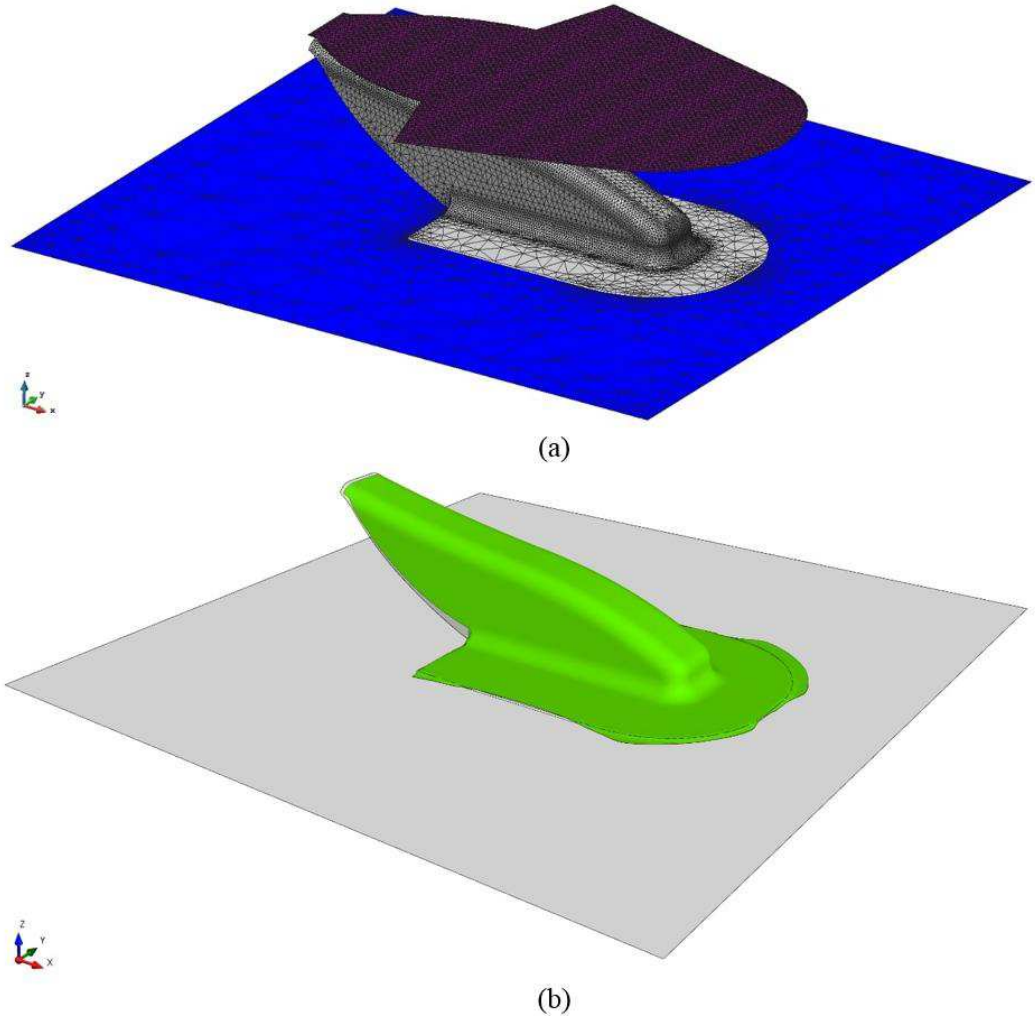

Figure 5.14: (a) Net ply shape for selected geometry, and (b) net-shaped part.

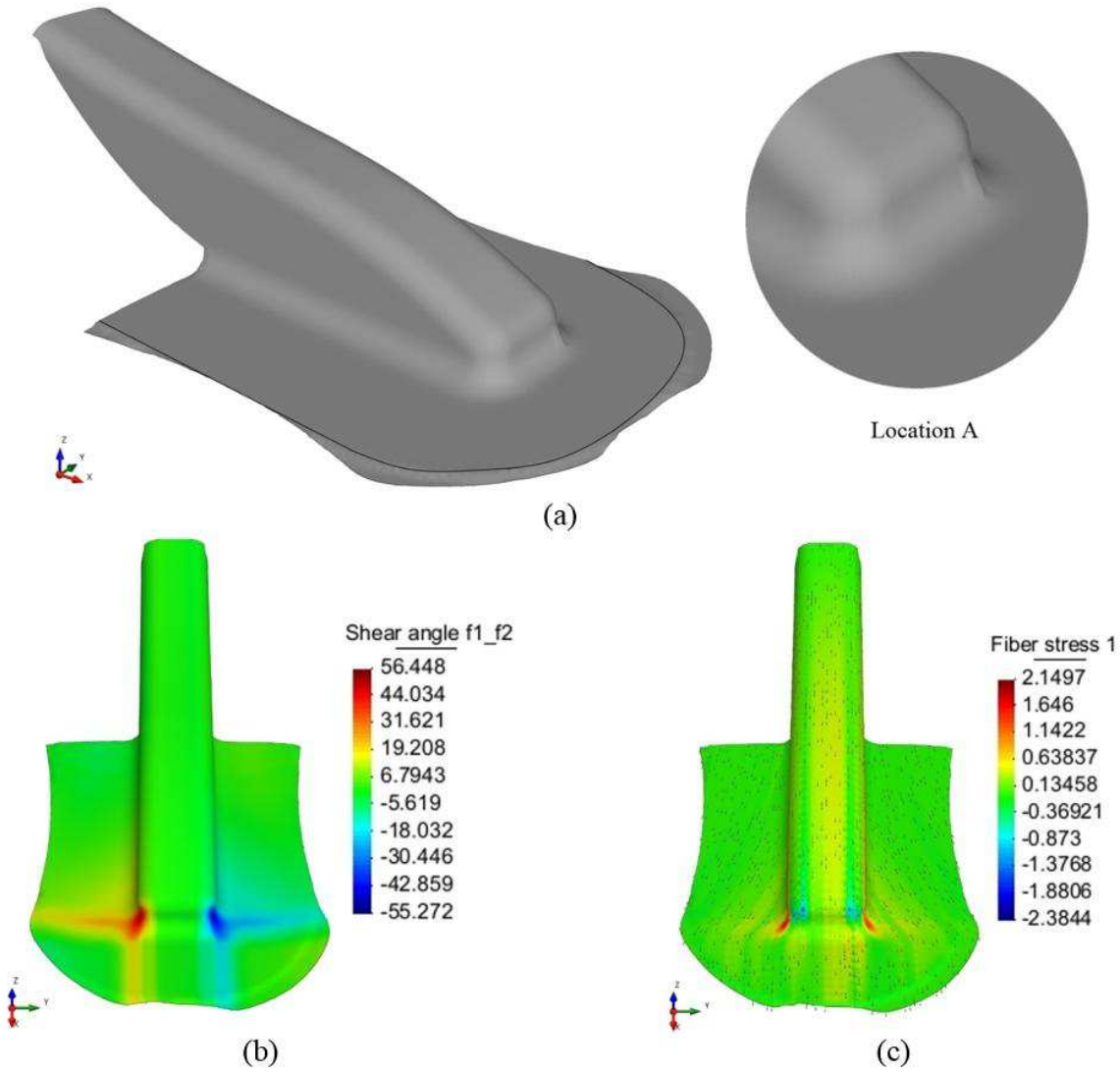

Figure 5.15: Forming predictions of single ply when the warp yarn direction is aligned with the x-direction: (a) observed defects, (b) shear angle distribution, and (c) fiber stress in warp direction.

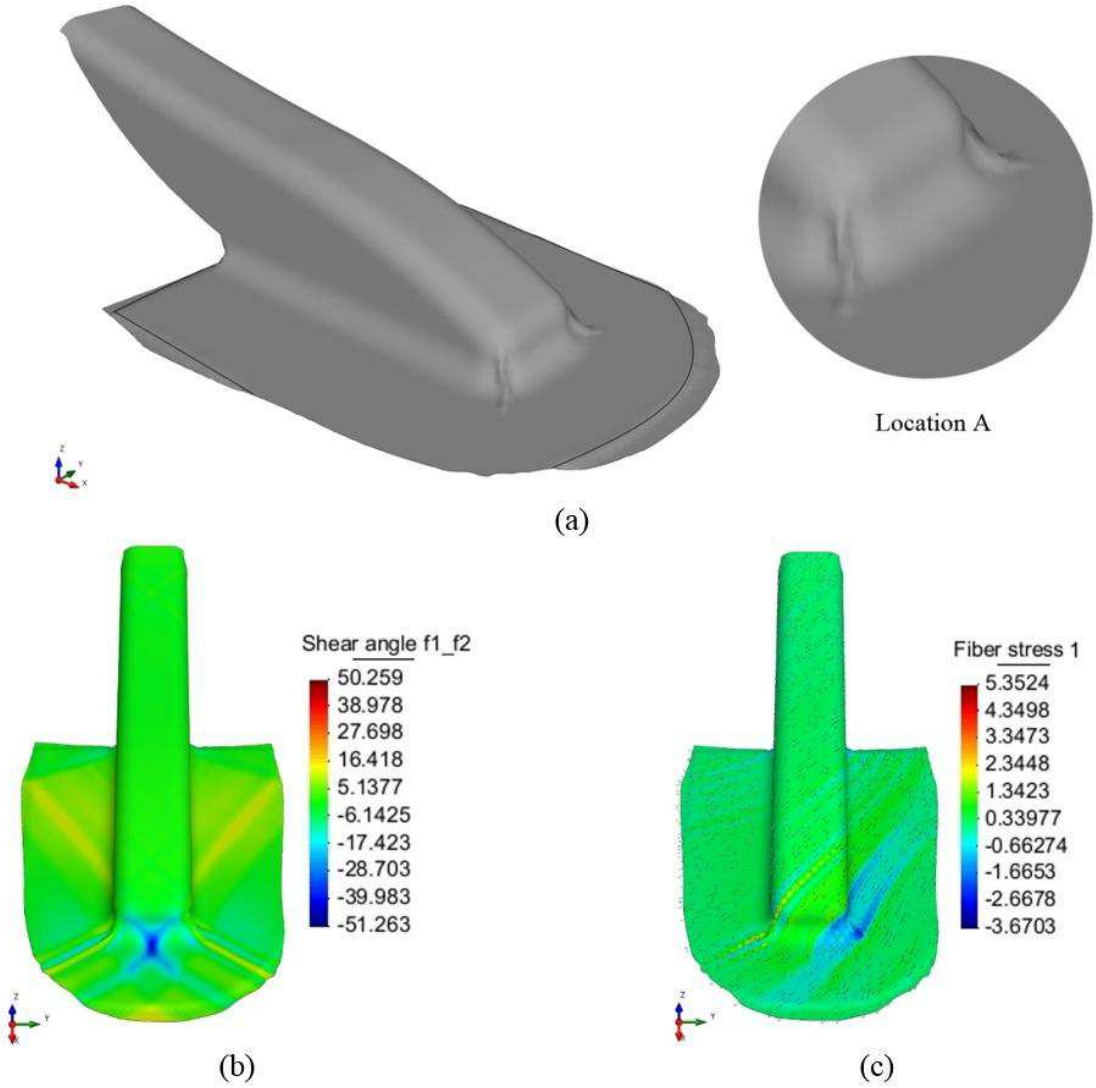

Figure 5.16: Forming predictions of single ply with -45° orientation respect to the x-direction: (a) observed defects, (b) shear angle distribution, and (c) fiber stress in warp direction.

The forming predictions for all three stacking sequences of [0/0], [0/90], and [0/45] over the selected geometry are shown in Figures 5.17, 5.18, and 5.19, respectively. The warp direction in ply 1 (top) was aligned with y-direction for all three selected sequences. Stacking [0/0] and [0/90] showed a similar number of wrinkle formations and locations. However, the size of the wrinkles is relatively smaller for the [0/90] lay-up, and it showed better tool conformity. On the contrary, the [0/45] lay-up shows severe wrinkles and less surface quality

(see Figure 5.19 (a)). Looking carefully to the shear angle distributions in each ply for all three sequences showed that the stack [0/90] has the highest in-plane shear deformations. Moreover, as discussed previously in [18], the rotation of fibers inside the laminate eased the sliding and thus decreased the frictional resistance, which allows for correct accommodation of the desired shape. However, stack [0/0] has the highest frictional resistance, but shows better forming results both experimentally and numerically when compared to the [0/45] lay-up. This is attributed to the difference in bending stiffness values between the two stacking sequences as explained in detail in [96]. Therefore, the stack is more sensitive to wrinkling when the lower bending stiffness and higher friction between plies are expected. Further analysis of the fiber stresses in each ply for all three stacks showed that wrinkles occurred at the locations having higher compressive stresses as shown in Figures 5.17 (c), 5.18 (c), and 5.19 (c). This compressive stress may provide a good indication for where the critical areas appear, mainly when the element size is much larger than the typical size of the defects. However, this also depends on the orientation of the ply and the chosen lay-up. Overall, concentrated compressive stresses in the most selected cases herein led to wrinkles in the DDF experiments. A summary of all performed simulations and experiments and how well the observed defects were predicted by the FE model is given in Table 5.4. This includes the overall part quality, which is described by a semi qualitative ranking scale (from 1 to 5), with 1 denoting very poor quality and 5 a flawless part (see Table 5.4).

The simulation results also showed less bridging defects around the curved-flanges compared to the formed parts from the DDF process. The variation in heating arrangements between the upper and lower diaphragms may cause different responses between the two diaphragms during the forming process [86]. This may further lead to folding and bridging defects during the DDF experiments. Therefore, future work is required to predict temperature gradients in the prepreg stack and the two diaphragms during the DDF process. However, the simulations show sufficient predictions in terms of when and where different kinds of wrinkles appear during the DDF over the selected geometry. Prior to investing in expensive trial and error tests, this prediction tool allows to redesign the part with further considerations such as material types, excessive materials locations, start contact angle,

appropriate stacking sequences and suitable process parameters.

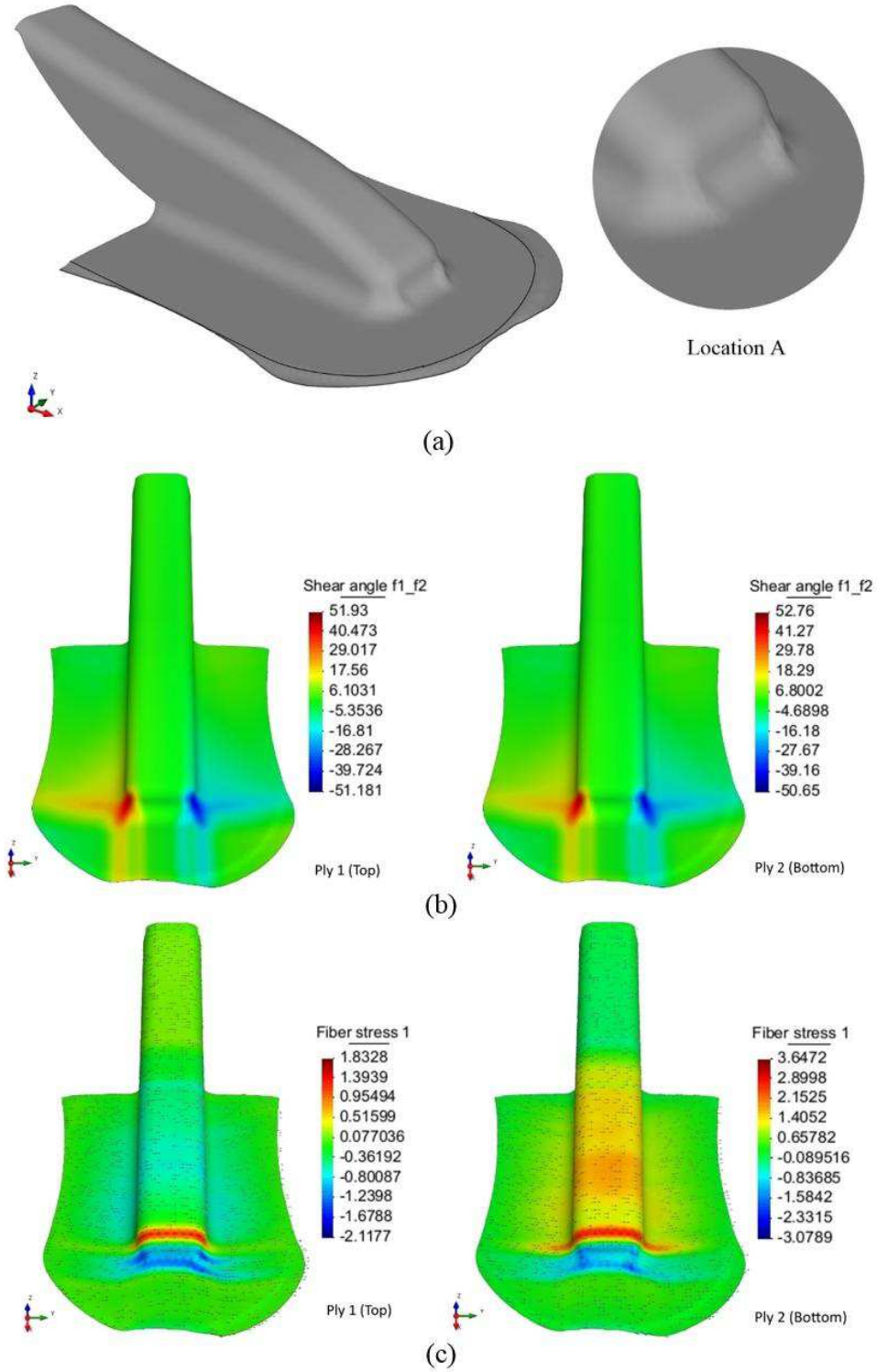

Figure 5.17: Forming predictions of [0/0] lay-up sequence: (a) observed defects, (b) shear angle distribution, and (c) fiber stress in warp direction.

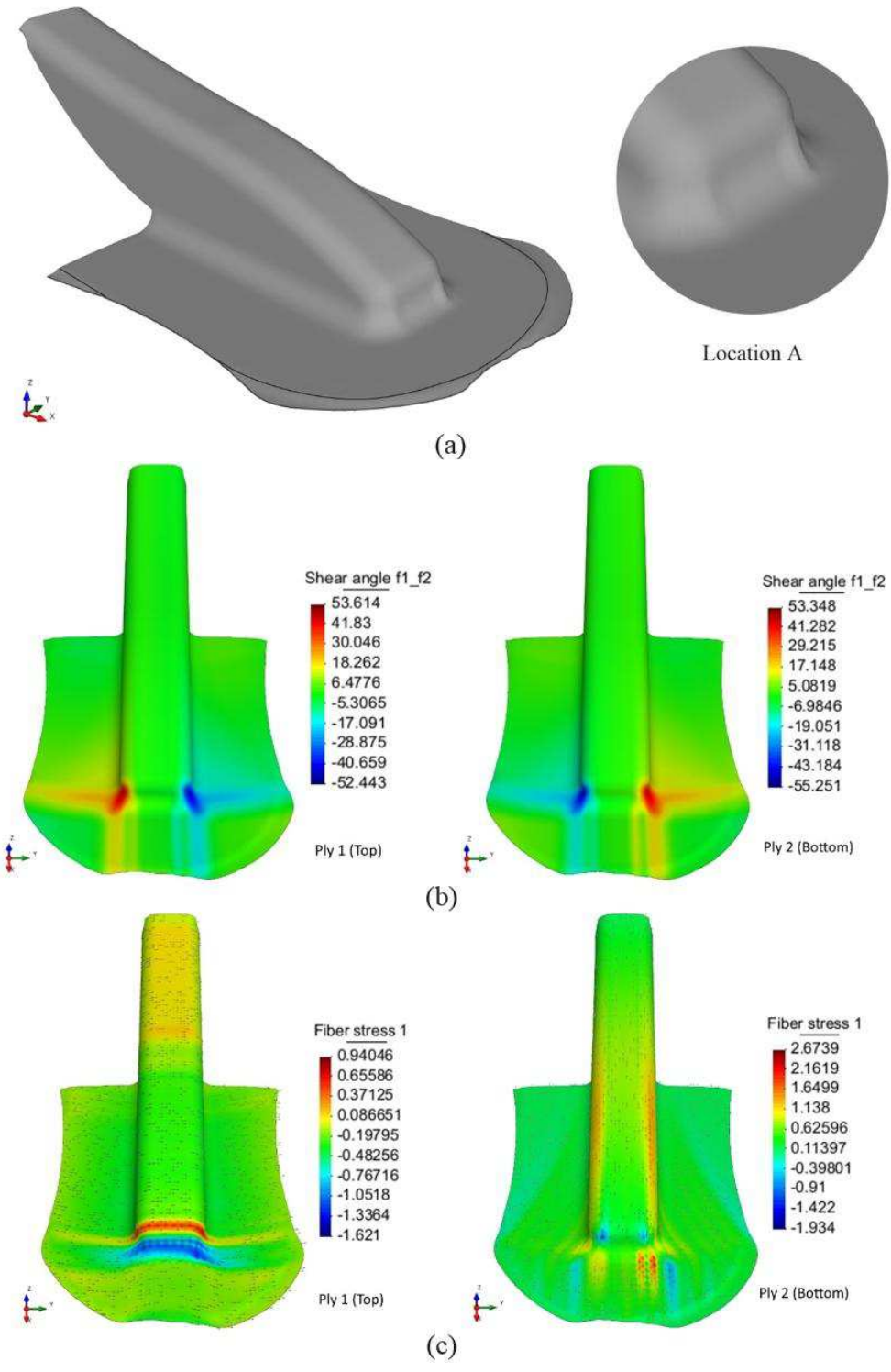

Figure 5.18: Forming predictions of [0/90] lay-up sequence: (a) observed defects, (b) shear angle distribution, and (c) fiber stress in warp direction.

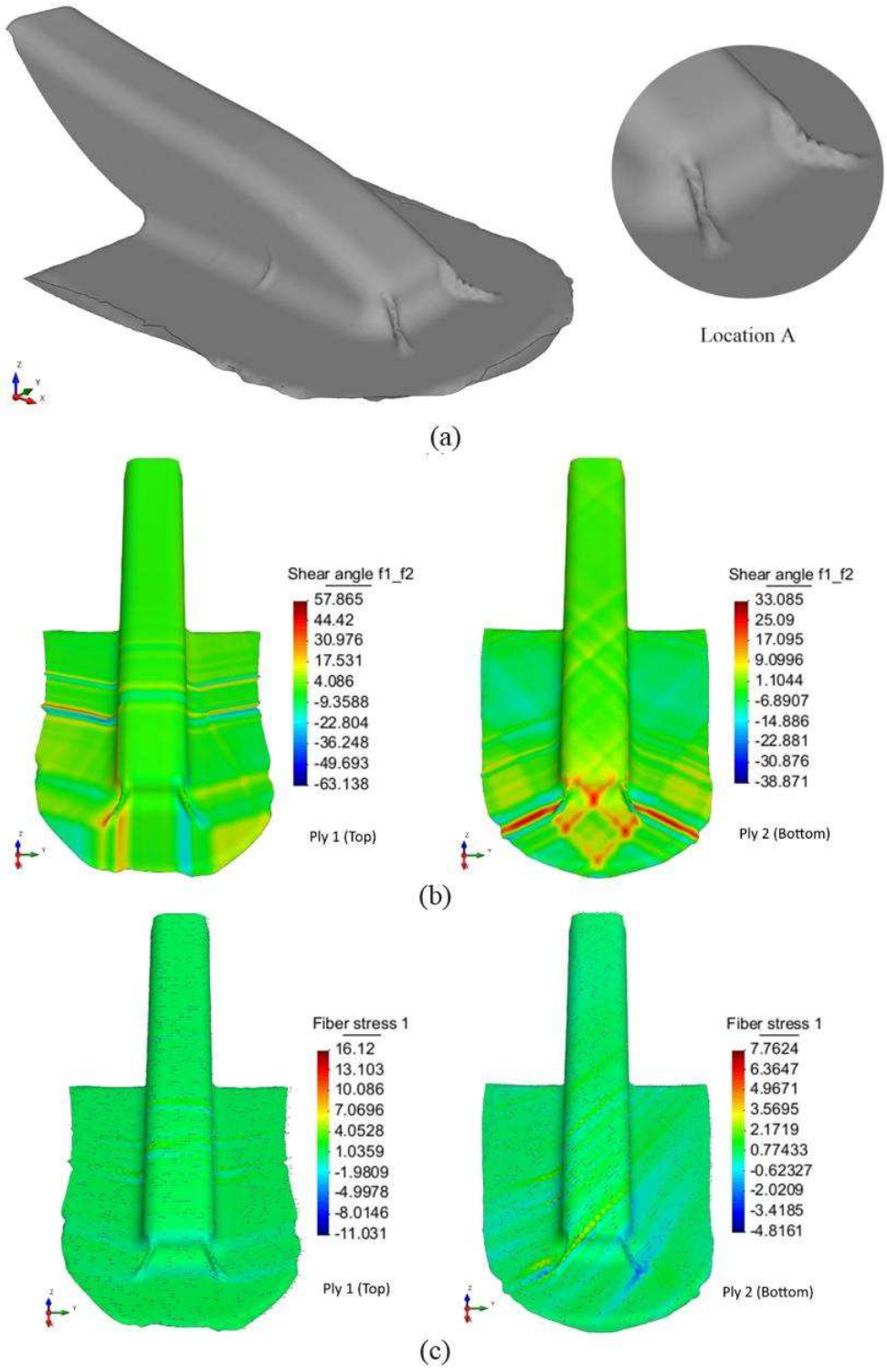

Figure 5.19: Forming predictions of [0/45] lay-up sequence: (a) observed defects, (b) shear angle distribution, and (c) fiber stress in warp direction.

Table 5.4: A summary of all performed experiments and simulations with their prediction capabilities.

Sample	**Part quality**(1)	**Observed defects**	**Defect Locations**	**Predicted defects**(2)	**Predicted shear angles**(2)
Single ply (warp yarn direction is aligned with the x-direction)	4	Small wrinkling	A	Y	Y
		Bridging	Between B and D	M	
Single ply (-45° orientation respect to the x-direction)	2	Large wrinkling	A	Y	Y
		Bridging	Between B and D	M	
		folding	B	N	
Two plies [0/0]	3	Small wrinkling	A	Y	Y
		Bridging	Between B and D	M	
		In-plane waviness	A	N	
Two plies [0/90]	3	Small wrinkling	A	Y	Y
		less Bridging	Between B and D	M	
Two plies [0/45]	2	Large size and number of wrinkles	A	Y	Top ply-Y Bottom ply-M
		Small wrinkling	Between B and D	M	
		Bridging	Between B and D	M	

(1) From 1 to 5 is used to describe the part quality, with 1 denoting very poor quality and 5 a flawless part.

(2) Y: simulation agrees with experimental result; N: simulation disagrees with experimental result; M: between Y and N.

5.5.3 Mitigation of wrinkle defects

In this section, different forming simulation scenarios were applied to reduce the wrinkle defects in [0/45] lay-up as this was the most challenging sequence for the geometry considered. First, stacking sequences [0/30] and [0/60] were examined to further understand the effect of ply orientation within the stacks as outlined in Figures 5.20 (a) and (b), respectively. It was shown that there is only a small reduction in the formed wrinkles compared to the [0/45] stack. However, the location of the wrinkle is different, as each layer shows different deformability depending on its relative fiber angle. Figure 5.20 (c) shows the forming outcome when the bending stiffness value is multiplied by 2. A slight improvement was seen in terms of minimizing the size of wrinkle formations. Also, the large wrinkle that appeared in the curved-flange zone vanished. Since the bending stiffness increases, bridging defects at locations with double curvature may tend to occur. Chen et al. [86] showed that the wrinkling decreases simultaneously as the number of bridging fibers decreases. However, this also depends on the tools and materials considered. On the other hand, a reduction in friction between plies showed no major difference compared to the reference stack (see Figure 5.20 (d)). Additionally, wrinkle size is smaller when friction is low.

From all applied scenarios, it seems that when there are fibers with certain angles (in this case, the x-direction), wrinkles cannot be avoided. The formability can be improved, however, when the fibers are parallel or perpendicular to the x-direction, as described in the previous section. Note that this was not the case for the UD stacks in [77]. Although forming a flat of textile OOA prepreg into a complex shape using the DDF process is not straightforward, a wrinkle-free part can be produced. However, more investigation into the process-induced defects is needed to improve the formability of OOA prepregs.

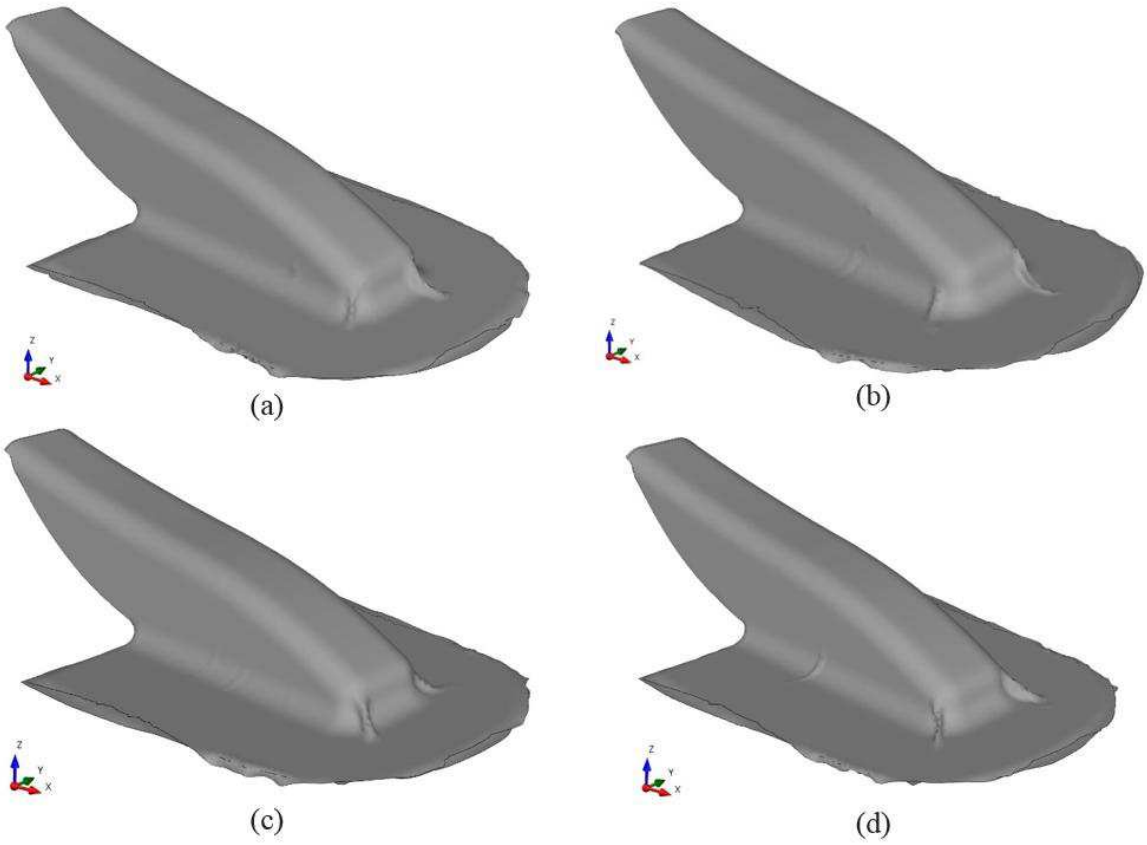

Figure 5.20: Observed defects in the predicted parts: (a) [0/30] sequence, (b) [0/60] sequence, (c) [0/45] sequence with high bending stiffness, and (d) [0/45] sequence with low friction properties.

5.6 Conclusion

The presented work experimentally and numerically investigated the formability of textile out-of-autoclave thermoset prepreg using double diaphragm forming to produce an aircraft component. A finite element model was developed to simulate the double diaphragm forming process. The experimental setup fully accommodated the forming and curing steps of the process, thereby providing a notable reduction in manufacturing time and cost.

Two main types of defects were noticed during the double diaphragm process for the geometry considered: first, the wrinkles with different numbers and sizes were concentrated near an area with double curvature; second, the prepreg bridging defect affected the tool

conformity, especially at deep concave locations. The experimental and numerical results indicated that a change in lay-up sequences significantly affects the formability. Depending on the lay-up arrangement, wrinkling in the formed part differed remarkably due to the deformation modes that occurred during the forming process and their resistances to the forming loads.

The forming simulations showed sufficient predictions in terms of when and where different kinds of wrinkles would appear during the DDF over the selected geometry. Higher local compressive stresses in each single ply during forming simulations led to wrinkles in the DDF experiments. This may be a good indication of where the critical areas will appear, and it can be considered when the small wrinkles cannot be predicted with the element size used.

Further work is needed to improve the formability of OOA prepregs through a focus on the process-induced defects, such as different temperature arrangements between the prepreg and the two diaphragms, unbalanced clamping forces, diaphragm material stiffness and thickness, and insufficient forming loads.

Chapter 6

Conclusions, Contributions, and Recommendations

This chapter summarizes the major conclusions arising from the work described in this thesis. Contributions and publications accomplished during the course of the current research work are highlighted. Moreover, several recommendations for future work are made.

6.1 Concluding remarks

The thesis focuses on the out-of-plane bending behavior of textile prepregs, which plays an important role in determining wrinkle formation during composite forming. A new test method for characterizing the bending behavior of prepreg materials at forming conditions was developed based on a vertical cantilever test associated with a linear actuator and load cell. This test method allowed for the sufficient control of deflection shape, testing rates, and processing temperatures within the range of thermosetting resin. Moreover, the developed experimental procedure allowed for investigation into viscoelastic effects and demonstrated good reproducibility of results. A new method for calculating the bending stiffness was proposed to minimize the effort needed to extract the data points for obtaining the deflection equation.

An experimental investigation of bending behavior of satin woven carbon/epoxy prepregs was assessed across different sample configurations, processing temperatures, and rates. The results revealed that bending stiffness is approximately 20% higher in the warp direction than in the weft direction; it decreased significantly with increasing temperature. This decrease is strongly correlated with resin viscosity reduction: higher temperatures reduce

the load required to achieve the same tip displacement. Note that increased temperature may also increase the incidence of wrinkling during the forming process, because the accompanying reduction in bending stiffness decreases the resistance to compressive loading in the plane of the material. A comparison between the prepreg sample and the dry sample indicated that the uncured resin matrix has a significant impact in the outcomes. Moreover, the experiments showed that bending behavior is rate-dependent, due to the viscoelastic behavior of the prepreg.

Reliance on the tensile modulus to assess bending stiffness of prepreg tends to produce an unrealistically elevated stiffness assessment. Thus, a theoretical model was developed that can be applied for a wide range of processing conditions to predict the bending behavior of thermosetting composite prepreg during the forming process. The model included the processing temperature and rate and was validated using a set of experimental tests. The predicted bending stiffness was found to be in good agreement with experimental values at selected conditions. However, slight differences occurred due to the complexity of undulation in a woven fabric structure. A new approach for considering the testing rate and temperature with respect to a reference value was also developed. The proposed approach reasonably captured the trend of the rate and temperature dependencies of selected materials without performing extensive experiments for relaxation test at the desired rates and temperatures. The bending properties obtained by the proposed model can be used as the initial inputs in a finite element model.

The developed test method was used to investigate the bending properties of multilayered textile thermosetting composite prepregs under conditions relevant to the forming process. A finite element model based on a viscoelastic approach was developed to predict the bending behavior of different stacking sequences at different processing parameters, including temperature and rate. The effect of textile stacking sequences on out-of-plane bending deformation was studied experimentally and numerically for the first time. The bending properties strongly depend on the fabric lay-up inside multiple stacked plies. The predicted bending properties were found to be in good agreement with the experimental results for selected stacking sequences. The feasibility of using a viscoelastic material model

to model the bending behavior of selected material and its application in forming simulation was analyzed. A notable difference in bending behavior was observed after comparing Kelvin–Voigt and elastic material models. Moreover, bending behavior is also influenced by the friction between plies, which plays an important role in terms of facilitating the through-thickness shearing during the bending experiments at processing temperature. The forming simulation outcomes showed that high bending stiffness along with low friction between the plies may help increase the limit of shear deformation (shear angles), ultimately providing a reduction in wrinkling.

Finally, this study investigated the formability of textile out-of-autoclave thermoset prepreg using double diaphragm forming over a complex structure for aerospace applications. A custom-built double diaphragm forming setup was developed. It consisted of three main parts: double diaphragm tool, vacuum system, and heating system. The experimental setup fully accommodated the forming and curing steps of the process, thereby providing a notable reduction in manufacturing time and cost. A finite element model was developed to simulate the double diaphragm forming process. The diaphragm and prepreg material properties at forming conditions, including their out-of-plane bending properties, were considered in the FE model. An evaluation of the double diaphragm forming process in terms of observed defects, stacking sequences, and pre–forming state was carried out.

Wrinkles and bridging were found to be the dominant defects during double diaphragm forming. The experimental and numerical results indicated that a change in lay-up sequences significantly affects the formability. Depending on the lay-up arrangement, wrinkling in the formed part differed remarkably due to the deformation modes that occurred during the forming process and their resistances to the forming loads. The forming simulations showed sufficient predictions in terms of when and where different kinds of wrinkles would appear during the double diaphragm forming over the selected geometry. Higher local compressive stresses in each single ply during forming simulations led to wrinkles in the double diaphragm forming experiments. This may be a good indication of where the critical areas will appear, and it can be considered when the small wrinkles cannot be predicted with the element size used.

6.2 Contributions

This work made an attempt to investigate the bending deformation behavior of textile woven out-of-autoclave thermoset prepregs both experimentally and numerically and to implement the findings into a forming simulation. The main contributions from the present PhD thesis include the following:

(1) A new approach for characterizing the bending behavior of prepreg materials at forming conditions was developed, offering more precise control of deflection shape, testing rates, and processing temperatures.

(2) For the first time, the bending behavior of out-of-autoclave thermoset prepregs including multilayered samples was studied under conditions relevant to the forming operation.

(3) A theoretical model for predicting the bending behavior of thermosetting composite perpreg during the forming process was proposed. This model can be applied to a wide range of processing conditions, including the processing temperature and rate.

(4) A new approach for considering the testing rate and temperature with respect to a reference value was presented. This proposed approach is beneficial for minimizing the efforts required for relaxation test at the desired rates and temperatures.

(5) A finite element model was proposed based on a viscoelastic approach to predict the bending behavior of multilayered textile thermosetting composite using commercial software (AniForm). This model will reduce the effort required by the experimental investigations and help the modeler determine the correct parameter values to set during the simulation process.

(6) The formability of out-of-autoclave thermoset prepregs using the double diaphragm forming process was investigated. A one-step procedure was used for both the forming and curing processes using the same experimental setup.

(7) A finite element model was built to simulate the double diaphragm forming process. Significant investigations were made to obtain the required properties for the material models in the FE simulation, including the diaphragm material properties.

(8) The relationships between important considerations during forming simulation, such as local fiber compressive stresses, shear angle distributions, and stacking lay-up sequences, were analyzed to identify potential causes for defect development.

In addition to the above contributions, the following publications have been accomplished during the journey of this study:

Journal Papers

(1) **Alshahrani H**, Hojjati M. A new test method for the characterization of the bending behavior of textile prepregs. Composites Part A: Applied Science and Manufacturing. 2017; 97:128-140.

(2) **Alshahrani H**, Hojjati M. A theoretical model with experimental verification for bending stiffness of thermosetting prepreg during forming process. Composite Structures. 2017; 166:136-145.

(3) **Alshahrani H**, Hojjati M. Bending behavior of multilayered textile composite prepregs: Experiment and finite element modeling. Materials & Design. 2017; 124:211-224.

(4) **Alshahrani H**, Hojjati M. Experimental and numerical investigations on formability of out-of-autoclave thermoset prepreg using a double diaphragm process. Composites Part A: Applied Science and Manufacturing. 2017; 101:199-214.

(5) **Alshahrani H**, Mohan R, Hojjati M. Experimental investigation of in-plane shear deformation of out-of-autoclave prepreg. International Journal of Composite Materials. 2015; 5(4):81-87.

(6) **Alshahrani H**, Hojjati M. Influence of double-diaphragm vacuum compaction on deformation during forming of composite prepregs. Journal of Science: Advanced Materials and Devices. 2016; 1(4):507-511.

(7) Mohan RP, **Alshahrani H**, Hojjati M. Investigation of intra-ply shear behavior of out-of-autoclave carbon/epoxy prepreg. Journal of Composite Materials. 2016; 50(30):4251-4268.

Conference Papers

(1) **Alshahrani H**, Mohan R, Hojjati M. Evaluation of in-plane shear deformation of out-of-autoclave carbon/epoxy prepregs using bias extension test. In: Proceedings of CAMX 2014 Conf. Orlando, FL. USA; 2014.

(2) **Alshahrani H**, Hojjati M. Optimum processing parameters for hot drape forming of out-of-autoclave prepreg over complex shape using a double diaphragm technique. In 20th International Conference on Composite Materials, Copenhagen, Denmark, 2015.

(3) **Alshahrani H**, Hojjati M. In-plane shear deformability of out-of-autoclave prepregs under double-diaphragm vacuum compaction. In ICANM 2015: International Conference and Exhibition on Advanced and Nano Materials, pp. 170-177, Ottawa, Canada, 2015.

(4) **Alshahrani H**, Hojjati M. Out-of-plane bending properties of out-of-autoclave thermosetting prepregs during forming processes. ICCET 2016: 18th International Conference on Composite Engineering and Technology. Dubai, UAE, 2016.

(5) **Alshahrani H**, Hojjati M. Comparison of horizontal and vertical cantilever tests for the characterization of bending behavior in woven fabric prepregs. In 3rd International Conference on Plastic, Rubber and Composites, Seoul, Korea, 22-23 July, 2016.

(6) **Alshahrani H**, Hojjati M. Analysis of formability of thick composite component under double-diaphragm forming process. In 2nd International Conference on Production Automation and Mechanical Engineering, pp. 185189, Montreal, Canada, 2016.

(7) **Alshahrani H**, Hojjati M. Bending behavior of woven fabric out-of-autoclave prepreg in forming. Accepted in CANCOM 2017 - Canadian International Conference On Composite Materials, Ottawa, Canada, 17-20 July 2017.

(8) **Alshahrani H**, Hojjati M. Investigation of shear-bending coupled properties in composite prepreg forming. Submitted to 21th International Conference on Composite Materials, Xi'an, China, 20-25 August 2017.

(9) R. Mohan, **H. Alshahrani**, M. Hojjati. The Effect of processing parameters on intra-ply shear property of out-autoclave carbon/epoxy prepreg. In 10th Canada-Japan Workshop on Composites, Vancouver, Canada, 2014.

6.3 Recommendations

6.3.1 Technical recommendations

To improve the formability of textile composites prepregs and minimize the possible failures during double diaphragm process, the following set of recommendations and guidelines are delivered to end-users:

- In the case of forming woven fabric over complex shapes, the satin weave style is preferred.
- The fabric lay-up inside multiple stacked plies with high bending stiffness and low friction properties is recommended as long as the desired tool shape can be correctly achieved.
- The forming work area should be three times larger than the tool size to obtain a better conformity.
- Forming temperature (70 °C) with a lower forming speed are preferred for processing of thermosetting matrix.
- Great care must be taken during placing of the samples between the two diaphragms.
- Initial orientation of sample respect to the direction of the largest curvature on the forming tool should avoid the 45° orientation.
- In forming simulation, the actual bending properties should be used according to the selected processing conditions.
- The analysis of observed defects during forming simulation should include the compressive stresses in the fiber, which can be a good indication of where the critical areas will appear.

6.3.2 Recommendations for future work

As an extension to this research, several recommendations for future work are made as follows:

(1) The present PhD thesis mainly investigates the bending behavior of woven out-of-autoclave thermoset prepregs in a macro-scale level. The out-of-autoclave prepregs are different from most autoclave prepregs in that the upper and lower fiber plies are partially impregnated with the resin system. Microscopic investigations are required to study the effect of resin-rich interlayer flow on bending deformation mechanism, especially at elevated temperatures and for thick samples.

(2) To further understand the material's formability for thick components, the contribution of transverse intra-ply shear to the bending behavior needs to be determined and explored through the finite element implementation with application to a forming simulation. This also requires some improvements in the current test method, including the load capacity and the temperature arrangement for different material types.

(3) As a continued work, the coupling effect of shear on bending properties should be studied as these deformation mechanisms during the actual forming process are combined. A numerical study using the combined shear-bending properties can be compared with those obtained from each separate test.

(4) The current viscoelastic bending model can be extended to include a non-linear viscous behavior, which can then be implemented in a finite element formulation to assess its effect on the forming simulation outcomes.

(5) The inherent undulation between yarns in woven-fabric structures should be considered to improve the prediction capabilities. A micro-model for woven fabric is recommended, which can be achieved through an appropriate description of the yarn geometry and the consideration of internal weave architecture. The application of the current model can be extended to study the defect formations during steering in

Automated Fiber Placement (AFP). This can be achieved by assuming the prepreg yarn is subjected to buckling load.

(6) The prediction of defects during double diaphragm forming requires considering the temperature development in the prepreg stack and the two diaphragms.

(7) In a double diaphragm forming process, the considerations of temperature arrangements between the prepreg and the two diaphragms, clamping forces, diaphragm material stiffness and thickness, and forming loads are necessary to improve the formability of OOA prepregs.

(8) Further work is needed to improve the rate control method during the double diaphragm forming process in order to elaborate its impact in detail on the forming results. Such work should also compare the results with those obtained from the press forming process, where the forming rate is well-controlled.

Bibliography

[1] Boeing 787, "Aircraft Rescue and Firefighting Composite Structure," accessed 15-March-2017.

[2] A. C. Long, *Design and manufacture of textile composites*. Elsevier, 2005.

[3] D. Bhattacharyya, *Composite sheet forming*. Elesvier, Amsterdam, 1997.

[4] C. Tucker, *Forming of advanced composites*. Wiley, New York, 1997.

[5] X. Yu, L. Zhang, and Y.-W. Mai, "Modelling and finite element treatment of intra-ply shearing of woven fabric," *Journal of materials processing technology*, vol. 138, no. 1, pp. 47–52, 2003.

[6] A. C. Long (editor), *Composites forming technolgies*. CRC Press LLC, Boca Raton FL, 2007.

[7] S. P. Haanappel, R. H. W. Ten Thije, U. Sachs, B. Rietman, and R. Akkerman, "Formability analyses of uni-directional and textile reinforced thermoplastics," *Composites Part A: Applied Science and Manufacturing*, vol. 56, pp. 80–92, 2014.

[8] J. S. Lightfoot, M. R. Wisnom, and K. Potter, "Defects in woven preforms: Formation mechanisms and the effects of laminate design and layup protocol," *Composites Part A: Applied Science and Manufacturing*, vol. 51, pp. 99–107, 2013.

[9] B. Zhu, T. Yu, and X. Tao, "An experimental study of in-plane large shear deformation of woven fabric composite," *Composites Science and Technology*, vol. 67, no. 2, pp. 252–261, 2007.

[10] G. Lebrun, M. N. Bureau, and J. Denault, "Evaluation of bias-extension and picture-frame test methods for the measurement of intraply shear properties of PP/glass commingled fabrics," *Composite Structures*, vol. 61, no. 4, pp. 341–352, 2003.

[11] P. Boisse, N. Hamila, E. Vidal-Sallé, and F. Dumont, "Simulation of wrinkling during textile composite reinforcement forming. Influence of tensile, in-plane shear and bending stiffnesses," *Composites Science and Technology*, vol. 71, no. 5, pp. 683–692, 2011.

[12] P. Harrison, M. Clifford, and A. Long, "Shear characterisation of viscous woven textile composites: a comparison between picture frame and bias extension experiments," *Composites Science and Technology*, vol. 64, no. 10, pp. 1453–1465, 2004.

[13] E. Guzman-Maldonado, N. Hamila, P. Boisse, and J. Bikard, "Thermomechanical analysis, modelling and simulation of the forming of pre-impregnated thermoplastics composites," *Composites Part A: Applied Science and Manufacturing*, vol. 78, pp. 211–222, 2015.

[14] I. Taha, Y. Abdin, and S. Ebeid, "Comparison of picture frame and bias-extension tests for the characterization of shear behaviour in natural fibre woven fabrics," *Fibers and Polymers*, vol. 14, no. 2, p. 338, 2013.

[15] H. Alshahrani, R. Mohan, and M. Hojjati, "Experimental investigation of in-plane shear deformation of out-of-autoclave prepreg," *International Journal of Composite Materials*, vol. 5, no. 4, pp. 81–87, 2015.

[16] R. P. Mohan, H. Alshahrani, and M. Hojjati, "Investigation of intra-ply shear behavior of out-of-autoclave carbon/epoxy prepreg," *Journal of Composite Materials*, vol. 50, no. 30, pp. 4251–4268, 2016.

[17] K. Vanclooster, *Forming of multilayered fabric reinforced thermoplastic composites*. Phd thesis, KU Leuven, 2009.

[18] H. Grewal, *Characterization of interply shear behaviour of out-of-autoclave thermosetting prepreg composites*. Master's thesis, Concordia University, 2015.

[19] J. Sun, Y. Gu, M. Li, X. Ma, and Z. Zhang, "Effect of forming temperature on the quality of hot diaphragm formed C-shaped thermosetting composite laminates," *Journal of Reinforced Plastics and Composites*, vol. 31, no. 16, pp. 1074–1087, 2012.

[20] Y. R. Larberg and M. Åkermo, "On the interply friction of different generations of carbon/epoxy prepreg systems," *Composites Part A: Applied Science and Manufacturing*, vol. 42, no. 9, pp. 1067–1074, 2011.

[21] K. A. Fetfatsidis, D. Jauffrès, J. A. Sherwood, and J. Chen, "Characterization of the tool/fabric and fabric/fabric friction for woven-fabric composites during the thermostamping process," *International journal of material forming*, vol. 6, no. 2, pp. 209–221, 2013.

[22] J. Sun, M. Li, Y. Gu, D. Zhang, Y. Li, and Z. Zhang, "Interply friction of carbon fiber/epoxy prepreg stacks under different processing conditions," *Journal of Composite Materials*, vol. 48, no. 5, pp. 515–526, 2014.

[23] K. A. Fetfatsidis, L. M. Gamache, J. L. Gorczyca, J. A. Sherwood, D. Jauffrès, and J. Chen, "Design of an apparatus for measuring tool/fabric and fabric/fabric friction of woven-fabric composites during the thermostamping process," *International journal of material forming*, vol. 6, no. 1, pp. 1–11, 2013.

[24] B. Liang, N. Hamila, M. Peillon, and P. Boisse, "Analysis of thermoplastic prepreg bending stiffness during manufacturing and of its influence on wrinkling simulations," *Composites Part A: Applied Science and Manufacturing*, vol. 67, pp. 111–122, 2014.

[25] S. Allaoui, P. Boisse, S. Chatel, N. Hamila, G. Hivet, D. Soulat, and E. Vidal-Salle, "Experimental and numerical analyses of textile reinforcement forming of a tetrahedral shape," *Composites Part A: Applied Science and Manufacturing*, vol. 42, no. 6, pp. 612–622, 2011.

[26] D. Soulat, A. Cheruet, and P. Boisse, "Simulation of continuous fibre reinforced thermoplastic forming using a shell finite element with transverse stress," *Computers & structures*, vol. 84, no. 13, pp. 888–903, 2006.

[27] W. R. Yu, M. Zampaloni, F. Pourboghrat, K. Chung, and T. J. Kang, "Analysis of flexible bending behavior of woven preform using non-orthogonal constitutive equation," *Composites Part A: Applied Science and Manufacturing*, vol. 36, pp. 839–850, 2005.

[28] E. Guzman-Maldonado, N. Hamila, N. Naouar, G. Moulin, and P. Boisse, "Simulation of thermoplastic prepreg thermoforming based on a visco-hyperelastic model and a thermal homogenization," *Materials & Design*, vol. 93, pp. 431–442, 2016.

[29] D. Dörr, F. J. Schirmaier, F. Henning, and L. Kärger, "A viscoelastic approach for modeling bending behavior in finite element forming simulation of continuously fiber reinforced composites," *Composites Part A: Applied Science and Manufacturing*, vol. 94, pp. 113–123, 2017.

[30] U. Sachs, *Friction and bending in thermoplastic composites forming processes.* Phd thesis, University of Twente, 2014.

[31] PAM-FORM, "Engineering System International. www.esi-group.com."

[32] AniForm Virtual Forming Tool, "Software and help-manual. www.aniform.com."

[33] D. Lukaszewicz, C. Ward, and K. Potter, "The engineering aspects of automated prepreg layup: History, present and future," *Composites Part B: Engineering*, vol. 43, no. 3, pp. 997–1009, 2012.

[34] P. Wang, N. Hamila, and P. Boisse, "Thermoforming simulation of multilayer composites with continuous fibres and thermoplastic matrix," *Composites Part B: Engineering*, vol. 52, pp. 127–136, 2013.

[35] S. Ropers, M. Kardos, and T. A. Osswald, "A thermo-viscoelastic approach for the characterization and modeling of the bending behavior of thermoplastic composites," *Composites Part A*, vol. 90, pp. 22–32, 2016.

[36] F. T. Peirce, "The Handle of Cloth As a Measurable Quantity," *Journal of the Textile Institute Transactions*, vol. 21, pp. 377–416, 1930.

[37] ASTM D1388-08, "Standard Test Method for Stiffness of Fabrics," *ASTM International*, 2012.

[38] E. Bilbao, D. Soulat, G. Hivet, and A. Gasser, "Experimental Study of Bending Behaviour of Reinforcements," *Experimental Mechanics*, vol. 50, no. 3, pp. 333–351, 2009.

[39] D. Soteropoulos, K. Fetfatsidis, J. a. Sherwood, and J. Langworthy, "Digital method of analyzing the bending stiffness of non-crimp fabrics," in *Proceedings of the 14th International ESAFORM Conference*, vol. 1353, pp. 913–917, 2011.

[40] L. M. Dangora, C. Mitchell, K. D. White, J. A. Sherwood, and J. C. Parker, "Characterization of temperature-dependent tensile and flexural rigidities of a cross-ply thermoplastic lamina with implementation into a forming model," *International Journal of Material Forming*, 2016.

[41] S. Kawabata, "The standardisation and analysis of hand evaluation," *The Textile Machinery Society of Japan, Osaka*, 1980.

[42] S. Lomov, I. Verpoest, M. Barburski, and J. Laperre, "Carbon composites based on multiaxial multiply stitched preforms. Part 2. KES-F characterisation of the deformability of the preforms at low loads," *Composites Part A: Applied Science and Manufacturing*, vol. 34, no. 4, pp. 359–370, 2003.

[43] T. A. Martin, D. Bhattacharyya, and I. F. Collins, "Bending of fibre-reinforced thermoplastic sheets," *Composites Manufacturing*, vol. 6, no. 3, pp. 177–187, 1995.

[44] J. Wang, A. C. Long, and M. J. Clifford, "Experimental measurement and predictive modelling of bending behaviour for viscous unidirectional composite materials," *International Journal of Material Forming*, vol. 3, pp. 1253–1266, 2010.

[45] T. Hove, *Bending of CF/PEEK prepregs*. Master's thesis, University of Twente, 2012.

[46] U. Sachs, R. Akkerman, and S. P. Haanappel, "Bending characterization of ud composites," in *Key Engineering Materials*, vol. 611, pp. 399–406, Trans Tech Publ, 2014.

[47] A. Margossian, S. Bel, and R. Hinterhoelzl, "Bending characterisation of a molten unidirectional carbon fibre reinforced thermoplastic composite using a Dynamic Mechanical Analysis system," *Composites Part A: Applied Science and Manufacturing*, vol. 77, pp. 154–163, 2015.

[48] T. Instruments, "Dynamic Mechanical Analysis, basic theory and applications training. http://www.tainstruments.com/wp-content/uploads/CA-2016-DMA.pdf ." accessed 14-December-2016.

[49] T. Centea, L. Grunenfelder, and S. Nutt, "A review of out-of-autoclave prepregs Material properties, process phenomena, and manufacturing considerations," *Composites Part A: Applied Science and Manufacturing*, vol. 70, pp. 132–154, 2015.

[50] D. Fertis, *Nonlinear structural engineering*. Springer-Verlag Berlin Heidelberg, 2006.

[51] L. M. Dangora, C. J. Mitchell, and J. A. Sherwood, "Predictive model for the detection of out-of-plane defects formed during textile-composite manufacture," *Composites Part A: Applied Science and Manufacturing*, vol. 78, pp. 102–112, 2015.

[52] X. Bian, Y. Gu, J. Sun, M. Li, W. Liu, and Z. Zhang, "Effects of Processing Parameters on the Forming Quality of C-Shaped Thermosetting Composite Laminates in Hot Diaphragm Forming Process," *Applied Composite Materials*, vol. 20, no. 5, pp. 927–945, 2013.

[53] Y. R. Larberg, M. Åkermo, and M. Norrby, "On the in-plane deformability of cross-plied unidirectional prepreg," *Journal of composite materials*, vol. 46, no. 8, pp. 929–939, 2012.

[54] H. Brinson and L. Brinson, *Polymer Engineering Science and Viscoelasticity An Introduction*. Springer New York Heidelberg Dordrecht London, 2015.

[55] T. Centea and P. Hubert, "Measuring the impregnation of an out-of-autoclave prepreg by micro-CT," *Composites Science and Technology*, vol. 71, no. 5, pp. 593–599, 2011.

[56] H. Alshahrani and M. Hojjati, "A new test method for the characterization of the bending behavior of textile prepregs," *Composites Part A: Applied Science and Manufacturing*, vol. 97, pp. 128–140, 2017.

[57] K. F. Choi and S. K. Tandon, "An energy model of yarn bending," *Journal of the Textile Institute*, vol. 97, no. 1, pp. 49–56, 2006.

[58] M. Realff, M. Boyce, and S. Backer, "A micromechanical model of the tesnile behavior of woven fabric," *Journal of Textile Research*, vol. 67, no. 6, pp. 445–459, 1997.

[59] E. Syerko, S. Comas-Cardona, and C. Binetruy, "Models of mechanical properties/behavior of dry fibrous materials at various scales in bending and tension: A review," *Composites Part A: Applied Science and Manufacturing*, vol. 43, no. 8, pp. 1365–1388, 2012.

[60] A.J.M. Spencer, *Continuum Theory of the mechanics of fibre-reinforced composites*. Springer-Verlag Wien, New York, 1984.

[61] S. Gatouillat, A. Bareggi, E. Vidal-Sallé, and P. Boisse, "Meso modelling for composite preform shaping - Simulation of the loss of cohesion of the woven fibre network," *Composites Part A: Applied Science and Manufacturing*, vol. 54, pp. 135–144, 2013.

[62] L. Galuppi and G. Royer-Carfagni, "Laminated beams with viscoelastic interlayer," *International Journal of Solids and Structures*, vol. 49, no. 18, pp. 2637–2645, 2012.

[63] Cytec Engineered Materials, "CYCOM 5320 toughened epoxy for structural applications, out-of-autoclave manufacturing. Product data sheet," 2015.

[64] M. Clifford, *Column buckling experiment, in structural mechanics*. Department of civil and municipal engineering, University College London, 1981.

[65] J. Hunt, H. Zhang, and Y. Huang, "Analysis of cantilever-beam bending stress relaxation properties of thin wood composites," *BioResources*, vol. 10, no. 2, pp. 3131–3145, 2015.

[66] M. L. Williams, R. F. Landel, J. D. Ferry, *et al.*, "The temperature dependence of relaxation mechanisms in amorphous polymers and other glass-forming liquids," *J. Am. Chem. Soc*, vol. 77, no. 14, pp. 3701–3707, 1955.

[67] R. Li, "Time-temperature superposition method for glass transition temperature of plastic materials," *Materials Science and Engineering: A*, vol. 278, no. 1, pp. 36–45, 2000.

[68] I. Emri and M. Gergesova, "Time-dependent behavior of solid polymers," *Rheology: encyclopaedia of life support systems (EOLSS), UNESCO. Eolss, Oxford*, pp. 247–330, 2010.

[69] P. Wang, N. Hamila, and P. Boisse, "Thermoforming simulation of multilayer composites with continuous fibres and thermoplastic matrix," *Composites Part B: Engineering*, vol. 52, pp. 127–136, 2013.

[70] H. Lin, J. Wang, A. Long, M. Clifford, and P. Harrison, "Predictive modelling for optimization of textile composite forming," *Composites Science and Technology*, vol. 67, no. 15-16, pp. 3242–3252, 2007.

[71] J. S. Lee, S. J. Hong, W. R. Yu, and T. J. Kang, "The effect of blank holder force on the stamp forming behavior of non-crimp fabric with a chain stitch," *Composites Science and Technology*, vol. 67, no. 3-4, pp. 357–366, 2007.

[72] M. Khan, T. Mabrouki, E. Vidal-Sallé, and P. Boisse, "Numerical and experimental analyses of woven composite reinforcement forming using a hypoelastic behaviour. application to the double dome benchmark," *Journal of materials processing technology*, vol. 210, no. 2, pp. 378–388, 2010.

[73] H. Alshahrani and M. Hojjati, "A theoretical model with experimental verification for bending stiffness of thermosetting prepreg during forming process," *Composite Structures*, vol. 166, pp. 136–145, 2017.

[74] H. Alshahrani, R. Mohan, and M. Hojjati, "Evaluation of in-plane shear deformation of outof-autoclave carbon/epoxy prepregs using bias extension test," in *CAMX 2014*, (Orlando, Florida, USA), 2014.

[75] T. Rogers, "Rheological characterization of anisotropic materials," *Composites*, vol. 20, no. 1, pp. 21–27, 1989.

[76] C. Macosko, *Rheology principles, measurements, and applications*. Wiley–VCH, 1994.

[77] J. Sjölander, P. Hallander, and M. Åkermo, "Forming induced wrinkling of composite laminates: a numerical study on wrinkling mechanisms," *Composites Part A: Applied Science and Manufacturing*, vol. 81, pp. 41–51, 2016.

[78] Y. Larberg and M. Åkermo, "In-plane deformation of multi-layered unidirectional thermoset prepreg–modelling and experimental verification," *Composites Part A: Applied Science and Manufacturing*, vol. 56, pp. 203–212, 2014.

[79] J. Kratz, K. Hsiao, G. Fernlund, and P. Hubert, "Thermal models for MTM45-1 and Cycom 5320 out-of-autoclave prepreg resins," *Journal of Composite Materials*, vol. 47, no. 3, pp. 341–352, 2013.

[80] H. Alshahrani and M. Hojjati, "Optimum processing parameters for hot drape forming of out-of-autoclave prepreg over complex shape using a double diaphragm technique," in *20th International Conference on Composite Materials*, (Copenhagen, Denmark), 2015.

[81] A. Murtagh, J. Lennon, and M. P, "Surface friction effects related to pressforming of continuous fibre thermoplastic composites," *Composites Manufacturing*, vol. 6, no. 3–4, pp. 169–175, 1995.

[82] A. Modin, "Hot Drape forming of thermoset prepreg," *In proceedings of Composites in Manufacturing, Pasadena, CA*, pp. 93–105, 1993.

[83] J. Krebs, K. Friedrich, and D. Bhattacharyya, "A direct comparison of matched-die versus diaphragm forming," *Composites Part A: Applied Science and Manufacturing*, vol. 29, no. 1, pp. 183–188, 1998.

[84] H. Bersee, S. Lindstedt, G. Niño, and A. Beukers, "Diaphragm forming of thermoset composites," in *16th International Conference on Composite Materials, Kyoto International Conference Center, Kyoto*, pp. 1–11, 2007.

[85] B. Christopher, *Technological advances in double diaphragm forming of advanced and uniform short fiber composites using fixed and reconfigurable tooling.* Phd thesis, Rensselaer Polytechnic Institute, 2006.

[86] S. Chen, O. McGregor, A. Endruweit, M. Elsmore, D. De Focatiis, L. Harper, and N. Warrior, "Double diaphragm forming simulation for complex composite structures," *Composites Part A: Applied Science and Manufacturing*, vol. 95, pp. 346–358, 2017.

[87] H. Alshahrani and M. Hojjati, "Influence of double-diaphragm vacuum compaction on deformation during forming of composite prepregs," *Journal of Science: Advanced Materials and Devices*, vol. 1, no. 4, pp. 507–511, 2016.

[88] P. J. Mallon, C. M. O'Bradaigh, and R. B. Pipes, "Polymeric diaphragm forming of complex-curvature thermoplastic composite parts," *Composites*, vol. 20, no. 1, pp. 48–56, 1989.

[89] S. Delaloye and M. Niedermeier, "Optimization of the diaphragm forming process for continuous fibre-reinforced advanced thermoplastic composites," *Composites Manufacturing*, vol. 6, no. 3-4, pp. 135–144, 1995.

[90] S. G. Pantelakis and E. Baxevani, "Optimization of the diaphragm forming process with regard to product quality and cost," *Composites Part A: Applied Science and Manufacturing*, vol. 33, no. 4, pp. 459–470, 2002.

[91] N. Haibin, G. Janowski, and U. Vaidya, "Processing and Nonisothermal Crystallization Kinetics of Carbon/PPS in Single Diaphragm Forming," *Journal of Composite Materials*, vol. 44, no. 8, pp. 915–929, 2010.

[92] M. Keane, M. Mulhern, and P. Mallon, "Investigation of the effects of varying the processing parameters in diaphragm forming of advanced thermoplastic composite laminates," *Composites Munufuchming*, vol. 6, no. 3, pp. 145–152, 1995.

[93] P. Hallander, J. Sjölander, and M. Åkermo, "Forming induced wrinkling of composite laminates with mixed ply material properties; an experimental study," *Composites Part A: Applied Science and Manufacturing*, vol. 78, pp. 234–245, 2015.

[94] P. Hallander, M. Akermo, C. Mattei, M. Petersson, and T. Nyman, "An experimental study of mechanisms behind wrinkle development during forming of composite laminates," *Composites Part A: Applied Science and Manufacturing*, vol. 50, pp. 54–64, 2013.

[95] L. Sorrentino and C. Bellini, "Potentiality of hot drape forming to produce complex shape parts in composite material," *The International Journal of Advanced Manufacturing Technology*, vol. 85, no. 5-8, pp. 945–954, 2016.

[96] H. Alshahrani and M. Hojjati, "Bending behavior of multilayered textile composite prepregs: Experiment and finite element modeling," *Materials & Design*, vol. 124, pp. 211–224, 2017.